Cape Peninsula University of Technology

Experimental and numerical modelling of defects in an additively manufactured aluminium propeller

By

ZWELISHA SENZOKUHLE SIYANDA NKWANYANA

(221666648)

Thesis

submitted in the fulfilment of the requirements

for

the Degree

Master of Engineering (M. Eng): Mechanical Engineering

In the faculty of Engineering & the Built Environment

at the Cape Peninsula University of Technology

Supervisor : Prof. G.J. Oliver

Co-supervisor : Mr. C. Magoda

Bellville Campus

Date submitted: 24 May 2025

DECLARATION

I, **Zwelisha Senzokuhle Siyanda Nkwanyana,** declare that the contents of this thesis represent my own unaided work, and that the thesis has not previously been submitted for academic examination towards any qualification. Furthermore, it represents my own opinions and not necessarily those of the Cape Peninsula University of Technology.

Signed 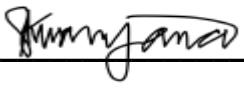 **-** **Date**____24/5/2025___

ABSTRACT

This research focused on conducting a numerical analysis of stress and strain distribution of defects and experimentally validating the presence of defect in an additively manufactured aluminium alloy propeller using advanced Non-destructive testing methods. The aim of this research was to understand the additively manufactured component behaviour when there are embedded defects that mimic inherent defects. The methods of investigation were numerical modelling using ABAQUS and laboratory experiments. The simulation findings from 20 steps had observed an increase in stress distribution along the blades. An analysis of a randomly sampled blade showed the stress results to be ascending from the tip of the blade to the root at increment of 0,5 MPa however at position 15 to 17 there an abrupt change of stress distribution which suggested a concentrated stress range of 105 MPa and 137 MPa. This led to a stress concentration factor of 1.36. This area was assessed using Micro X-ray CT which suggested the presence of the linear defect. This research concludes that crack propagation of inherent defects of additive manufacturing (AM) components are significantly influenced by:

- cyclic loading conditions on defective AlSi10Mg AM components, results in a crack propagating easily along the interfaces, leading to delamination or inter-layer cracking.
- Stress Concentration: Linear defects (cracks) create localised stress concentrations. When the component is subjected to loading, these areas experience higher stress, which can accelerate crack initiation and growth in AlSi10Mg AM components.

The solutions obtained in this research demonstrate to create a data of effect-of-defect behaviour of AM aluminium component.

Keywords

Additive manufacturing, Non-destructive testing, X-ray CT, stress intensity factor, fracture toughness, number of cycles, defects, Modelling, tomogram analysis, NDT tolerance standards

ACKNOWLEDGEMENTS

I wish to thank:

- Professor G.J Oliver and Mr C. Magoda, my research Supervisors and Prof. Ngonda for their effort in mentoring me complete my thesis despite all the troubles.
- My father S.C Nkwanyana for believing in me
- Father almighty and I for believing that it is possible I just must start this journey.
- My partner J.M. Nkosi and son for understanding and helping me achieve my goals and
- Vaal University of Technology faculty of Applied and Computer Sciences for supporting and giving me the opportunity to study further.

The financial assistance of RNF-UCDP funding through Vaal University Technology (VUT) towards this research is acknowledged. Opinions expressed in this thesis and the conclusions arrived at, are those of the author, and are not necessarily to be attributed to the National Research Foundation.

Contents

LIST OF FIGURES

List of tables

Abbreviations and definitions

AM	Additive Manufacturing
CAD	Computer Aided Design
CT	Computed Tomography
CR	Computed Radiography
DR	Direct Radiography
ISO	International Organization Standards
NDT	Non-Destructive Testing
PBF	Powder Bed Fusion
RTR	Real-time Radiography

SYMBOLS & MEANING

μ	Attenuation coefficient
$\boldsymbol{\varepsilon}$	Strain
D	Gradient operator matrix
∇	Gradient operator
I_o	Incident radiation intensity
$I(j,k)$-	secondary radiation intensity at j and k directions
$\boldsymbol{K^e}$	Element stiffness matrix
$\boldsymbol{F^e}$	Load vector
μ, λ	Lames constants
$\boldsymbol{\rho}$	Slope of the projection line
N_f	Number of circles to fracture
a_i	initial crack
m	geometry factor
σ_{max}	Maximum stress
σ_{min}	Minimum stress
K	stress intensity factor
Θ^e	Element nodal values
$\boldsymbol{B^e}$	Strain displacement matrix
S_0	Space function
$\boldsymbol{\Gamma}$	Total boundary

U_1	Dirichlet boundary condition

GLOSSARY

Defects or Imperfection- A product especially that creates an unreasonable risk of harm in its normal use.
Fracture mechanics- The discipline concerned with analysing the failure of materials containing cracks and flaws.

Chapter 1.

Introduction.

1.1 Background.

The accidents and human injuries from propeller's failures are not as prevalent, even though they are serious and are preventable. To date the accidents that are blamed on the propeller are up to fourteen, resulting to fatalities and three serious injuries. Four incidents had involved propeller blade (Price and Muszynski, 2014) and no further review has been done this far however it is still concerning.

Additive manufacturing (AM) is described as a latest production skill that improves manufacturing processes by constructing thin layers of materials from digitized three-dimensional (3D) designs which are virtually constructed using advanced computer aided design (CAD) software, Dufera and Science, (2019). According to Grasso, M. *et al.* (2018), AM offers the construction of new types of complex component with exceptional material properties as compared to other manufacturing processes such as subtractive manufacturing. This manufacturing process provide an added advantage of developing a one-piece propeller at a reasonable duration.

This manufacturing process however carries some drawbacks amongst other the development of inherent defects. Charalampou et al. (2020) discussed that most of the discontinuities in AM are mostly noticeable around the layered or flattened plane structure of the components. These types of defects are caused by various factors such as imperfect melting on certain layers (Charalampous, Kostavelis and Tzovaras, 2020). Duplessis (2018) as well had articulated that the development of defects such as cracking, pores, delamination are a result of poor quality of powder is poor such as powder particle shapes, the presence of satellites, the particle size distribution, oxidation level, humidity, static charge etc. the poor quality leads to lack of geometrical accuracy which agrees with Chen et al. (2021) statement stated that, these defects may occur due to different melt pool dynamics that depend on process parameters, complex shapes, and internal structures of PBF produced components. Once the crack has initiated in this process, it spreads along the molten layer, resulting in affecting the material properties such as mechanical properties of the component. It is for this reason that this research addresses the detectability of these defects by Non-Destructive Testing (NDT).

Since additive manufacturing (AM) is a merging manufacturing system, there is a gap and deep research is still conducted in the development of non-destructive testing (NDT) acceptance standards for AM components, which delays the full adoption of AM and permanently eliminate subtractive manufacturing by

industry (Diego, 2016). NDT has numerous methods depending on the material type, thickness, geometry and location of a defect, a method can be selected. The NDT basic methods are visual testing (VT), Liquid penetrant Testing (LPT), Magnetic Particle testing (MPT), Eddy current Testing (ECT), Ultrasonic Testing (UT) and radiographic Testing (RT). Previous research had demonstrated that these basic methods are not sufficient to evaluate for the integrity of Additive Manufacturing as they carry various disadvantages that will be discussed in chapter 2.

Consequently, advanced NDT methods were established, these methods are Ultrasonic Phased Array, Time of Flight Diffraction (TOFD), Computerised Radiography (CR) and computed Tomography (CT). Chapter 2 in the literature has a discussion more of the most suitable NDT methods for AM components for assessing internal structural integrity and explicitly highlight the gaps and drawbacks which are a result of AM in industries that benefit from this type of manufacturing process. The defect characteristics (size, location depth &geometry) (Khorshidi, Khosrowpour and Hosseini, 2020) data will be collected from using a modelling system and validate experimentally and further be analysed, where fracture mechanics computations will be adopted for the estimation of life span.

The study by Chau et al. (2017) had observed that, according to ASTM standard, AM processes is classified into seven categories namely: VAT Photo-polymerization, Material Extrusion, Sheet Lamination, Material Jetting, Binder Jetting, Powder Bed Fusion (PBF), and Directed Energy Deposition (DED). This research project therefore had investigated whether NDT can be used as an acceptable method for AM components which were developed by one of these manufacturing processing.

1.2 Research problem statement

The function of the tolerance or acceptance criteria in NDT must be to determine whether, the NDT method selected, is feasible to detect a smallest defect found in AM propellers. The establishment of tolerance (accept/reject criteria) for the NDT inspection is the most important commitment for the AM designer and NDT inspection since it provides the designer with input from material integrity so that further decisions can be made for improvement and quality control and assurance.

This is sufficient to portray the importance for understanding the effects of defects in AM components so that developing and improving NDT acceptance standards for the additively manufactured aluminium propellers through can be achieved. NASA released a paper in (2020) had stated in their presentation Military Additive Manufacturing Summit, that there is lack of physical reference standards with same material, processing and history of actual AM components (demonstrate NDE capability), also there is a lack of effect-of-defect behaviour studies on AM. Hence the research addresses the application of modelling and Computed

Tomography on additively manufactured aluminium propellers. Consequently, the research shall project on the importance and function of NDT in manufacturing industry.

1.3 Research questions

- What are the life-span impacting defects that are inherently originate in AM components?
- How is the stress distributed in a defective component?
- How is crack propagation influenced by AM component inherent defects?
- How are the NDT methods used for evaluation of defects?
- How can NDT methods be used to uncover and characterise lifespan impacting defects in AM components? (case study of AM propeller)

1.3.1 Sub-questions

- How is the built-in beam employed in combination with a digital X-ray detector in a backscatter X-ray imaging setup for quality control of a component built with the PBF-E process?
- Which simulations approach may be adopted to approximate the typical growth rate of the defect of specific size?
- How does NDT link with fracture mechanics of AM products?

1.4 Objectives of the research

The following research objectives were formulated:

(a) Developing a modelling system for prediction of component life span (Failure Analysis) by:
   - Determining stress intensity factor
   - Determining and analysing the intensity factor vs defect growth

(b) Characterisation of defects using NDT method:
   - To assess the structural integrity of aluminium propellers by Characterising sub-surface defects using Computed Tomography.

1.5 Research Methodology

The research uses a quantitative technique approach. The methods of investigation will be numerical modelling using ABAQUS and laboratory experiments. The design of this research will be based on experimental study using and analysing the primary data which will be extracted by ABAQUS models. Random sampling approach of defects will be applied in this research. The below shows a flow step to be

taken for the proposed research methodology.

ABAQUS modelling and MATLAB computing

- **Step 1**: Simulate stress and deformation acting on the propeller using ABAQUS
- **Step 2:** Compute intensity factor using MATLAB
- **Step 3:** Compute the prediction model of components
- **Step4:** Compare the stress distribution acting on the blade with the defect location on the blade

NDT experiments

- **Step 5**: Conduct NDT experiments using a CT scan
- **Step 6**: Obtain the defect characteristics (i.e. size)

1.6 Research significance.

The significance of the research is to advance NDT-CT procedure for AM components and address and support engineering principles such as testability, maintainability, integrity, ethics and management of components by conducting numerical estimation for life span on additively manufactured aluminium propellers and also by using computed tomography as an NDT method of inspection to improve standard tolerance in NDT.

1.7. Expected outcomes and contributions of the research.

The expected outcomes shall be:

- To author and co-author peer at least two reviewed papers that will be published by Science direct or Springer. The papers will have the following topics:
  (a) The impact of NDT in engineering design of additive manufacturing: A review
  (b) An experimental comparison of NDT inspection efficiency between Tomography and phased array.
- Attaining the Master of Engineering (MEng: Mechanical)

Other outcomes of this research that are expected are:

- to create a defect catalogue where other researchers may continue to populate the effect-of-defect studies furthermore the results will qualify NDE method capability at the critical flaw size for high value fracture of critical AM components and ultimately in future,
- to suggest an NDT acceptance criteria standard for AM components

Chapter 2.
Literature review.

2.1 Introduction.

This Chapter reflected on work done previously by other researchers in understanding the application of different simulation methods in additive materials. This chapter reflected on the three modelling methods namely finite volume, finite element, and finite difference methods. The chapter also explored the research used simulation equations that are functional on these distinct modelling methods. This chapter also links the review done by other researchers on the types of Additive manufacturing processes that are currently used by the industry. Seven processes were reflected and amongst those, the powder bed fusion additive manufacturing process was of interest. This research focused on giving a brief of the working principle of the powder bed fusion, an AM process and its discontinuities that are associated with this AM process.

Fracture mechanic was covered with an intension to uncover the behaviour of AlSi10Mg alloy when there is a presence of a defect both at the simulation and experimental reviews. The equations to estimate the defect growth rate which were unpacked by in Hosseini et al. on ductile material under an applied load. There were three modes of fracture that were reviewed in this research namely tensile, sliding and tear modes. These modes are associated with the defect propagation. This literature led to the research to review the Paris law equation, that when the reciprocal of Paris law is integrated, results in finding an equation that determines the number of cycles a ductile material such as AlSi10Mg shall endure before failure.

This chapter further reviewed on the Non-Destructive testing (NDT) as a science of investigating the integrity of material without impairing its intended use or integrity. Firstly, it was alluded that NDT is a centre of three pillars of engineering concepts namely, quality control and assurance, engineering design and additive manufacturing. It was explained that NDT addresses a control of risk management and quality improvement in the industrial products. The researcher also reviewed that NDT utilises six basic NDT methods namely, Visual Testing (VT); Magnetic Particle Testing (MPT); Liquid Penetrant Testing (LPT); Eddy Current Testing (ECT); Ultrasonic Testing (UT) and Radiographic Testing (RT). These methods were reviewed whether they are feasible for the inspection of additively manufactured metal components. A further unpacking of NDT was done on advanced NDT methods with a same intention of measuring testability and reliability of methods. These methods were Phased Array Ultrasonic Testing (PAUT) and Computed Tomography (CT).

The chapter lastly reviewed the Destructive testing for determination of tensile strength and bend resistance. The intention was to establish the impact of defect on the AM material. These concepts were intended to

address the quantitative approach that this research had taken in chapter three.

2.2 Additive Manufacturing Process

The final production of all additively manufactured components requires an inspection for measuring integrity or fit for purpose without impairing their usual and expected functions. Rohib (2018) mentioned that it is the desire of most engineering designers to develop a component that have a safety factor value that is well above 1 (Rohib, and Irawan, 2018). The factor of safety (SF) can be described as a measure of how capable a component is, compared to the minimum expected capability. This applies to also AM components produced such as propellers.

A propeller (informally called a screw) is a component that is assembled with a rotating hub and blades which are arranged to be at a pitch that forms a helical spiral when rotated to employ a linear drive upon a working fluid such as water or air. The main function of the propeller is to create thrust to force a boat through water or an aircraft through the air.

There are several types of propellers namely, Voith Schneider propellers, modular propellers, Skewback propellers and a variable-pitch propeller. This research conducts a study on a variable-pitch propeller which is used in air space. A variable-pitch propeller is a type of propeller with blades that can be rotated around their long axis to change the blade pitch, this is a Reversible propeller meaning that the pitch can also create reverse thrust for going backwards or braking without the need to change the direction of shaft revolution.

Propellers are some of the components that can be manufactured by either subtractive or additive manufacturing. This research explores the additive manufacturing of aluminium variable-pitch propeller component. The propeller blades are manufactured to satisfy Bernoulli's principle as their shape designed in a way that when in rotational motion through the fluid or air, the pressure difference will be caused between the two surfaces of the blade.

Additive Manufacturing (AM) is described by Bajaj et al. (2020) to be a process that produces a multidimensional object based on a 3-dimensional (3D) computer Aided design (CAD) model by adding layers of material. The manufacturing of materials by additives of layers is developing technology with a high degree of freedom in the design of light and heavy-weight components and structures that serves the aerospace, military, automotive, electrical, medical, and power industries (Haghdadi *et al.*, 2021).

These components and structure are bound to be manufactured with consideration of safety and reliability to be of prime importance (Plessis *et al.*, 2018; Haghdadi *et al.*, 2021). Chen et al. (2021) cited in their research the benefits of choosing AM to have the ability to manufacture complex structures, short product manufacturing cycle, high material utilisation and no need for tools or moulds as compared to other metal

manufacturing processes or technologies such as forging, machining, casting, and welding.

The choice of using Additive Manufacturing of components is motivated by four group criteria namely: cohesive design, individualization, lightweight design, and efficiency (Haghdadi *et al.*, 2021). The modifications between the product of the two methods that is, additive Manufacturing (AM) or subtractive manufacturing (SM) are different since AM components are formed in stack of thin layers, rather than as a full body object (Rohib and Irawan, 2018).

The study by Chau et al (2017) had observed that, AM processes are classified into seven categories namely: VAT Photo-polymerization, Material Extrusion, Sheet Lamination, Material Jetting, Binder Jetting, Powder Bed Fusion (PBF), and Directed Energy Deposition (DED). Four processes have the ability of processing metallic materials as shown in figure 2.1(net near shape component), these processes are sheet lamination, material jetting, binder jetting, PBF and DED.

- Vat photopolymerization: selective layer by layer photopolymerization of a holder of liquid photopolymer resin.
- Material extrusion: selective layer by layer extrusion of material through a nozzle e.g., fused deposition modelling (FDM, polymers).
- Sheet lamination: Selective cutting of material sheets that are laminated together to form 3D geometries e.g., laminated object manufacture (LOM, various materials).
- Material jetting: selective layer by layer deposition of liquid material droplets onto a substrate where it then solidifies, e.g., ink jetting, metal jetting (various materials).
- Binder jetting: a layer by layer pouring of liquid binder droplets into a bed of powdered material forming a 3D printing (polymers and ceramics).
- Powder bed fusion: careful layer by layer fusion of a powdered material on a bed form, the following techniques are used; selective laser melting (SLM, metals), electron beam melting (EBM, metals), direct metal laser sintering (DMLS, metals), selective laser sintering (SLS, polymers and ceramics).
- Directed energy deposition: Deposition of material fed into an energy source to form a melted pool, frequently attached on a multi axis arm, such as a direct metal deposition (DMD), laser engineered net shaping (LENS, also metals).

Research by Hossain et al. (2018) explained that adding aluminium alloying elements can increase chances of attaining strength as high as 1 GPa. When elements such as Borron is added, the size of grain reduces and thus improve its strength. The modification of a 7075-alloy or AA7075 using nickel and boron can be possible to achieve exceptional mechanical properties that are beneficial for strength related applications.

This research hence it focuses only on an aluminium propeller that is AM manufactured which by the virtue of their design are made to be subjected to high cyclic loading and high performance when in-service, therefore, if not properly evaluated by NDT methods prior and in-service, catastrophic events are likely to occur when there is presence of defects.

Additive manufacturing is further classified by categorising it according to their physics as shown in figure 2.1 below:

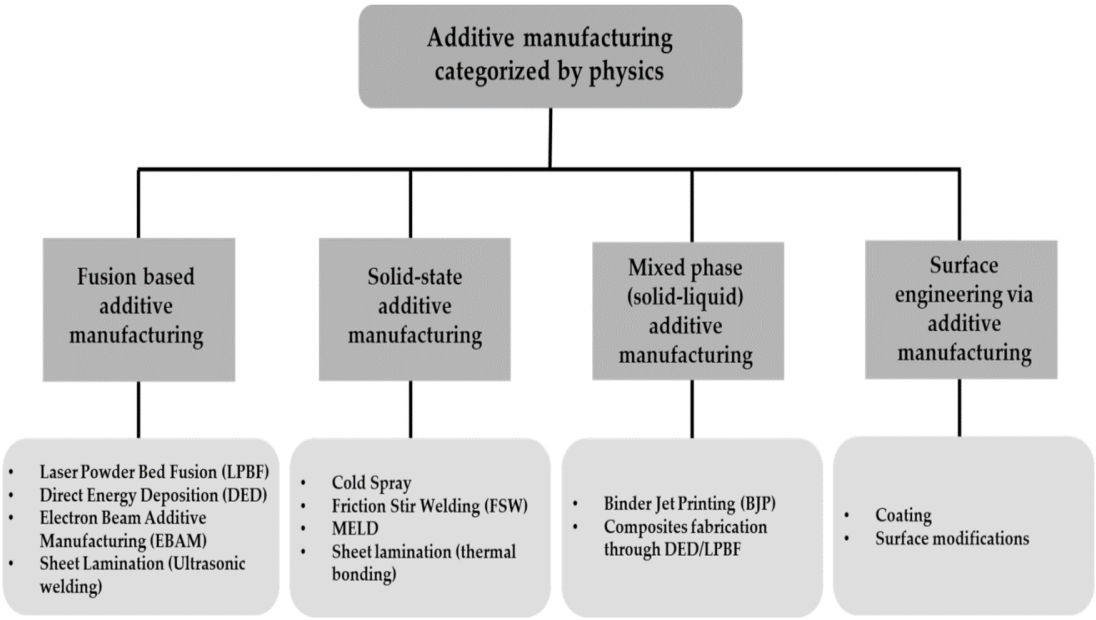

Figure 2.1 Arrangement of additive manufacturing processes (Vo, T. H. et al. (2018))

This classification to some extent agrees to those presented and explained by Chau et al (Chua, Ahn and Moon, 2017), however it is proposed to be more precise since it had grouped the categories by their physics. Therefore, this research focuses only on aluminium propeller product that is developed using Powder Bed Fusion (PBF).

2.2.1 Powder Bed Fusion (PBF).

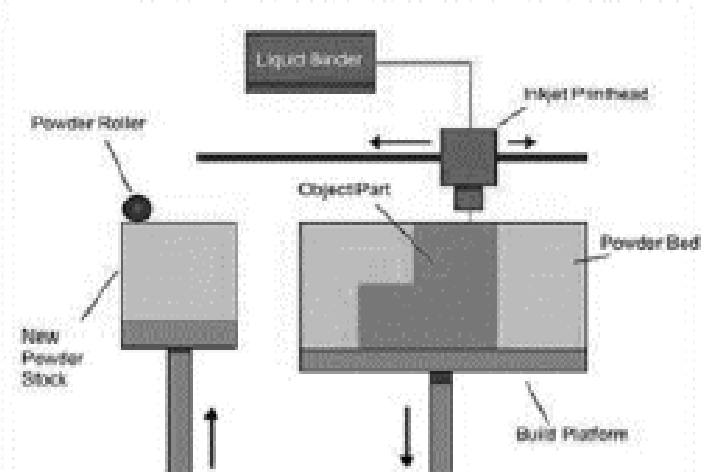

Figure 2.2: Schematic view of powder bed fusion process (Singh R. et al (2020))

The PBF system make use of admission of a powder methodology, where it spreads on the substrate layer by layer. The energy from the electron beam or laser is utilised to sinter the powder once the powder is distributed, so that a digital 3D model (cross-sectional) of the component is formed. The building platform shall be lowered automatically once the layer is completed, and the manufacturing operation is carried out continuously until a completed structure is formed. The following are the PBF parameters for manufacturing dimensions of AM complex AlSi10Mg components:

Metrix	Typical PBF value
Dimensional accuracy	$\pm 0.1\ mm$ (can be low as 0.03mm)
Surface roughness (as built)	Ra approx. 5-10μm
Layer thickness	20-50 μm
Minimum feature size	150-300μm
Wall thickness	Above 0.5 mm (geometry dependent)

These values depend on size of laser spot, scanning speed, quality of powder, and machine calibration. The manufactured components are also subjected to production drawbacks such as possible failures of producing required geometrical accuracy and defective (internal or external) components and are comparable in different AM methods. The continuous quality improvement in the processes of components manufacturing

is important so that the challenges will be reduced to meet industry requirements.

2.2.2 AM inherent defects from Powder Bed Fusion (PBF) process.

Chen et al. (2021) research made mention that most of the discontinuities in AM, such as cracking, porosity and balling, are a result of the discontinuity from categories that includes manufacturing processes, build preparation choices, equipment and powder. Discontinuity which are induced by equipment are caused by unsuitable setting and calibration of the main system components. The discontinuities which were induced by the manufacturing process are viewed to be linked with the interaction of various factors such as powder quality, the beam parameters used and the quality of the previous layer of the material. The research done by Museau et al (2018) had describe discontinuities in AM to be classified into four categories as shown in Figure 2.3 below, which turns to agree mostly with the research done by Chen et al (2021).

AM process demonstrated to be a considerable manufacturing process since it shows significant benefits as compared with other conventional manufacturing processes. Although this process is promising, there limiting factors that makes it difficult to endorse in areas where stringent standards are used such as aeronautical standards due to few qualities that need to be addressed on structural components. Air bus was the first aeronautical compony to use AM component which was manufactured by Laser Powder Bed Fusion (L-PBF) on a commercial cabin bracket connector which was made of Ti6Al4V on aircraft A350. This led to a rapid production of AM components in this industrial sector where Ti6Al4V and AlSi10Mg components were produced using a Direct Energy Deposition (DED) process in a Boeing 787 Dreamliner in 2017.

Despite of these profound developments in the AM production system, there are drawbacks that holds the endorsement of AM, the oxides which are inherently in the Al powder causing a high degree of porosity defects in the final component produced. The other drawback is the poor surface finish of the competence component which may hinder and cause fatigue in structures where fatigue resistance is crucial and lastly the drawback of shrinkage during solidification stage. The cracking may be a result of the following characteristics: the building direction may result into parallel direction cracks. Secondly, the coalescence of pores due to notch effect can lead to cracks, thirdly, the intergranular cracks could propagate along grain boundaries, and lastly equiaxed semisolid structures partially accommodate the strain and mitigate the cracking.

During AM processing it was observed that the adjacent layers comprise of microcracks and microporosity which are transversal to the building direction. This resulted to high brittleness and lower strength in such a material as compared to those material which have a diagonal or a horizontal building direction (Montanari, R. *et al.*, 2023). The materials such as Al--Mg alloy exhibited a fatigue strength of 100.5MPa which was found to be more superior for a material deposition were in a transversal direction and when the material deposition

was horizontal 57 MPa of strength was found.

There were two factors that were noted during the parallel deposition namely, the high stress concentration in areas with lack of fusion defect and lastly the microstructure variations. The different columnar grains/equiaxed grains area ratio contribute toward the intergranular cracking and the propagation. Some grains of transversely deposited samples contribute to enhance the fatigue resistance because of the exceptional dislocation formation (Montanari, R. *et al.*, 2023). These are the defects which may be susceptible towards the manufacturing of the AlSi10Mg propeller. When a propeller creates a spinning to lift there are five expected forces acting on it. These forces are centrifugal, centrifugal twisting, aerodynamic, thrust bending and torque bending force, The centrifugal force is a dominant force in a propeller, and it is a physical force that tends to throw (pull) the rotating propeller blades away from the hub. The blade stresses are assessed to be using an application of beam bending theory with the basic assumptions to be (a) the blade acts as a cantilevered beam, (b) normal stresses are due to bending and centrifugal forces, (c) sheer stresses are negligible, and (d) the blade has zero rake and skew. Therefore, in the presence of discontinuity or defect, these forces then create a localised stress which causes propagation of defects. The AM development of defects could be due to surface quality, microstructure, mechanical properties or geometric complexity. The below chat assists by showing the classical defect categories based on their origin.

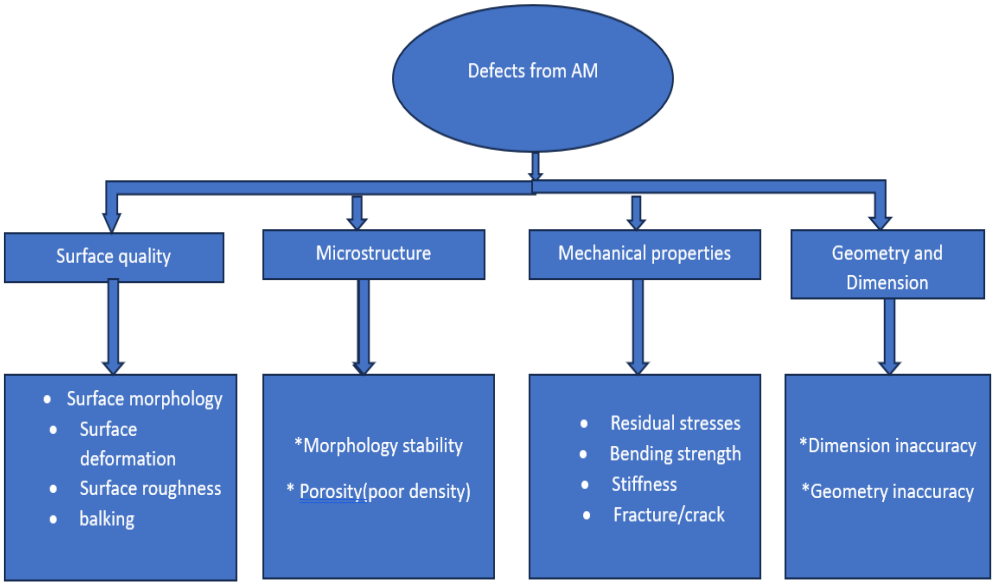

Figure 2.3: Defect classification in Additive manufacturing

Charalampou et al (2020) discussed that most of the discontinuities in AM are mostly located in a layered or flattened Plane of the component and these types of defects can be explained to result from the deficient melting on specific layers (Charalampous, Kostavelis and Tzovaras, 2020).

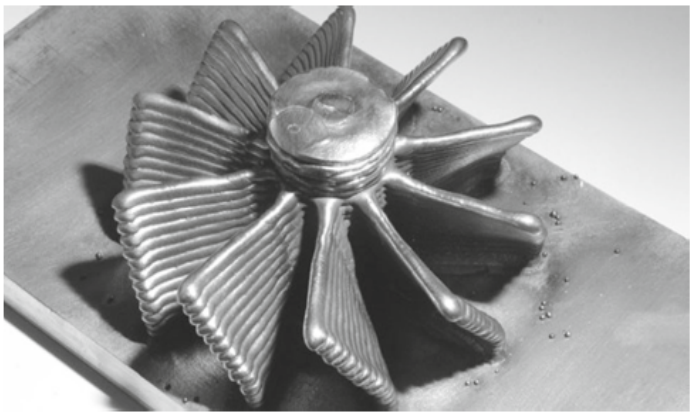

Figure 2.4: Near net shape propeller component *(Lopez* et al*., 2019)*

Duplessis (2018) articulated that when quality of powder is poor such as shapes of the powder particle, the presence of satellites, the particle size distribution, oxidation level, humidity, static charge etc. will result in development of defects such as porosity, lack of fusion, cracking, lack of geometrical accuracy which agrees with Chen et al (2021) statement stated that, these defects may occur due to different melt pool dynamics that depend on process parameters, complex shapes, and internal structures of PBF produced components.

The mechanical properties of the component from AM process are compromised when the defect such as crack has occurred because it spreads it spreads along the molten layer. Porosity is a typical phenomenon in PBF process resulting from a lack of fusion and trapped gas, and this directly affects the density and mechanical properties of the finished components which agrees with Chen et al (2021). This research however focuses on the discontinuities that compromise the mechanical properties. The discontinuities such as cracks, porosity and delamination are said to be life span compromising the AM components. These life span impacting defects are articulated below.

(a) Cracking

Cracks are types of discontinuities that are linear in nature. When a continuous and semi-continuous liquid film forms on the grain boundaries of the heat-affected zone and when tensile stresses form within the component, the linear discontinuities in PFB are formed within the component. The growth of the linear discontinuity is determined by the direction of the grain, and they are a result of uneven thermal stresses in an AM process.

(b) Porosity

The plural term used in describing many pores which are spherical in shape that are either clustered or scattered is called porosity. Porosity in PBF is explained to be a result of a gas entrapped in the molten pool

of the material that had been exposed to rapid meting and solidification processes during the PBF component manufacturing process. Porosity is one of the process-induced discontinuities that may also possibly exist before the melting process.

This occurs when the arrangement of the feed material is atomised, the preparation setting is thus argon purged which leaves indications on the solidified powder particles. The melting process will thus make the gas to formulates in metal powder resulting to pores forming and remaining in the component if these gases are not released on time. There are various types of pores can be observed in the components fabricated by PBF namely:

i. Structural (engineered) porosity is introduced in the component for a particular purpose. The intentionally induced pores. It is cited as the empty sections in lattice structures, which decrease the overall weight without any effect on the loading capacity of the component.

ii. Functional porosity which results from de-binding where they are described as open and connected. They can be eliminated by applying heat at low melting point of raw materials, pressure post-treatment, and intrusion of similar secondary materials to attain fully dense composite components.

iii. Microstructural porosity: are unintentionally formed and should be prevented so that the negative impact on mechanical properties is not compromised. This porosity is resulting from residual voids which existed in the microstructure of the fabricated component;

Therefore, this research also assesses detectability of porosity among other defects. It should be noted that the internal discontinuities mostly result from residual thermal stresses and are the most common discontinuities that are found in AM components which could be found in AM propellers.

Studies have found that the development of residual stresses in AM components are resulting from factors such as material properties, component height, powder layer thickness, scanning strategy, and related process parameters.

The temperature of the metal powder differs substantially in AM process, and this results to the residual thermal stresses to form easily within the component. The trapped stress will release itself in a form of cracks developing on the surface. The formation of residual stress will compromise the mechanical properties which will ultimately hinder the quality of the final product and affecting the performance and life of the component.

2.2.3 Fracture Mechanics methods for AM

Fracture mechanics is useful since it gives a platform to estimate a components life span in the event where

there is presence of defects. This is a stage in manufacturing where first NDT inspection takes part to validate the integrity of the component whether it shall serve its purpose, this paper extends the precision of inspection by first creating a catalogue of simulated defect which are under certain physical properties. The defect propagation modelling requires the determination of the next growth direction.

The research by Wang P et al. (2019) noted that AlSi10Mg powder contains hollow particles, which partially originated the void defects. It was articulated that the liquid metal solidifies too rapidly and at time making it impossible to release the internally entrapped gases. At low energy input per layer, the void defects are generated due to lack of fusion, whereas, at higher energy input per layer, large voids are generated because of unstable melt pools, which are inferred by real-time monitoring of AM processes.

This research focuses in two dimensional problems where the stress fields surrounding the defect are dependent on the defect propagation direction or vice versa. The modes (mode I, II,III) of fracture in fracture mechanics is directly proportional to the stress intensity factor. The defect growth is determined by the following criteria:

(1) The maximum hoop stress principle,
(2) The maximum potential energy release rate principle, and
(3) The minimum strain energy density principle.

These three principles appear to show that they provide almost similar results. This research focuses on the first principle. The assumption from the hoop stress mentions that the defect extension will occur in the direction that maximises the circumferential stress in the region close to the defect tip (e.g., crack tip). The polar coordinate system r, θ, on the circumferential stress $\sigma_\theta$and the shear stress $\sigma_{r\theta}$ are given as

$$\sigma_\theta = \frac{1}{2\pi r} cos\left(\theta/_2\right)\left[K_I cos^2\left(\theta/_2\right) - K_{II} sin\theta\right] \quad (2.1)$$

$$\sigma_{r\theta} = \frac{1}{2\sqrt{2\pi r}} cos\left(\theta/_2\right)[K_I sin(\theta) - K_{II}(3cos\theta - 1)] \quad (2.2)$$

where K_I and K_{II} are stress intensity factors at mode I and II respectively. The stress σ_θ becomes principal when $\sigma_{r\theta} = 0$, meaning that

$$K_I sin\theta + K_{II}(3cos\theta - 1) = 0$$

and the defect propagation direction becomes,

$$\sigma_\theta = 2arctan\left[\frac{1}{4}\left(\frac{K_I}{K_{II}} \pm \sqrt{\frac{K_I}{K_{II}} + 8}\right)\right] \quad (2.3)$$

The ± sign in equation (2.3) contained is depended on the direction of the defect and the two values of θ given by the equation, the one resulting in the higher hoop stressσ_θ is taken by the direction of crack propagation. The modelling of the initial crack propagation is then attached to the use of fracture mechanics techniques.

The defect propagation model articulated by F Kelil et al (2013) suggested that the intraspecimen and interspecimen scatter should be considered when conducting severe propagation analysis. This research therefore looks at the possibility of estimating the lifespan of the component with specimen-to-specimen scattering using equation 2.4 for stochastic crack growth. The stress intensity factor *K* is a measure of the severity of a crack situation as affected by crack size, stress, and geometry. The stress intensity factor is a function of the defect (e.g. crack) size and applied load (Hosseini *et al.*, 2018). The mathematical definition for the stress intensity factor is,

$$K = Y\sigma\sqrt{\pi a} \quad (2.4)$$

Where Y is the defect (e.g. crack) geometry factor and σ represents applied load (stress). Once the defect reaches section of growth it is already propagating. This propagation rate is outlined using the Paris law equation as referenced by Hosseini (Hosseini *et al.*, 2018),

$$\frac{da}{dN} = C\Delta K^m \quad (2.5)$$

The paper by Olivier D et al (2018) looked at the modelling of powder bed manufacturing defects found that the defects arising from the powder bed fusion process had compromised the mechanical properties of the product such as strength. Furthermore, they concluded that the thermal input used to create the workpiece leads to the development of residual stresses and distortion.

The local stress concentration that is induced by defects in AM was found to be closely related to the defect morphology. The fatigue crack initiation can be accelerated mainly because the irregular morphology can produce higher stress concentrations. They further noted that the distributions of defect sphericity follow the trend of high localised stress concentration. These trends were like those found by other researchers where the defect size was shown to have an influence on buffer crack nucleation and failure and NDT was the best approach to investigate such defects Cheng (2021).

2.3 Non-Destructive Testing.

The term non-destructive testing according to Cherfaoui, (2012) is a science of diagnosis of industrial components and equipment by implementing scientific investigation methods to assess the health condition

of components and equipment without destruction and articulating an opinion on their ability to fulfil the function which they are intended. Kumar V et al.s' (2021) research also agrees with Cherfaoui that NDT methods are employed on components including those that are manufactured additively with the aim of locating and characterising a variety of flaws which are less visible but capable of threatening both the lifespan and properties of components.

2.3.1 NDT as a quality control tool

Krishnamoorthy (2009) stated that NDT plays a key role in quality assurance (QA), reliability and control since its services are inspection, condition monitoring and diagnostic in a variety of applications (Krishnamoorthy, 2009). The figure 2.8 below shows the vital role of NDT in engineering design and additive manufacturing for quality production. NDT demonstrates that it is the centre of the three principal spheres, and simply the lamination of NDT creates a gap in quality and safety of engineering products.

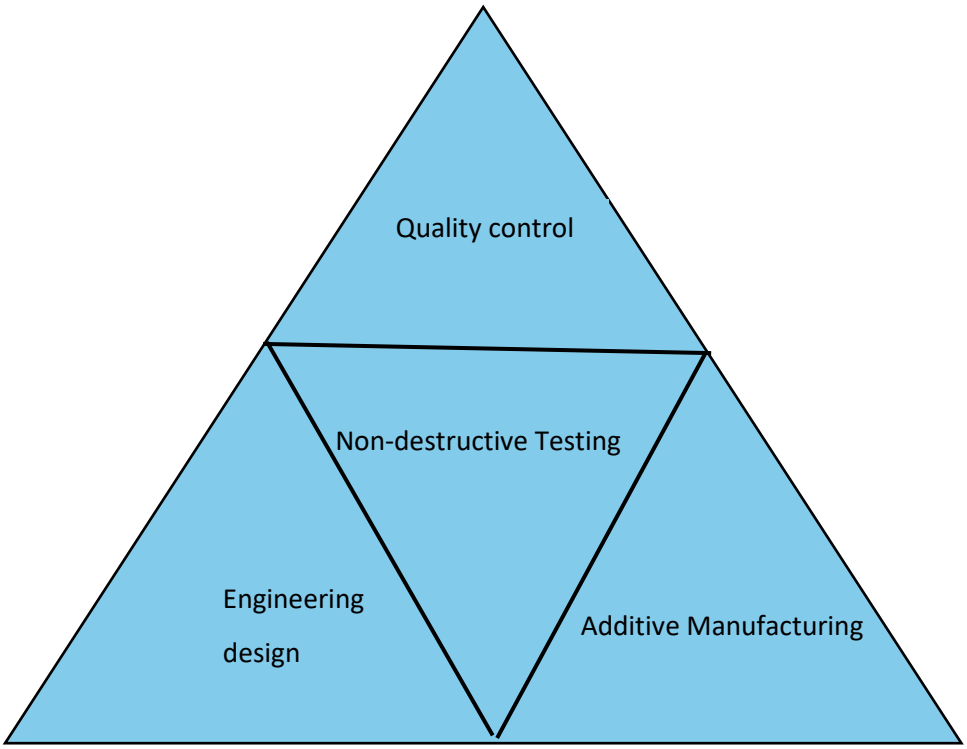

Figure 2.5: *Quality dependence for products*

It is noted that regardless of the advantages that AM poses, discontinuities occur in components which can be harmful to the mechanical properties of the produced components (Rohib and Irawan, 2018). The quality of parts made by AM technologies are strongly dependent on the actual geometrical designs.

Kumar V et al. (2021) also extends and explained that the development of quality and risk management for industrial products necessitates extensive expertise and knowledge, particularly in the inspection of surfaces through Non-Destructive Testing (NDT) during the manufacturing process. The assessment methods for detecting and evaluating weld components are influenced by the critical size of defects.

NDT processes have gathered global attention for their essential role in advancing engineering practices and enhancing industrial operations while mitigating risks associated with services. The choice of NDT methods is contingent upon the specific requirements of the equipment involved. It is important to note that not all defects that may arise during inspection can be identified by a single NDT technique.

2.3.2. NDT methods of inspections

NDT utilises six basic methods that are employed frequently by industry. These NDT methods are divided into two namely, surface methods and volumetric methods. The methods each has different testing techniques, since all these techniques can detect defects or flaws that are situated on the surface or inside the component Gbenga, E. E. (2016). NDT can investigate for defects such as porosity (internal and external),

cracks, voids, delamination etc. RT however has a drawback on in ability to detecting defects that are positioned parallel to the radiation beam direction such as cracks and lack of fusion.

The lack of data for determining an appropriate NDT method is a serious challenge when it comes to determining the best NDT method in terms of the tolerance (acceptance/rejection) for the defects in any components that are manufactured additively including propellers.

NDT standards provide guidance for the appropriated method and techniques which are used to detect flaws and provides an indication to engineers whether the components are fit for purpose (Obaton, 2020) hence this research seeks to find the tools that satisfies the measurements of engineering principles such as testability, maintainability, integrity, external integration, ethics, and management in additively manufactured (AM) components for assessing the defects in materials are either present because of the faulty manufacturing processes or due to fatigue, corrosion, or similar damage during service.

It is of course important to have components of the right quality before they are accepted for service. NDT methods offer not only the advantages of discovering potential or real problems early in the production programme but also definite feedback as to how to correct production problems at the earliest possible point.

The most critical non-destructive testing (NDT) methods used to perform detection of internal structural integrity are ultrasonic testing (UT) and radiographic testing (RT). Ultrasonic testing is an NDT method that uses acoustic sound energy level of above 20KHz as cited by Sharma, A. et al (2018). RT techniques are primarily comprising of either X-radiation(X-rays) or gamma radiation which is generated from a tube or from a disintegrating isotope of Iridium-192, or Cobalt-60 respectively.

This radiation type can penetrate extensive ranges of most material types with fluctuating densities by acquiring 2D images (radiograph) of the component (Teng et al., 2021). The current drawback of conventional radiography which uses films, is that it does not provide an understanding of the volume integrity of multifaceted materials and defect depth (Khorshidi, Khosrowpour and Hosseini, 2020). This method is said to be exceptional at finding defects such as cracks, porosity and delamination.

The RT method, further, can be further categorized in terms of the newer digital processing techniques such as computed radiography (CR) and direct radiography (DR), real-time radiography (RTR) and computed tomography (CT). Therefore, for the purpose of this research CT using X-rays will be selected since it can reconstruct 3D representations of complex shaped components by taking several of single 2D images(slices) at different projection angles. X-ray CT had then become a solution to address the findings of defects that are not found by the conventional RT method.

2.3.3. NDT surface methods

The surface method is one of the NDT methods that used to identify and locate surface and near surface defects such as cracks and surface porosity. Surface methods used in NDT are visual inspection (VT), magnetic particle testing (MPT), liquid Penetrant testing (LPT), electromagnetic or eddy current testing (ECT). all these techniques can detect defects or flaws that are situated on the surface or subsurface of the component and only the location and length of the defect can be reported.

(a) Visual Testing

Visual testing is the mostly used NDT technique which utilises the human eye as the main tool that is used for inspection. Leutenecker C., et al (2014) articulated that VT regularly serves as a pre-inspection technique to that is used to determine the dimensional accuracy and visible surface defects (such as cracks) of the component before it is tested using other NDT techniques. The visual testing technique is often paired with other NDT techniques. The technique can be carried out using directly (using the naked eye) and indirectly (using optical aids) Leutenecker C., et al (2014). During indirect testing, optical aids are used when direct viewing of the component inspected is impossible. The optical aids for visual testing have evolved from a simple mirror or magnifying glasses to sophisticated devices such as video scopes, borescopes, microscopes, optical flats, and optical comparators.

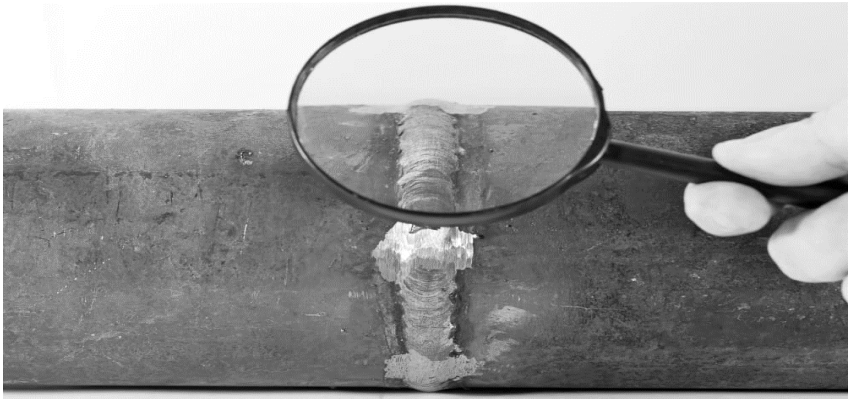

Figure 2.6: visual testing equipment for indirect technique (https://www.zetec.com/blog/is-visual-inspection-an-effective-ndt-method/)

The advantages of using optical aids are that it is portable, you can have real-time photo images. You can store and transfer images, furthermore blurriness can be reduced by using polarization. Accurate measurement of defect length and area can be made when paired with a computer and software. The disadvantage on the other hand is that this technique is only limited to surface flaws and is highly dependent on the experience of the NDT inspector or scientist.

(b) Magnetic Particle Testing (MPT)

Magnetic particle testing (MPT) is used for the inspection of surface integrity of ferromagnetic components which are made of either cobalt, steel or nickel to characterise defect such crack and surface porosity, Sacarea, et al (2021) research articulated. The sensitivity of this technique relies on the properties of the magnetic fields such as magnetic flux and strength.

The working principle of this technique is that the permanent magnet or an alternating current yoke is used to induce the magnetic flux or field lines of force onto the ferromagnetic components. The field lines will travel steadily from the north to the south poles of the yoke, and during that process, the magnetic particles (either suspended or powder) are sprayed around the area that is magnetised.

When a discontinuity or flaw such as a crack is present, secondary poles are created at the crack face. The secondary magnetic field will appear at the surface of the component by filling flux leakage and clump round the flaw, making it visible as seen in the figure 2.10 below.

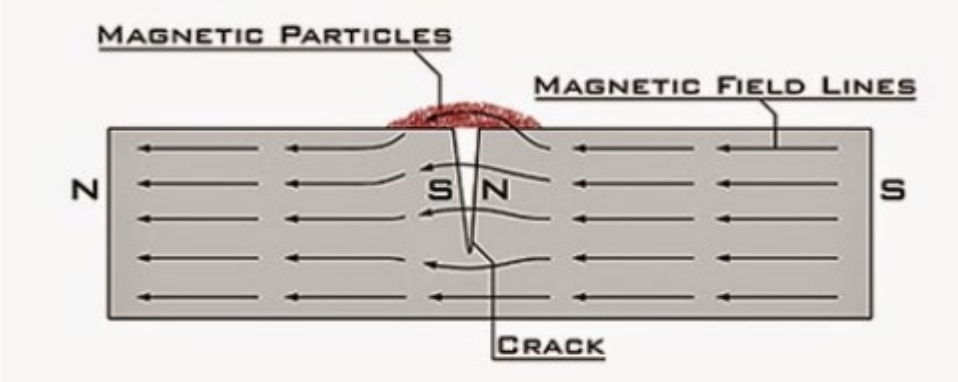

Figure 2.7: Magnetic particle testing working principle (Jim Worman (2021); Senior Staff Engineer-National Board source: http://www.nationalboard.org/index.aspx?pageID=164&ID=377)

The best visibility of indications is when the magnetic flux lines are at 90 ˚ to discontinuity or flaw. This technique can be done by either using white contrast or florescent methods depending on the sensitivity requirements. The ability to show a discontinuity depends on the magnetic field strength induced during magnetisation, the angle of the flaw to the lines of force, and the depth of the flaw.

The work done by several researchers like Sacarea, A. (2021) also mentioned that this method can be applied both manually and semi-automated with the following advantages: It is relatively fast quick and uncomplicated, indications of discontinuities are observed immediately, both surface and near surface-

defects can inspect, and the method can be used for both on-site or workshop. Paramagnetic and diamagnetic materials cannot hold a flux which is strong enough to attract particles and in the case of this research, aluminium is non-magnetic, also testing complex shape components is not possible. Therefore, this method is not recommended to be useful for this research.

(c) Liquid penetrant testing (LPT)

Liquid penetrant testing is an NDT method that is used to assess for the surface-breaking discontinuities in all non-porous materials such as metals, plastics, or ceramics. LPT is used to detect components which are manufactured by casting, forging, and welding for surface defects such as hairline cracks, surface porosity, leaks in new products, and fatigue cracks on in-service components.

The American Society of Materials (ASTM) classifies liquid penetrant testing based on the penetrant type either fluorescent (Type I), visible (Type II), water washable (Method A), post emulsifiable lipophilic (Method B), solvent removable (Method C), or post emulsifiable-hydrophilic (Method D). Penetrants are also divided into five levels of sensitivity namely, ultralow (Level 1/2), low (Level 1), medium (Level 2), high (Level 3), and ultrahigh (Level 4).

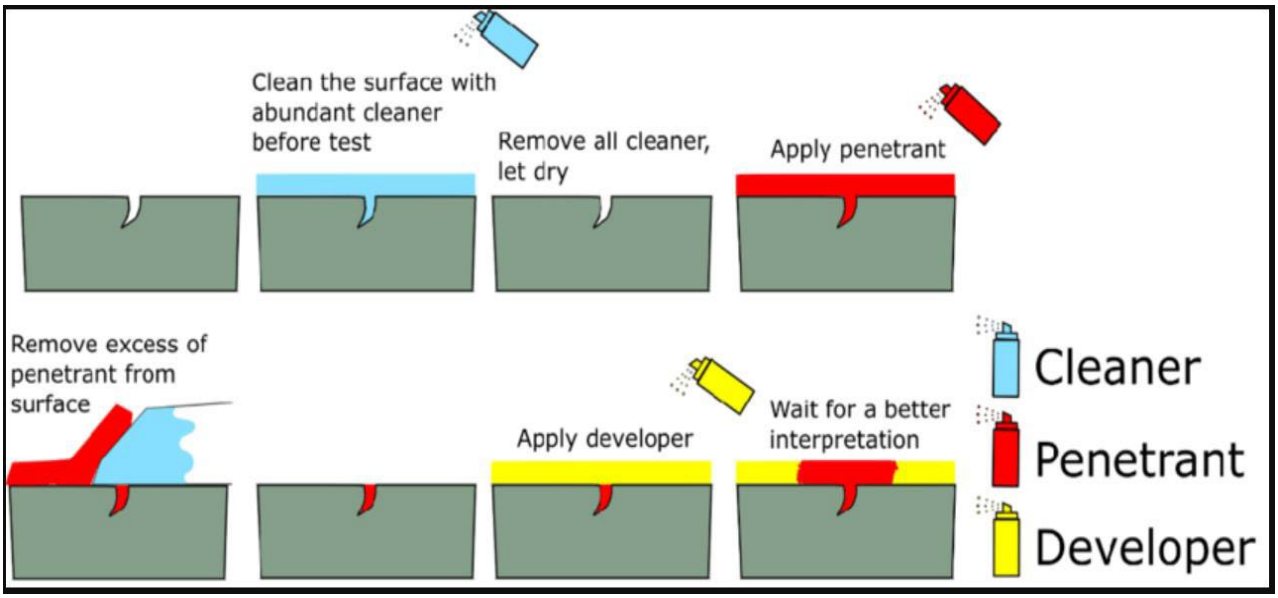

Figure 2.9: Liquid penetrant testing working principle Muhsen, A. A. (2022)

The basic principle of liquid penetrant testing (PT) is capillary action, which allows the penetrant to enter the opening of the defect, remain there when the liquid is removed from the material surface, and then re-emerge on the surface on the application of a developer, which has a capillary action like blotting paper. The term penetrant material includes all penetrants, solvents or cleaning agents that are used in this examination process.

A penetrant material has the capacity to enter the crevices opening on the surface of a material. Figure 2.11 shows the following stages: 1. Soiled crack, 2. Ideally pre-cleaned, 3. Application of test agent, 4. Intermediate cleaning, 5. Optimally cleaned intermediately, 6. Drying, 7. Application of developer and 8. Crack indication.

Solvent removable technique is mostly used in industry and further describes the description step by step as follows: the pre-cleaned components are coated with an excessive visible or fluorescent dye solution for a given time called a dwell time (usually 10 minutes) depending on the material type inspected. The excess penetrant is carefully removed from the surface using a clean damped with water cloth or penetrant remover, and a developer in liquid or powder form is applied for a specific dwell time.

The function of the developer is to act as a blotter, that should be able to draw the entrapped penetrant out of the crevice opening of the discontinuity to the surface and reveals a colour contrast between the penetrant and developer (usually red on white). While with fluorescent dyes, ultraviolet light is used to make the bleed-out to fluoresce brightly, allowing the discontinuity to be readily seen and inspected.

AM is not capable of producing parts with acceptable mechanical properties and surface roughness that meet the requirements which makes this method not useable for the surface inspection of AM components.

(d) Eddy current Testing (ECT)

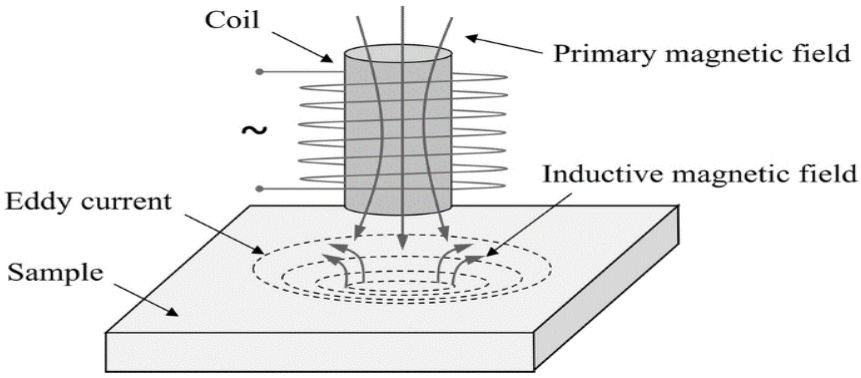

Figure 2.13: Eddy current working principle Bhagi, R. (2014)

Bhagi, Purna Chandra. (2011) stated that Eddy current testing is an electromagnetic non-destructive evaluation method extensively utilized across various sectors, including power generation, aerospace, and petrochemicals, for identifying surface cracks and subsurface damage in metallic components.

Eddy current testing relies on the principle of electromagnetic induction. An alternating current passing through a wire coil creates an oscillating magnetic field within an eddy current transducer. When the probe,

along with its magnetic field, approaches a conductive material, such as a metallic specimen, it induces a circular flow of electrons, referred to as an eddy current, which moves through the metal akin to swirling water in a stream. This eddy current, in turn, produces its own magnetic field that interacts with the coil and its magnetic field through the process of mutual inductance.

Alterations in metal thickness or the presence of defects, such as cracks near the surface, disrupt or modify the amplitude and pattern of the eddy current and the associated magnetic field. This disruption subsequently influences the movement of electrons within the coil by changing the electrical impedance of the coil. The eddy current instrument records variations in both the impedance amplitude and phase angle, which can be analysed by a qualified operator to detect changes in the test specimen.

The density of eddy currents is greatest at the surface of the component, making this area the most sensitive for testing. The standard depth of penetration is defined as the depth at which the eddy current density reaches 37% of its surface value, a measurement that can be determined based on the test frequency along with the magnetic permeability and conductivity of the material being tested.

2.3.4 NDT volumetric methods

The industry uses either radiography or an ultrasonic testing method for volumetric inspections. Many researchers apply either radiographic testing or ultrasound testing techniques to detect internal failure and damage in components. Some studies used ultrasonic testing (UT) method that is widely used for non-destructive evaluation method for the integrity evaluation of components however this paper will not consider applying UT method the material geometry is complex for probes positioning and the varying thickness of the manufactured component this then becomes a most crucial drawback of UT in this research. Radiographic testing method will be used instead.

(a) Radiographic Testing (RT)

The South African Health product regulation authority defines industrial radiography as work that examines the structure of materials by non-destructive methods, utilising ionising radiation. Radiographic testing has the following methods that make use of either gamma or X-radiation: conventional radiography, Computerised radiography, Digital imaging radiography, and computed tomography.

There are other CT modalities where gamma (γ)-rays, synchrotron x-rays and neutron radiations energy sources are used for materials characterization and industrial applications alternative to the X-ray source. These modalities are denoted as γCT, SRCT, XCT and NRCT. Other radiographic testing methods used in number of research are, Proton radiography, and Neutron radiography. This research focuses on the use of computed tomography using X-radiation. Computed tomography is also known as “Computed Axial

Tomography" scanning. The working principle of computed tomography inspection requires a radiation source, a rotation bench, and a component to be inspected.

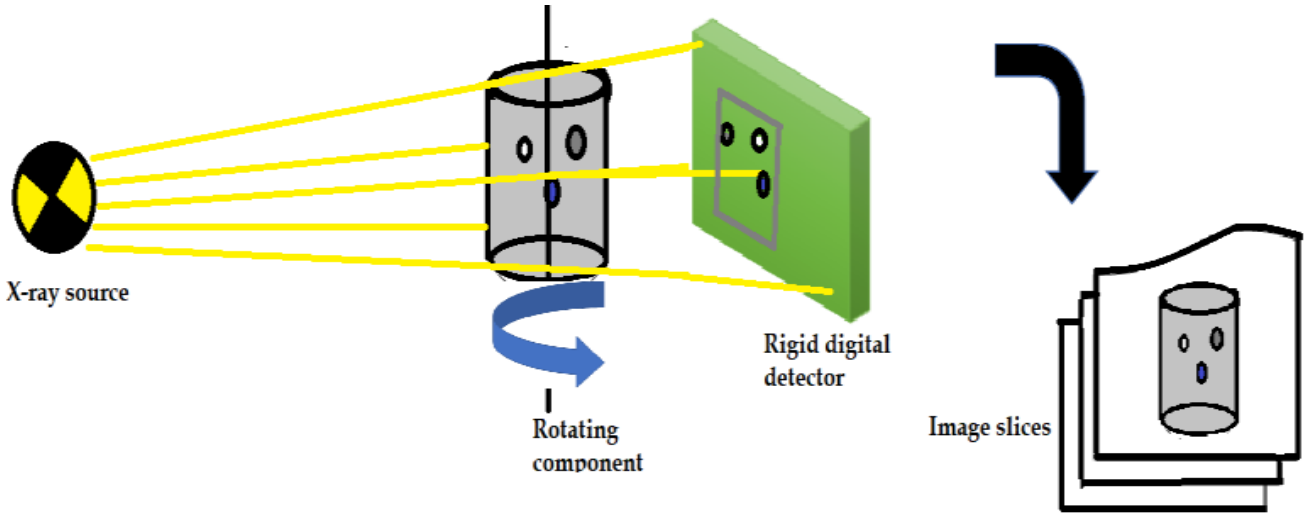

Figure 2.10: Arrangement of X-ray Computed tomography

The x-ray beam is characterized by its photon flux density or intensity and spectral energy distribution. When a beam of x-rays passes through a homogenous isotropic slab of material, the intensity of the rays is decreased due to scattering and absorption. For monochromatic radiation with an incident intensity $\mathbf{I_0}$, the x-ray beam is attenuated after passing through a test object infinitely thin slab of incremental thickness dx; The thin slab consists of a material with linear attenuation coefficient The yield is an attenuation intensity (transmitted intensity) **I**, which is proportional to the number of photons per unit time and unit area. The change in intensity of the x-ray beam after transmission through the slab may be expressed by considering the rate of decrease of the x-ray intensity as it passes through the test material.

CT can view the internal and external structure and measure the volumetric details of an object or component in 3-D planetary. CT takes several 2D digital radiography projections around 360° rotation of a component, proprietary algorithms are used to reconstruct the 2-D images into a 3-D volume images which allows viewing and slicing the part/component at any angle. The advantage of using X-ray CT is that both linear and rounded defects can be detected by this method because of its ability to produce a three-dimension internal shape of the material.

Image reconstruction by Tomography (Non-Destructive testing)

CT is essential to the development and enhancement of additive manufacturing techniques. In order to optimize process parameters like laser power, speed, scan strategy, and others, this stage improvement involves microscopic inspection of small representative slip samples. The issue with the superimposition of structures in conventional radiographs is what led to the use of CT image production. CT offers

comprehensive defect characterization and information.

According to Du Plessis et al (2018) it is difficult to detect defects such as lack of fusion, debonding, voids and porosity, deformation, and micro crack etc. by other NDT means such as traditional radiographic testing but Computed Tomography (CT), due to their size, geometry and the complexity of the object.

Charalampous et al (2020) also supported the statement from Du Plessis et al. It is therefore important to measure whether the choice of selecting NDT micro-CT method portrays capabilities of detecting defects of micro sizes and average the measured using the automated defect analysis module.

The research done by Senck *et al* (2020) stated that the intensity of the transmitted beam is recorded as a transformation function of the position parameter ***t*** (see figure 2.3) and the transmitted intensity is expressed by Beer Lambert's law as:

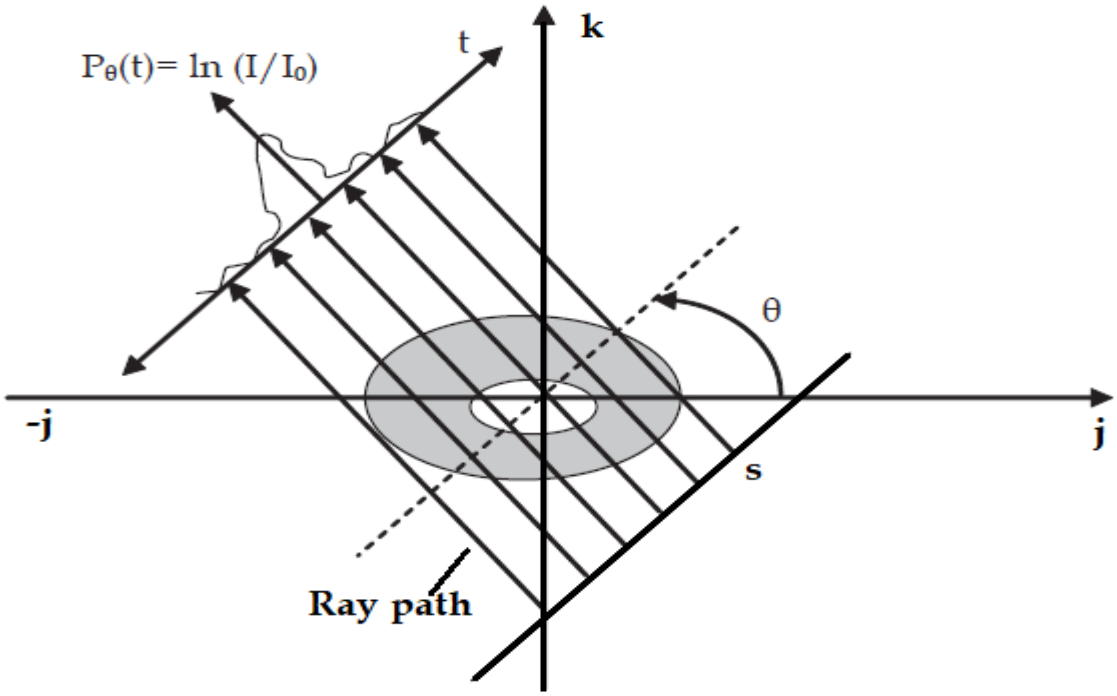

Figure 2.11: A scanned layer in the plane (j,k) along the angle θ and the transmitted intensity is stored in a system (t,s) of rotational coordinates *(Kharfi, 2019).*

$$I(j,k) = I_o Exp\left(\int \mu(j,k)ds\right) \qquad (2.44)$$

where I_0 is the incident X-ray beam intensity and $\mu(j,k) = f(j,k)$ is the rebuild function for 2D plane of heterogenous attenuation coefficient which will apply to this research for the analysis of radiation beam coordinates (Hilgendorff *et al.*, 2016).

The below figure: 2.4 shows a new square and rotational coordinates system (t, s) which is defined by Senck (2018) to be an expression to detect the system rotation that is in comparison to the fixed component coordinates system or vice versa, if the object is rotating and the detection system is fixed.

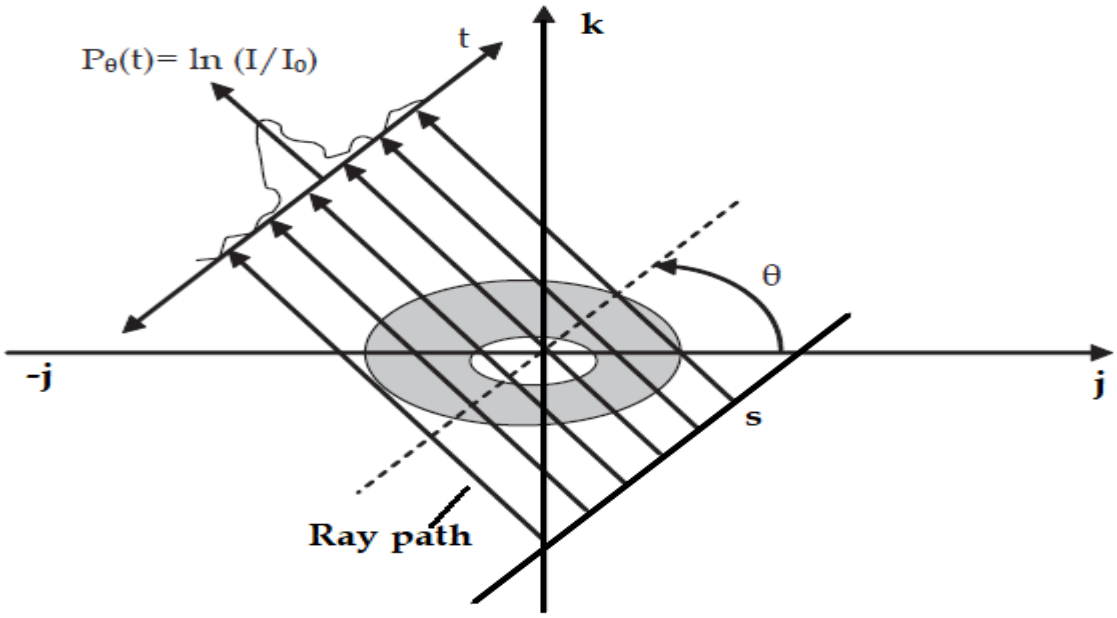

Figure 2.15: Scanning of a single layer in the plane (j, k). Note that z is the axis of rotation which coincides with the z-axis of the rotational coordinate's system {s, t, z}(Kharfi, 2019).

The transformation from the system (j, k) to the system (t, s), t is given by

$$t = jcos\theta + ksin\theta \tag{2.45}$$

and determines the X-ray (path) through the component which will be expressed in terms of $\boldsymbol{t}$ and $\boldsymbol{\theta}$. The Daric function is related to the X-ray beam (comb-shaped) influencing to the projection P_θ *(t)* which is expressed as

$$P_\theta(t) = \int \mu(j,k)ds = ln\left(\frac{I}{I_O}\right) \tag{2.46}$$

The coordinates of the system transformation from (j, k) system to (t, s) system was proven by Du Plessis (Plessis *et al.*, 2018) to have no influence on the values of the object function $\mu\,(j,k)$ $((\mu\,(j,k) = \mu\,(s,t))$ and (Senck *et al.*, 2020) confirmed.

The presence of defects in localised thin-walled component sections also high stress cross sectional areas are problematic, hence it is imperative to conduct a non-destructive testing of high-performance in components. Charalampous *et al* (Charalampous, Kostavelis and Tzovaras, 2020) discussed that X-ray micro-CT can be an ideal tool to characterize the type of defect by sizing, locating, and measuring the geometrical shapes hence this research will be committing into experimentally conducting NDT inspection and validating a comprehensive study on defect Characterization using Computed Tomography method.
The research done by Villarraga et al, (2015) showed that a 3D wall thickness analysis on the CT software system for volume data, is applicable to locate and size the positions of the individual areas with thinner and

thicker components walls. The color-coding can be used to visualized defects which agrees with Charalampous *et al*.

Another paper studied by Villarraga *et al*, (2018), had concluded with CT scans that has a voxel resolution of V_x= 65 μm have the capability of displaying the voids with volumes in the order of 0.002 mm^3 or less. These voids were concluded to be not assessable as residual internal deformations and spatial deformations were detectable in the manufacture of flexures with the AM process. They discussed that the deviations of up to 4 mm were detected with CT scans between measured and nominal dimensions from the CAD model of the flexure. This proves that the X-ray CT scan can detect defects of 0.002 mm^3 and therefore this research will be able to accumulate any small defect within the mentioned size. The demonstration of the tomographic projection is thus expressed by one of the Radon's transform expressions by Kharfi (2019) as

$$R(\rho,\tau)(f(j,k)) = \int_{-\infty}^{\infty}\int_{-\infty}^{\infty} f(j+\tau+\rho j)\, dj \tag{2.47}$$

which is further expressed as

$$R(\rho,\tau)\big(f(j,k)\big) = f(j,k)\delta(k-\tau+\rho j)djdk) \equiv U(\rho,\tau) \tag{2.48}$$

where ρ is the slope of the projection line and $\boldsymbol{\tau}$ is its intersection with the k axis. This equation will be employed. It is important to establish the mathematical basis of image projection and reconstruction in CT in the case of analytical method such as Filtered Back Projection (FBP). When the image is captured, interpretation will follow (Kharfi, 2019; Khorshidi, Khosrowpour and Hosseini, 2020).

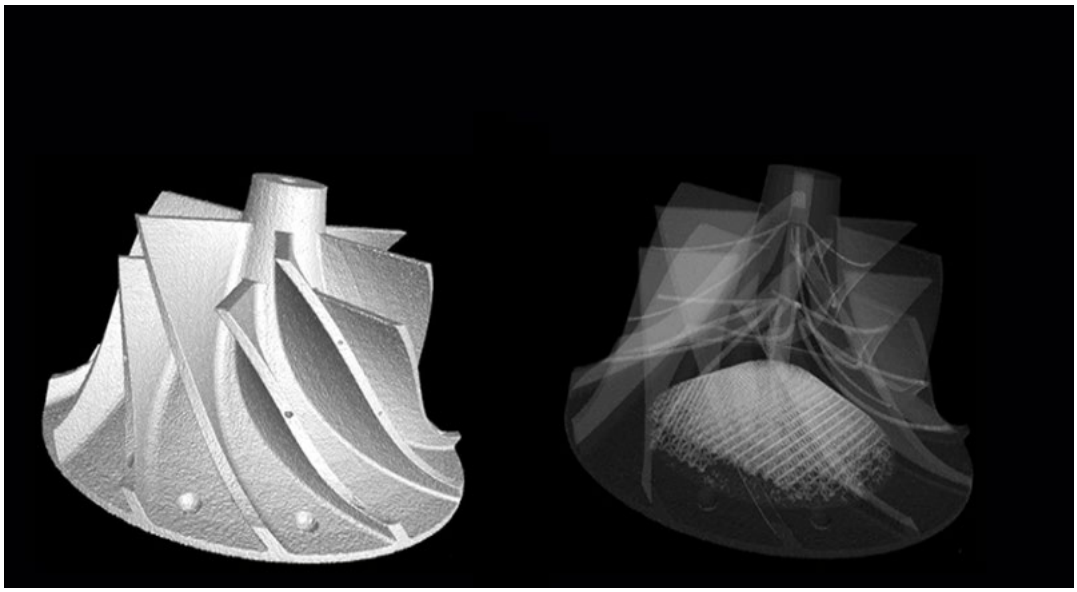

Figure2.12: The micro–X-ray CT for AM components Bamberg et al (2016)

This shows that the remaining technical gap from all the researchers is to estimate the life span of the additively manufactured components to influence NDT international standards for inspection and acceptance criteria of flaws or defects. This approach is meant to improve the understanding of the potential of NDT using X-ray tomography in advancing additive manufacturing processes as shown in figure 2.16. X-ray tomography is therefore suggested to play a crucial role in the evaluation, adoption and qualification of high-quality metal additive manufacturing.

2.4 The use of NDT in AM products

Gathering data on the mechanical characteristics of printed materials can lessen qualification expenses and assist in the creation of standards for this approach. Recently, standards have been developed for defining feedstock material, acceptable defects, and potential NDT inspection techniques; however, research on damage tolerance continues for further advancements. According to the research, Al alloys are widely utilized in the production of structural parts for the aerospace sector because of their excellent specific mechanical characteristics and strong resistance to corrosion.

The research done by Lupez (2019), on Non-Destructive Testing (NDT) noted that Liquid Penetrant Testing (LPT) technology specifically the florescent technique which is the best method for inspection of surface breaking defects in aluminium (aluminium propeller in this case), is not suitable for testing porous or rough additively manufactured parts. The researcher, therefore, presumed that the AM materials have a rough surface when they are at complete state. LPT is highly sensitive to surface-opening defects such as surface cracks, surface porosity (clustered or linear) and intuitive results especially when the part has not undergone post-processing or polishing.

It is stated that AM components frequently exhibit intricate temperature distributions, making it challenging to precisely identify flaws using eddy current testing (ECT). Ongoing advancements are still being made in the related signal processing techniques by creating an appropriate probe shape to mitigate the effects of temperature and surface roughness on the detection outcomes by ECT.

As stated earlier, conventional ultrasonic testing introduces energy into the workpiece via a couplant. The use of this technology for detecting defects in AM is restricted because of factors like temperature fluctuations that influence the grain structure of the part. As a result, the laser ultrasonic technique (LUT) was created and showed significant promise in detecting defects in real-time. The LUT technique employs a pulsed laser (pulse duration 7 ns) to produce ultrasonic waves in a part where a laser interferometer is used to observe the surface wave of the additively manufactured item. The spread of ultrasonic waves in additively manufactured components was influenced by defects, enabling the characterization of those defects. This Ultrasonic Testing method was employed to identify flaws like cracks and pores. These research efforts, nevertheless, remain in the primary validation phase.

Phased array ultrasonic testing PAUT method, is articulated by Lopez, A. B. *et al.* (2019) as a method that uses high frequency however the difference for UT is on the transducer configuration. The PAUT transducer has elements up to 64 which can be used at different sweep of angles for defect detection. In essence, the PAUT probe array contains multiple piezoelectric transducers that simultaneously emit (transmitters) and capture (receivers) the backscattered ultrasonic waves. In PAUT utilizing full matrix capture (FMC) and total focusing method (TFM), the initial step involves a data acquisition process known as FMC, where all transducers of the probe emit independently and sequentially while simultaneously recording with each transducer, producing a graph that illustrates the amplitude of the reflected ultrasonic wave over time. This screen is referred to as an A-scan display. Obaton (2020) created a metal part through AM that features a star artifact. The implementation of FMC and TFM has allowed for the detection of many internal characteristics within the star artifacts, but it does not include those smaller than 200 μm.

This limit is reported to be associated with the transducer frequency utilized, which was 10 MHz in their case. Utilizing higher frequency benefits allows for the detection of smaller imperfections. The main disadvantage of using this method primarily depends on the NDT operator's experience, as it involves significant interpretation. The understanding of the images would have been significantly more difficult if the position of the features (simulated AM defects) had not been identified.

An article written by Zenzinger, G. et al. (2014) states that the high resolution of computed tomography makes it possible to describe the quality of an AM metal products, this capability has made them to conclude that the use of X-ray CT in aviation and aerospace for production is feasible. This paper considers a selection of an NDT method as well that portrays high resolution (ability to detect defects that are close to each other) during inspection.

Their article also noted that the surface texture of components made through AM makes many surface inspections unfeasible, as superficial imperfections may be wrongly recognized as fractures. The NDT inspection methods presently accessible for validating components indicate that the most beneficial for AM producers are radiographic internal examinations. Radiography, particularly Digital Radiography (DR) and CT, currently offers the most dependable evaluations.

Both are utilized to identify major flaws and verify internal shapes. Nonetheless, CT is more effective for geometry verification, while digital radiography (slice size) excels in identifying major defects. Both methods lack the sensitivity to determine whether defects exist (or do not exist) at the individual layer level, and there is a potential for defects in each thin layer of an AM component. Although both DR and CT can detect larger flaws, the existing resolution of single-layer inspections poses significant challenges, leading many manufacturers to validate a build using a destructively tested sample.

2.5 Modelling Methods

The are several numerical problem-solving methods that can be used in engineering to resolve structural mechanical challenges such as methods to estimate mechanical properties (stresses, stiffness, ductility, malleability, hardness etc.), but at times most methods often fail because of the structural specification and properties such as geometric shape, load, the quantities and mixtures of alloying elements used with various metals which affects strength, ductility, temperature resistance, corrosion resistance, and other properties of AM aluminium alloy propellers.

This is where computational modelling is useful for this research since it can allow an estimation of the approximate number of stresses and strain that an AM component can sustain without failure. Petro et al. (2005) had articulated that there are three classical choices for the numerical solution of partial difference equations (PDEs) which are useful to estimate components properties, namely:

(a) The finite volume method (FVM),
(b) The finite element method (FEM) and
(c) Finite difference method (FDM).

It is therefore assumed that an AM aluminium propeller can also adopt these methods for the estimation of its mechanical performance. These PDEs methods, each carries both advantages and disadvantages which will be discussed shortly below, depending on the area of interest (ROI) one is expected to model. Each method is quite similar in that it represents a systematic numerical method for solving PDEs.

There are three important steps to consider in the computational modelling of any physical process applied in mechanical engineering, these steps are namely, (i) problem definition, (ii) mathematical model, and (iii) computer simulation

2.5.1 Finite volume method (FVM)

The finite volume method is a discretization method which is well suited for the numerical simulation of various types (elliptic, parabolic, or hyperbolic, or instance) of conservation laws; it has been used in several engineering fields, such as fluid mechanics, heat and mass transfer or petroleum engineering.

FVM may be used on arbitrary geometries, using structured or unstructured meshes, and it leads to robust schemes. One of the features FVM possesses is the local conservative of the numerical fluxes, that is the numerical flux is conserved from one discretization cell to its neighbour. When modelling problems for which

the flux is of importance this feature is useful. The finite volume method uses balance approach, that is, a local balance is written on each discretization cell which is regularly called a control volume. The use of the divergence formula and an integral formulation of the fluxes over the boundary of the control volume is then obtained.

The fluxes on the boundary are discretized with respect to the discrete unknowns. The discretization of general conservation laws by finite volume schemes. As suggested by its name, a conservation law expresses the conservation of a quantity. This method is more advantageous when modelling heat transfer and in chemical engineering.

2.5.2 Finite element methods

The finite-element method is a computational technique that divides a CAD model into tiny but finite elements of geometrically simple forms of the entire intricately shaped aluminium component. The assembly of all basic shapes constitutes the finite-element mesh.

The creation of the mesh in 2D with FEM necessitates that the domain be initially divided in its x and y directions to form the nodes. Once the nodes are established, the elements will be formed as either triangular, quadrilateral, or tetrahedral. A tetrahedral mesh offers the benefit of producing excellent outcomes for both static and dynamic mechanical characteristics. It is advisable to employ higher-order elements, such as quadratic interpolating. In many cases a 3D 10-node tetrahedral elements, in intricate structures like this propeller in the study is preferred, rather than using 4-node elements that can only perform linear interpolation.

A tetrahedral mesh represents a 3D perspective of a 2D triangular mesh. The precision is significantly greater than that of a basic cubic grid used in 3D, or a quadrilateral utilized in 2D. The component created by PBF and DED presents difficulties related to the layer- or track-specific structure during production with a tetrahedral mesh; meanwhile, Mehemert P (2023) noted that uneven surfaces arising from partial element activation may be accepted, albeit with potential inaccuracies at these temporary interfaces. Tetrahedral elements are considered to be particularly well-suited for this study, especially due to the intricate geometries they exhibit

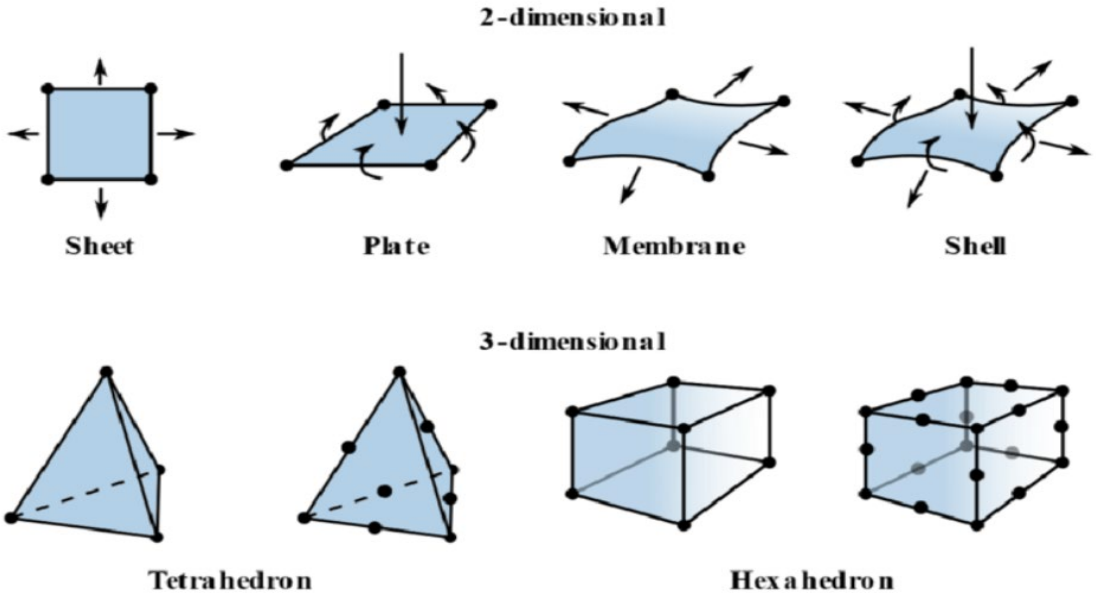

Figure 2.5: Different types of 2D and 3D elements (Dugan U (2018)),

The choice of mathematical formulation of linear or non-linear (quadratic) interpolation (shape) function depends on the user and the phenomenon to be analysed. Since quadrilateral elements cannot offer accurate analysis of results this research shall consider exploring the tetrahedral elements. The figure below shows an example of a mapped hexahedral mesh on blades:

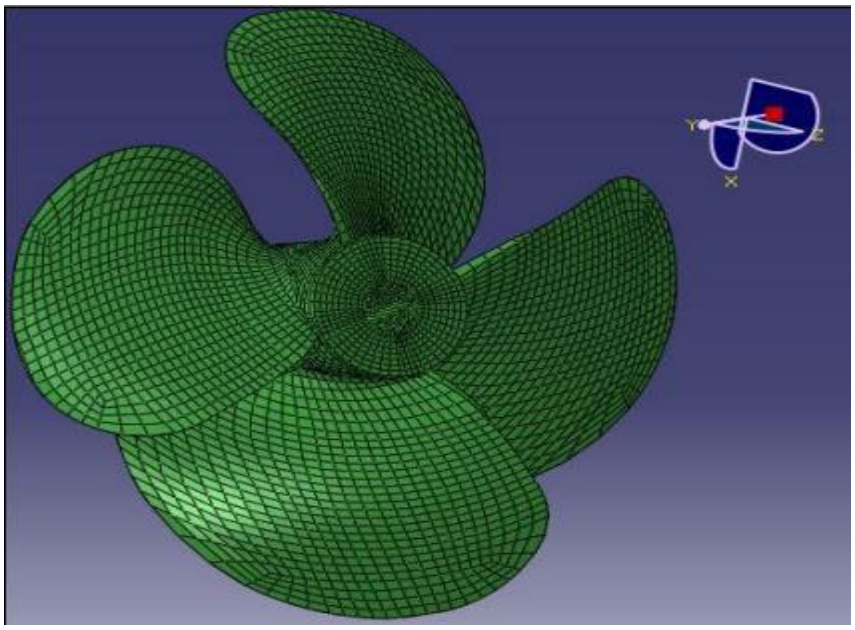

Figure 2.6: *Finite element mesh model of propeller Rao, R., Mohan, S. and Kumar, G. (2016)*

FEM is also used to estimate the mode of vibration, optimising the designs of components, estimate maximum stress; it can also be used to analyse a wide range of solid mechanic problems (example static analysis, dynamic analysis, buckling analysis and modal analysis) and estimate the life condition of components, which are applicable to the analysis of the AM aluminium propeller.

Research by Suryanarayana Ch. et al. (2015) also articulated other benefits of applying FEM to the propeller component to be reasonably accurate by properly selecting the element time and size in both static and dynamic loads, the stress contours are obtainable over the entire propeller section, lesser processing time, easy to determine unsteady loading conditions and behaviour of the blade.

The partial differential equations (PDEs) represent the set of field equations that characterize the behavior and establish equations for each element of the system. This is achieved by estimating the fields within each element using a basic function, like a linear or quadratic polynomial, which has a limited number of degrees of freedom (DOFs). Consequently, this idea will be implemented for the structural analysis by simulating various characteristics of the aluminium propeller to provide an estimated local representation of the physics through establishing a straightforward linear or nonlinear equation in this study.

Bessling, B., et al. (2022) noted that when the inputs from all components are combined, a significant sparse matrix equation system emerges, which can be resolved using various established sparse matrix solvers. The kind of solver selected relies on the original physics, as each type of physics leaves its distinct mark on the matrix's structure. Modelling defect propagation necessitates identifying the direction of the defect in which it will advance next

The Galerkin method is said by Thomas R. (2017) in his thesis to be the base of the finite element method (FEM). This thesis then briefly outlines the formulation and the resulting static equations of the FEM which is used by the ABAQUS modelling software (to be used in chapter 3 in this research).

Galerkin method propose a solution method for problems of linear self-adjoint differential equations. Thomas R. (2017) articulated that the Galerkin method provides the greatest estimates of the actual solution as compared to methods such as Ritz Methods, the minimum complementary energy principle, and the minimum potential energy principle.

2.5.2.1 Galerkin method as a base of FEM

The Galerkin method considers that, if the required solution u to the differential equation $\frac{dL}{du} = 0$ and is represented in terms of a series $u_n = \sum_{i=1}^{n} a_i \chi_i$ with suitable properties, leading to the orthogonality situations, meaning that, as $n \to \infty$, then;

$$\int_{\Theta}^{0} L(\sum_{i=1}^{n} a_i \chi_i)\chi_i d\Theta = 0 \qquad (2.4)$$

and are equivalent to $L(u) = 0$. In the event that u_n series has n terms, the eq. (2.4) gives a set of n

simultaneous equations to determine the coefficients a_i.

When the space S_0 which is a space function that is continuous up to the first derivative on the interval $\langle 0, l\rangle$ and vanishing at the points where an important boundary condition is given as:

$$S_0 = \{s \in C^1\langle 0, l\rangle : s(0) = 0\}$$

on a condition that the test function is $s \in S_0$, the multiplication of $f = (-AEu')'$ in the test function v and integrated by parts using $\langle 0, l\rangle$ as limits. The given boundary force called a natural or Neumann boundary condition is expressed as

$$A(l)E(l)u'(l) = F_l \tag{2.5}$$

where sectional area A, Young's modulus E, of length l and force F_l of a natural boundary acting on the right end $x = l$. If equation 2.5 is affected into the equation given as force $f = (-AEu')'$ so that eq. 2.6 is obtained

$$\int_0^l fv\, dx = \int_0^l [(-AEu')']\, vdx$$

$$\int_0^l fv\, dx = -fu(l) + \int_0^l (AEu'v')dx \tag{2.6}$$

The space trial $W = \{w \in c^2\langle 0, l : w(0) = d_0\rangle\}$ can provide the solution for u by satisfying the Dirichlet boundary condition, leading to the weak form as:

$$u \in W \text{ so that } a(u, v) = (f, v) + fv(l) for\ all\ v \in V_0 \tag{2.7}$$

Therefore, this hypothesises informs that the governing differential equations should be multiplied with the trial functions to obtain the set of simultaneous equations for the formation finite element method equations.

2.5.2.2 The set of Finite Element Method (FEM) computations

The crack propagation prediction computation is practically offering solutions to complex structures such as propellers with complex geometries that requires numerical analysis. In some applications, accurate computation of stresses in the vicinity of crack tips in complex component configurations is important for the analysis.

The variation of the test function v is $v_n(x)$ is:

$$dv_n(x) = \sum_{i=1}^{n} \frac{\partial v_n(x)}{\partial a_i} da_i \quad (2.8)$$

on a condition that the test function is in a series of the form of $v_n(x)$, where a_i is initial crack coefficient .This is conditioned when the test function v is assumed to be a series of the form $v_n(x) = \sum_i^n a_i \varphi_i(x)$. When substituting the variation into Eq. (2.4) becomes,

$$\int_0^l f \sum_{i=1}^{n} a_i \varphi_i(x)\ dx = -F_l \sum_{i=1}^{n} a_i \varphi_i(l) + \int_0^l (AEu' \sum_{i=1}^{n} \varphi_i(x) dx d\, a_i) \quad (2.9)$$

Equation 2.9 shows a basis of the finite element method, in which both the functions (u) and(v) are constructed using the finite element shape functions and φ_i is the geometric function. The test function v satisfying the important boundary conditions. Equation 2.9 thus leads to a set of finite element equations.

The use of Galerkin weak form for a plane strain or stress problem gives a solution of two functions that are called the displacement functions $v_1(x,z)$ and $v_2(x,z)$ in the directions of the two coordinate axes. This research uses the tensor notation to introduce new matrices based on the governing equations for plane stress and strain for the unknown problems and the body forces which are collected in vectors: the following are the governing equations:

Equilibrium, $\boldsymbol{D^T\sigma} + \boldsymbol{f} = 0$ (2.10)

Constitutive, $\boldsymbol{\sigma} = \boldsymbol{E\varepsilon}$ (2.11)

Kinematics, $\boldsymbol{\varepsilon} = \boldsymbol{DU}$ (2.12)

Where **D** is the gradient operator matrix, $\boldsymbol{\sigma}$ is the stress tensor $\boldsymbol{\varepsilon}$ is the strain tensor and $\boldsymbol{f}$ are the body forces satisfying the natural boundary conditions. They are defined as:

$$Body\ forces = \boldsymbol{f}[f_1, f_2]^T$$

$$Stress: \boldsymbol{\sigma} = [\sigma_{xx} \quad \sigma_{xx} \quad \sigma_{xz}]^T \quad (2.13)$$

$$Strain\ \boldsymbol{\varepsilon} = [\varepsilon_{xx} \quad \varepsilon_{xx} \quad \varepsilon_{xz}]^T = \left[\frac{\partial v_1}{\partial x}, \frac{\partial v_2}{\partial z}, \frac{\partial v_1}{\partial x} + \frac{\partial v_2}{\partial z}\right]^T \quad (2.14)$$

$$Displacement = \boldsymbol{U}[U_x, U_z]^T$$

The gradient operator matrix **D** is expressed as:

$$\boldsymbol{D} = \begin{bmatrix} \partial/\partial x & 0 \\ 0 & \partial/\partial y \\ \partial/\partial y & \partial/\partial z \end{bmatrix} \quad (2.15)$$

$$\boldsymbol{E} = \frac{E}{1-v^2}\begin{bmatrix} 1 & v & 0 \\ v & 1 & 0 \\ 0 & 0 & \frac{(1-v)}{2} \end{bmatrix} \tag{2.16}$$

And the plane strain

$$\boldsymbol{\varepsilon} = \frac{E}{(1-v)(1-2v)}\begin{bmatrix} 1-v & v & 0 \\ v & 1-v & 0 \\ 0 & 0 & \frac{(1-2v)}{2} \end{bmatrix} \tag{2.17}$$

We note that the lames constant is $\mu = \frac{E}{2(1+v)}$, plane stress $\lambda = \frac{vE}{1-v^2}$, plane strain $\lambda = \frac{vE}{(1-v)(1-2v)}$, leading to the stress-strain matrix to be:

$$E = \begin{bmatrix} \lambda + 2\mu & \lambda & 0 \\ \lambda & \lambda + 2\mu & 0 \\ 0 & 0 & \mu \end{bmatrix} \tag{2.18}$$

The Dirichlet Boundary conditions on displacements are,

$$U_1 = d_1, U_2 = d_2 \text{ on } \boldsymbol{\Gamma_u} \tag{2.19}$$

And on the Neuman boundary $\boldsymbol{\Gamma_t}$, for the static boundary conditions are:

$$\begin{aligned} \sigma_{xx}n_x + \sigma_{xz}n_z &= T_1 \\ \sigma_{zz}n_z + \sigma_{xz}n_z &= T_2 \end{aligned} \tag{2.20}$$

where $\boldsymbol{n}$ in Eq. (2.20) is the unit vector for the outward normal to the total boundary $\boldsymbol{\Gamma}$. The total boundary condition is to be given as:

$$\boldsymbol{\Gamma} = \boldsymbol{\Gamma_u} \cup \boldsymbol{\Gamma_t} \text{ and } \boldsymbol{\Gamma_u} \cap \boldsymbol{\Gamma_t} = \emptyset$$

where$\boldsymbol{\Gamma_u}$ and $\boldsymbol{\Gamma_t}$ are respectively Dirichlet and Neuman boundaries.

The function $v(x,z) = (v_1(x,z), v_2(x,z))^T$ couple of a space $X = \{(v|v_1(x,z) \in H^1(\Omega), (V|v_2(x,z) \in H^1(\Omega)\}$ where Ω is the domain of the two-dimensional body and H^1 is a space of the square – integrable functions which are derived up to the first derivative.

The static equilibrium equations (2.10) is the expressed as

$$\partial\sigma_{xx}/_{\partial x} + \partial\sigma_{xz}/_{\partial z} + f_1 = 0; \partial\sigma_{zz}/_{\partial z} + \partial\sigma_{xz}/_{\partial x} + f_2 = 0 \tag{2.21}$$

$$N^e = \begin{bmatrix} N_1^e & 0 & N_1^e & 0 & \cdots N_1^e & 0 \\ 0 & N_1^e & 0 & N_1^e & \cdots 0 & N_1^e \end{bmatrix} \tag{2.22}$$

Then eq. (2.21) is multiplied by v_1 and v_2 respectively and integrated over Ω. This is analogous to the procedure used in Galerkin method and when applying the Greens theorem, kinematic equation, Neuman boundary condition and Hooke's law. The following is obtained:

$$\int_{\Omega}^{0} \left[\left({}^{\partial \sigma_{xx}}/_{\partial x} + {}^{\partial \sigma_{xz}}/_{\partial z} + f_1 \right) v_1 + \left({}^{\partial \sigma_{zz}}/_{\partial z} + {}^{\partial \sigma_{xz}}/_{\partial x} + f_2 \right) v_2 \right] dxdz =$$

$$\int_{\Gamma}^{0} [(\sigma_{xx} n_x + \sigma_{xz} n_z) v_1 + (\sigma_{zz} n_z + \sigma_{xz} n_z) v_2] ds$$

$$- \int_{\Omega}^{0} \left(\sigma_{xx} \frac{\partial v_1}{\partial x} + \sigma_{xz} \frac{\partial v_1}{\partial x} + \sigma_{xz} \frac{\partial v_2}{\partial z} + \sigma_{zz} \frac{\partial v_2}{\partial z} \right) dxdz + \int_{\Omega}^{0} (f_1 v_1 + f_2 v_2) dxdz \tag{2.23}$$

Leading to,

$$\int_{\Gamma}^{0} \left[\left[\left({}^{\partial \sigma_{xx}}/_{\partial x} + {}^{\partial \sigma_{xz}}/_{\partial z} + f_1 \right) v_1 + \left({}^{\partial \sigma_{zz}}/_{\partial z} + {}^{\partial \sigma_{xz}}/_{\partial x} + f_2 \right) v_2 \right] dxdz \right.$$

$$\left. = \int_{\Gamma}^{0} (T_1 v_1 + T_2 v_2) dS - \int_{\Omega}^{0} \boldsymbol{\varepsilon}(\boldsymbol{v}) \cdot \boldsymbol{\sigma} dxdz + \int_{\Omega}^{0} \boldsymbol{v} \cdot \boldsymbol{f} dxdz \right]$$

$$\int_{\Omega}^{0} \left[\left({}^{\partial \sigma_{xx}}/_{\partial x} + {}^{\partial \sigma_{xz}}/_{\partial z} + f_1 \right) v_1 + \left({}^{\partial \sigma_{zz}}/_{\partial z} + {}^{\partial \sigma_{xz}}/_{\partial x} + f_2 \right) v_2 \right] dxdz$$

$$= \int_{\Gamma}^{0} (T_1 v_1 + T_2 v_2) dS - \int_{\Omega}^{0} \boldsymbol{\varepsilon}(\boldsymbol{v}) \cdot \boldsymbol{\sigma} dxdz + \int_{\Omega}^{0} \boldsymbol{\varepsilon}(\boldsymbol{v}) \cdot \boldsymbol{\sigma} dxdz + \int_{\Omega}^{0} \boldsymbol{v} \cdot \boldsymbol{f} dxdz \tag{2.24}$$

Giving a simplified form as,

$$\int_{\Gamma}^{0} (T_1 v_1 + T_2 v_2) - \int_{\Omega}^{o} \boldsymbol{\varepsilon}(\boldsymbol{v}) \cdot \boldsymbol{\sigma} dxdz + \int_{\Omega}^{0} \boldsymbol{v} \cdot \boldsymbol{f} dxdz = \int_{\Gamma}^{0} \boldsymbol{T} \cdot \boldsymbol{v}\, dS - \int_{\Omega}^{0} \boldsymbol{\varepsilon}(\boldsymbol{v}) \cdot \boldsymbol{\sigma} dxdz + \int_{\Omega}^{0} \boldsymbol{v} \cdot \boldsymbol{f} dxdz \tag{2.25}$$

This means that we may express the weak form of plane stress/strain as:

$$L(v) = \int_{\Gamma}^{0} \boldsymbol{T} \cdot \boldsymbol{v}\, dS + \int_{\Omega}^{0} \boldsymbol{v} \cdot \boldsymbol{f} dx dz \quad (2.26)$$

And the weak form for discrete plane stress/strain is:

$$L_h(v) = \sum_{\Gamma_e \in \Gamma_t} \int_{\Gamma_e}^{0} \boldsymbol{v} \cdot \boldsymbol{T} d\Gamma_e + \sum_{e \epsilon \Omega} \int_{\Omega}^{0} \boldsymbol{v} \cdot \boldsymbol{f} d\Omega_e \quad (2.27)$$

Gauss quadrature was used to evaluate the boundary element edge Γ_e of the integral over an element Ω_e. Now the finite element can be formulated in a weak form by defining the base function on an element with *n* node which are arranged in a matrix as:

The element nodal Θ^evalues of a test function are expressed in a vector form as;

$$\Theta^e = [\Theta_{11}^e \quad \Theta_{12}^e \quad \Theta_{21}^e \, \Theta_{22}^e \quad \cdots \quad \Theta_{n1}^e \quad \Theta_{n2}^e] \quad (2.28)$$

And the element nodal displacement U^e also as vector

$$\mathrm{U}^e = [\mathrm{U}_{11}^e \quad \mathrm{U}_{12}^e \quad U_{21}^e \, \mathrm{U}_{22}^e \quad \cdots \quad \mathrm{U}_{n1}^e \quad \mathrm{U}_{n2}^e] \quad (2.29)$$

$$a_h(U_h, v) = \sum_{e \epsilon \Omega} \int_{\Omega}^{0} \boldsymbol{\epsilon}(\boldsymbol{v}) \cdot \boldsymbol{E} \boldsymbol{\epsilon}(U_h)\, d\Omega_e \quad (2.30)$$

The value of the components U_1 and U_2 of the discretised solution U_h can be denoted as U_{j1} and U_{j2} respectively at node P_j and the components v_1 and $v_2$of the test function *v* are denoted as Θ_{i1} and Θ_{i2} at node P_i, leading to a test function as a function of *(x; z)* being expressed as:

$$v(x,z) = \sum_{i=1}^{IN} [\Theta_{i1} \quad (x,z) + \Theta_{i1} \quad N_i(x,z)] \quad (2.31)$$

the strain-displacement matrix B of size (3 *x 2n*) where *n* is the number of element nodes is given as:

$$\boldsymbol{B^e} = \boldsymbol{DN^e} = \begin{bmatrix} \partial N_1^e/\partial x & 0 & \partial N_2^e/\partial x & 0 & \cdots & \partial N_n^e/\partial x & 0 \\ 0 & \partial N_1^e/\partial z & 0 & \partial N_2^e/\partial z & \cdots & 0 & \partial N_n^e/\partial z \\ \partial N_1^e/\partial z & \partial N_1^e/\partial x & \partial N_2^e/\partial z & \partial N_2^e/\partial x & \cdots & \partial N_n^e/\partial z & \partial N_n^e/\partial x \end{bmatrix} \quad (2.32)$$

Assuming that the matrix of the stiffness **E** is constant over the elements and by giving an allowance to

express the kinematic relation from Eq 2.12 in discrete form then we get:

$$\boldsymbol{\varepsilon} = \boldsymbol{BU}$$

This then allows this research to express Eq 2.26 as:

$$\int_{\Omega_e}^{0} \varepsilon^e(v) \cdot E^e \varepsilon^e(U_h) d\Omega_e = [\Theta^e]^T \int_{\Omega_e}^{0} [\boldsymbol{B}^e]^T E^e \boldsymbol{B}^e d\Omega_e U^e$$

$$[\Theta^e]^T \int_{\Omega_e}^{0} [\boldsymbol{B}^e]^T E^e \boldsymbol{B}^e d\Omega_e U^e = [\Theta^e]^T \boldsymbol{K^e U^e} \tag{2.33}$$

And the Newman boundary condition as

$$\int_{\Omega_e}^{0} \boldsymbol{v} \cdot \boldsymbol{f}\, d\Omega_e = [\Theta^e]^T \int_{\Omega_e}^{0} [\boldsymbol{N}^e]^T f d\Omega_e$$

$$[\Theta^e]^T \int_{\Omega_e}^{0} [\boldsymbol{N}^e]^T f d\Omega_e = [\Theta^e]^T \boldsymbol{F^e} \tag{2.34}$$

And,

$$\int_{\Gamma_e}^{0} \boldsymbol{v} \cdot \boldsymbol{T}\, d\Gamma_e = [\Theta^s]^T \int_{\Gamma_e}^{0} [\boldsymbol{N^e}]^{\boldsymbol{T}} \boldsymbol{T} d\Gamma_e$$

$$[\Theta^s]^T \int_{\Gamma_e}^{0} [\boldsymbol{N^e}]^{\boldsymbol{T}} \boldsymbol{T} d\Gamma_e = [\Theta^s]^T \boldsymbol{F^s} \tag{2.35}$$

The summation on eq (2.28),(2.29) and (2.30) results to

$$[\Theta^e]^T \boldsymbol{K^e U^e} - [\Theta^e]^T \boldsymbol{F^e} = [\Theta^s]^T \boldsymbol{F^s} \tag{2.36}$$

and the ratio of the nodal element and the nodal displacement $\frac{[\Theta^e]^T}{[\Theta^s]^T} = 1$, leading to the recognisable finite element equation at element:

$$\boldsymbol{K^e U^e} = \boldsymbol{F^e} + \boldsymbol{F^s} \tag{2.37}$$

Where $\boldsymbol{K^e}$ is called the element stiffness matrix and the $\boldsymbol{F^e} + \boldsymbol{F^s}$ is the load vector. The computation of industrial modelling problems is challenging when using a computer simulation of fracture processes. Fleming et al. (2020) introduced the modelling for cracks in components, here a mapping algorithm is needed to align the discontinuity with the crack geometry. This analysis starts by slitting the body into the number of small meshes.

(i) Discretisation

It is useful since the equilibrium method requires a satisfaction over a finite number of elements. Several element shapes can be selected such as first order elements which are: (a) surface elements (example triangular, I and quadrilateral elements) (b) solid elements such as prisms which are useful for 3-dimension (3-D) elements; and (c) line elements. The second order elements such as tetrahedral are useful in determining stress and strain which are useful for this research.

Historically, FEA method was first applied to structural analysis and also in a large class of multi-physics problems. Therefore, this method can be tried on for the plane analysis of an aluminium propeller.

The accuracy of FEA is articulated to be said that it depends on mesh generation and the application of the right boundary conditions. The finite element method has the benefit of coupling results found using NDT and ultimately resulting into fracture mechanics computations. This coupling analysis extracts data from NDT and accurately changes it to resemble the characteristics of the test components and inputs it into the finite element model.

Therefore, This makes the FEA method to be exceptional in the prediction of the performance of components when in service so that an increased margin of safety can be developed to quantitatively measure the components' acceptance criteria, hence this research extends to assess the prediction of performance in AM components under various loadings.

Symmetric boundary conditions are limitations that are used for stabilizing the finite element model and drastically simplify the model. The finite element method for this research will use two-dimensional solid elements to analyse the plane stress and strain as Mabuza (2018) has used in their research.

2.5.3 Finite difference methods

The finite-difference method is defined as a method that uses dimensions per dimension to develop an easy increase of the element order so that a higher-order accuracy is obtained. The finite difference method performs optimally for simulations in Hexahedral geometries using a uniform grid, as efficient implementations are simpler compared to finite-element and finite-volume methods. Standard grids are beneficial for extensive simulations on supercomputers.

The finite difference methods are defined by Peiro et Al. (2005) as a numerical technique that is used when solving differential equations in numerical techniques to find the approximate solutions, and it is acclaimed

to be the oldest and simpler to execute than several the numerical techniques for finding exact solutions or formulas for solutions.

This method when there is a derivative in the differential equation, it is substituted with an algebraic approximation equation to the derivative. This means that the finite difference equations will have no derivatives. It is also used to obtain numerical approximations of PDEs written in the strong form, which is derived from Gauss's theorem given as:

$$\int_V^0 \nabla \cdot f(dxdydz) = \int_{dydz}^0 f \cdot \boldsymbol{n} d(dydz) \quad (2.38)$$

and for which in the case of the integral expression needs to be zero for any volume V, therefore the integrand must be equal to zero, which is expressed in a strong form as,

$$\frac{\partial N\,(\boldsymbol{x},t)}{\partial t} + \nabla \cdot f(N) - U = 0 \quad (2.39)$$

The approach is said to take the algebraic equations that are approximations, to be changed from differential equations and to solve the algebraic equations to get an approximate solution to the original differential equation. It is also important to know the kind of algebraic approximation. The derivative of $N(x)$ with respect to x can be evident to be the most common approximation in finite difference method which is the quotient technique given as:

$$N_{(x|i)} = \lim_{x \to 0} \frac{N(x_i + \Delta x) - N(x_i)}{\Delta x} = N'(x) \quad (2.40)$$

For relatively small Δx, the limit inequality can be replaced with an approximation so for some small Δx, $N'(x)$ the derivative of $N(x)$will be approximately equal to this difference quotient. Therefore equation 2.1 can be mathematically expressed as:

$$\frac{N(x_i + \Delta x) - N(x_i)}{\Delta x} \approx N'(x) \quad (2.41)$$

Equation (2.2) is referred to as a forward finite difference method. The finite difference method is disadvantageous for this research since it is more difficult to use for handling material with discontinuities, and moreover, it does not provide itself for local grid refinement or anything like an adaptive mesh refinement. This may be needed to resolve local rapid variations in solutions such as around a corner of a complex shape aluminium propeller components.

This method works precisely in weather calculations, astrophysics, seismology, physical realism in computer graphics, and special effects. Compared to FDM and FVM, therefore FEM is reviewed to be the best suitable

for the application of this research as it can assess complex hydro and aerodynamic geometries including complex geometries such as an aluminium propeller.

2.6 Fracture mechanics in Additive manufacturing

The modelling concept was historically introduced in 1970's by Elber, and became a significant concept of modelling a plasticity induced cracking in solid structures. This concept became a base line for the development of the recent modeling tools in mechanical structures where procedures such as the retardation in crack growth occurring after an overload in the stressing sequence was adopted.

There are two types of effects of variable amplitude or "complex" loading. The first effect is ignoring overloads which may be prone to an unnecessary overdesign of structures for fatigue and the second is a life load that is experienced to be less severe than has been predicted may lead to a material failing prematurely. Davy (2020) anticipated an attempt of arranging the amplitude variables for the fatigue loading that excites the defect propagation known as an acronym PREFFAS, that mean "Pr´evision de la fissuration en fatigue a´erospatiale". This method relies on a alteration of the variable amplitude time history of stresses that were applied into a constant amplitude, sinusoidally varying stresses, which is making use of Elber's crack closure concept.

The research selected the finite element methods where the use of a linear-elastic fracture-mechanics approach and relating a defect to a half-elliptical surface defect for ductile components. The stress intensity factor *K* is a measure of the severity of a defect (crack) situation as affected by the size, location, stress, and geometry. The stress intensity factor is a function of the defect (e.g. crack) size and applied load (Hosseini *et al.*, 2018). The mathematical definition for the stress intensity factor is defined in eq 1.1.

where Y is the defect (e.g. crack) geometry factor and σ represents applied load (stress). Once the defect reaches section of growth it is already propagating. This propagation rate is outlined using the Paris law equation as referenced by Hosseini (Hosseini *et al.*, 2018),

$$\frac{da}{dN} = C\Delta k^m \tag{2.42}$$

There are three different modes of fracture that AlSi10Mg may be subjected to fractures based on the angle concerning stress namely, mode I, mode II, and mode III see the image below. Mode I displacement is described as an opening or tensile mode and is entirely extensional. These fractures develop at an orientation perpendicular to normal stress. Mode II displacement is described as a forward shear mode, where the fracture surfaces slide over one another in a direction perpendicular to the fracture tip and lastly Mode III displacement is described as a transverse shear mode, where the fracture surfaces move relative to one

another in a direction parallel to with the fracture tip.

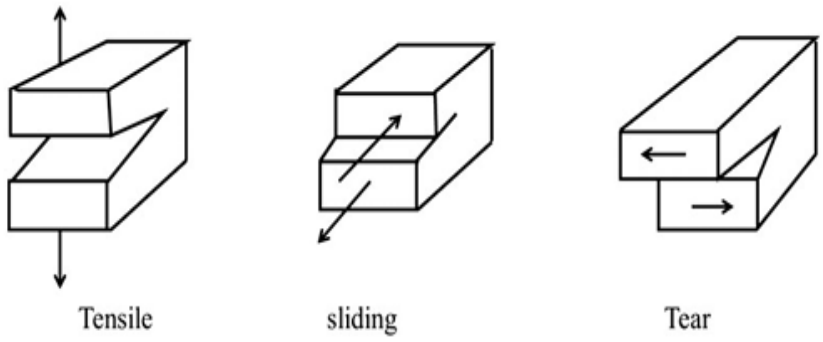

Figure 2.8: *modes of fracture (Siddique, A. et al. (2021))*

This thesis findings, therefore, depend on the above equations for the computation of number of cycles of the component as denoted in Eq (1.3). The integration of the reciprocal of the Paris law shall result in equation 2.43 which can be used to determine the number of circles that the component can run. The prediction for the life span is either in days, months, or years (Muñiz-Calvente and Fernández-Canteli, 2020)

$$N_f = \frac{a_i}{\Delta a_0}\left(\frac{\Delta k_o}{\sqrt{\pi a_i}}\right)^m \cdot \frac{2}{2-m}\left[\left(\frac{\pi a_i}{K_{IC}^2}\right)^{\frac{m-2}{2}} (Y\sigma_{max})^{-2} - (Y\sigma_{max})^{-m}\right] \quad (2.43)$$

The mechanical properties of aluminium are articulated by Suryawanshi (2018) who investigated the tensile strength and ultimate tensile strength of SLM $AlSi_{12}$ and found that mechanical properties (as tabulated below in table 2.1) were relatively good quality than the cast equivalents.

Table 2.1: Material properties of Aluminium powder.

Properties		Build orientation
Density	2.7 g/cm^3	Vertical
Yield strength	~270 MPa	Vertical
Ultimate tensile strength	~325 MPa	Vertical
% Elongation	~4.4	Vertical
Youngs Modulus	70 GPa	
Strain	0.33	
Yield stress (heat treated)	~530 MPa	
Poisson ratio	0.34	

This research will therefore adopt Suryawanshi values are expected to resemble a close approximation of samples and the trial composition of the printed full propeller component for experimental purposes. The

mechanical properties of this type of sample are often improved by heat treatment where it is recommended that the annealing, quenching and age hardening be used on the T6 cycle of solution. The laser-sintering process is characterized by extremely rapid melting and re-solidification. However, this research will not conduct the heat treatment processes at this stage, will focus on the as built material.

This produces a metallurgy and corresponding mechanical properties in the as-built condition which is like T6 heat-treated cast parts. For the purpose of this research, the cast components of the propeller and the destructive testing samples are proposed to be articulated as to that such hardening heat treatments will not be recommended for laser-sintered parts, but rather a stress relieving cycle of 2 hours at 300 °C due to the vertical layer wise building method that will be used and the parts that have certain anisotropy, which can be reduced or be removed by appropriate heat treatment. The below is the planned for use chemical composition of the AlSi10Mg AM propeller and samples that shall be developed for experimental purposes.

Table 2.2: Chemical composition of Al propeller and samples

Probe	**Charge** **Lot no. 0538/2/5**	**Chemical composition of cast**								
		Al%	**Si%**	**Mg %**	**Fe%**	**Cu%**	**Zn%**	**Ti%**	**Mn%**	**Ni%**
Normal value		Bal.	9-11	0.20-0.45	< 0.55	<0.55	<0.1	<0.15	<0.45	<0.05
Actual value		Bal.	10.7	0.43	0.11	<0.01	<0.002	<0.02	<0.005	<0.01

A paper by Kempen et al (2012) had articulated the observation that SLM AlSi10Mg components demonstrate similar mechanical properties or higher, comparable to the casted AlSi10Mg material.

The paper had discussed that the pores were more frequent when the parts are produced in the Z direction, compared to parts which were produced in the XY direction. The high stress level of 395MPa for both testing directions were noticed. A stress strain graph results were presented for the AlSi10Mg material.

The defects that are located close to the edge of the component were articulated to lack space for wide or deformation leading to a complete fracture of the sample. This literature also notices that the development of material in the Z direction will cause high stress levels to be reached sooner and
as a result, the elongation in tensile test is lower: 3,47% compared to 5,55% for XY developed samples.

It was argued that the mechanical property such as an ultimate tensile strength of the as built AlSi10Mg AM

parts was always higher than those of the high pressure die casts (HPDC). This mean that there is a possibility of the material to be brittle when the of the as-built AlSi10Mg sample in the Z-direction is comparable to the HPDC samples show less plasticity, while the elongation for parts built in XY – direction is almost 2% higher and the strength and hardness are higher.

Amin S. (2024) in their paper had investigated the structural integrity on an additively manufactured Aluminium by generating a computational methodology to analyse the properties of notch geometry, subsurface porosity, and their interaction on the metallic components. It was observed the stress concentration at the notch geometry, combined with other phenomena like hydrogen cracking, were leading to post-process cracking or serving as a preferred location for fatigue cracking throughout the materials lifespan. Their findings also noticed that the internal pores may have a significant impact on the structural integrity of the material. The progressed cracks on the surface interacted with the pores, leading toward the influence of the behaviour of crack growth and material lifespan.

The article by Chan Guo at el. (2023) found that the high level of residual stresses is generated from the high degree of temperature gradient that is induced by the rapid heating and cooling processes in AM components leading to severe metallurgical defects. In this regard, cracks demonstrated to be the greatest threat to these materials' integrity as they can rapidly propagate and thereby cause sudden and non-predictable failure. During the powder bed fusion (PBF) processes, the metal powders experience rapid heating and cooling where the molten metal is in a non-equilibrium solidification condition, such that distribution and segregation of the solute occur at the front of the solidification interface.

2.7 Conclusion

This chapter concludes by noting that the AlSi10Mg is a casting alloy with good casting properties for AM and is normally used for cast parts with thin walls and complex geometry. This material affords exceptional good strength, hardness and dynamic properties. Therefore, it be used for parts that are subjected to high loads such as AM propellers. The chapter also demonstrated that as much as the powder fusion bed is beneficial to produce complex shaped metal, it also has one of the drawbacks of noted that there a dynamic solidification equilibrium. This chapter further concludes the finite element method was the befitting method for the determination of stress and deformation distribution in complex shaped components.

Chapter 3

Numerical modelling.

3.1 Introduction.

This chapter introduced the simulation of a defective Additively Manufactured component, figure 3.1 below shows a propeller that was drawn by SolidWorks in order to simulate for mechanical properties response when it is subjected under load. In this propeller the researcher had analysed using ABAQUS in application of finite element method.

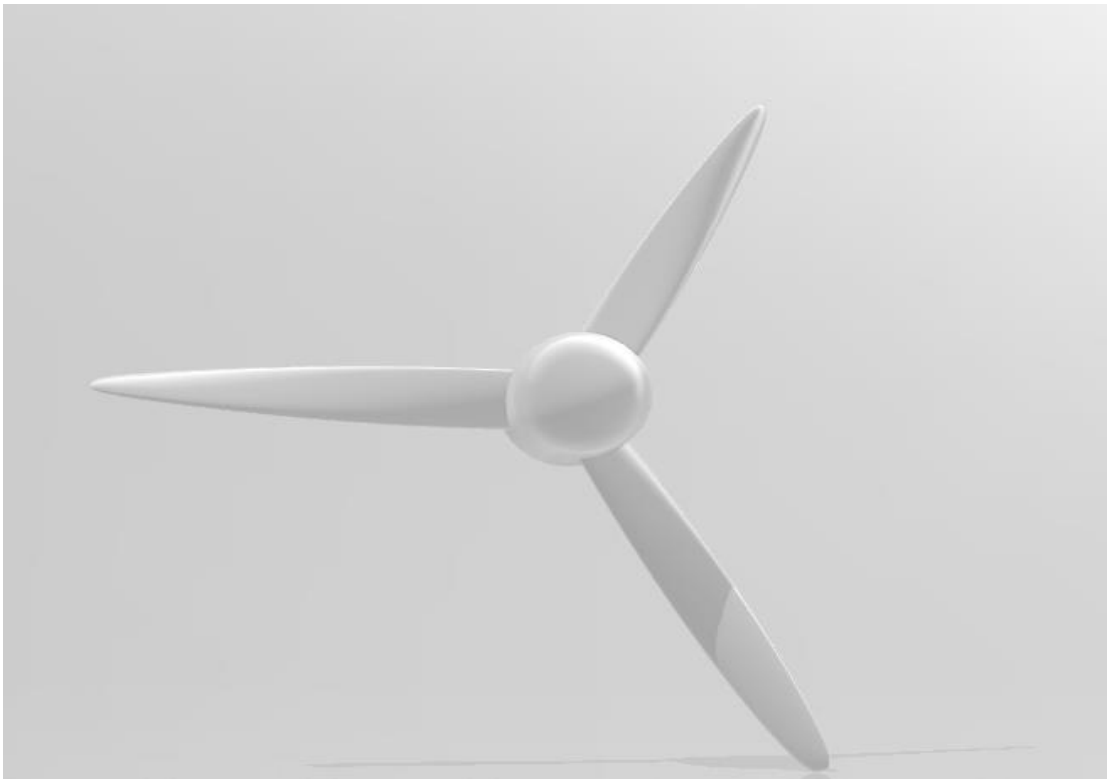

Figure 3.1: a three-blade propeller drawn by SOLIDWORKS.

The analysis had to give mechanical property results on strain distribution, stress distribution, stress concentration and stress intensity factor etc to ultimately assist in computing the for the life span.

Table 3.1: features of the AM propeller

Blade Diameter (mm)	Number of blades	Pitch rotation (0.7r)	Hub diameter (mm)
400mm	3	140mm	58mm

Table 3.2: Defects information

Defect	**Length**	**Location**
crack	10mm	Closer to the hub
Delamination	13 mm	Closer to the hub
Cluster Porosity	10 mm	Middle of the blade

The defects were positioned at various positions internally in the blades. The crack was simulated in the in solid works where it was drawn and was positioned at the root of one of the blades. The crack was positioned there as the area is that it high stress levels moreover the area that has different thickness variation is likely to create defects such as crack during solidification. The cluster porosity was developed in circular form and positioned in the centre of one of the blades due to gas entrapment and other contaminating features. The location of this defect was opted to be there due to thickness variation which affect solidification. Delamination is a defect that result from poor powder deposition and poor feed characteristics and parameter that may affect solidification.

The application of the ABAQUS system had followed the procedure as described in figure 3.2 where the problem definition is divided into three i.e. pre-processor, processor, and post processor. In the event where post processing was not satisfactory, repeating the problem definition was done until Analysis and design decision was satisfactory.

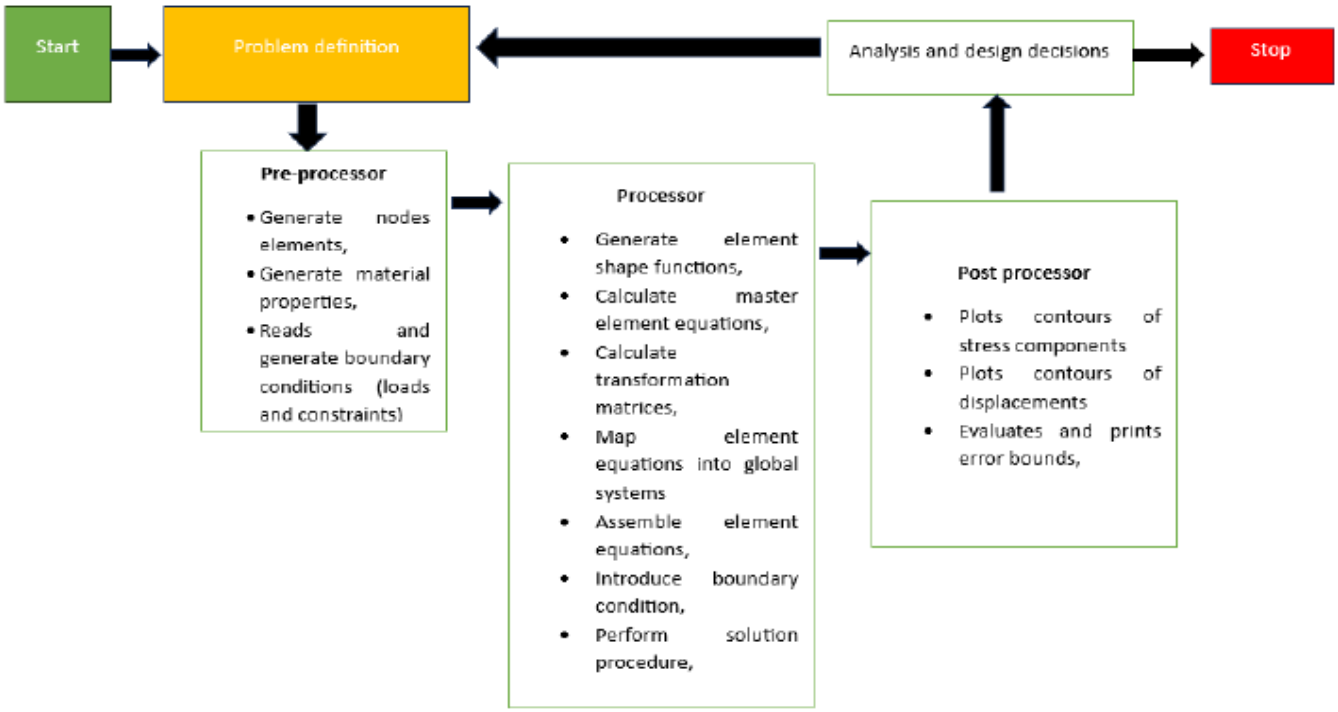

Figure 3.2: procedure for stress and displacement contour development

The content in chapter 3 is assuming that the load was static with fixed values (i.e., minimum, and maximum) on the propeller blades leading stress response may cause defects to propagate. The assumptions and conditions were made in this chapter as follows:

(a) The defect propagates in one direction and was a homogeneous body, isotropic,
(b) The propagation was in the plane plate under mixed mode conditions,

The figure 3.3 below show a flow chat that is describing the research methodology followed in chapters three and four:

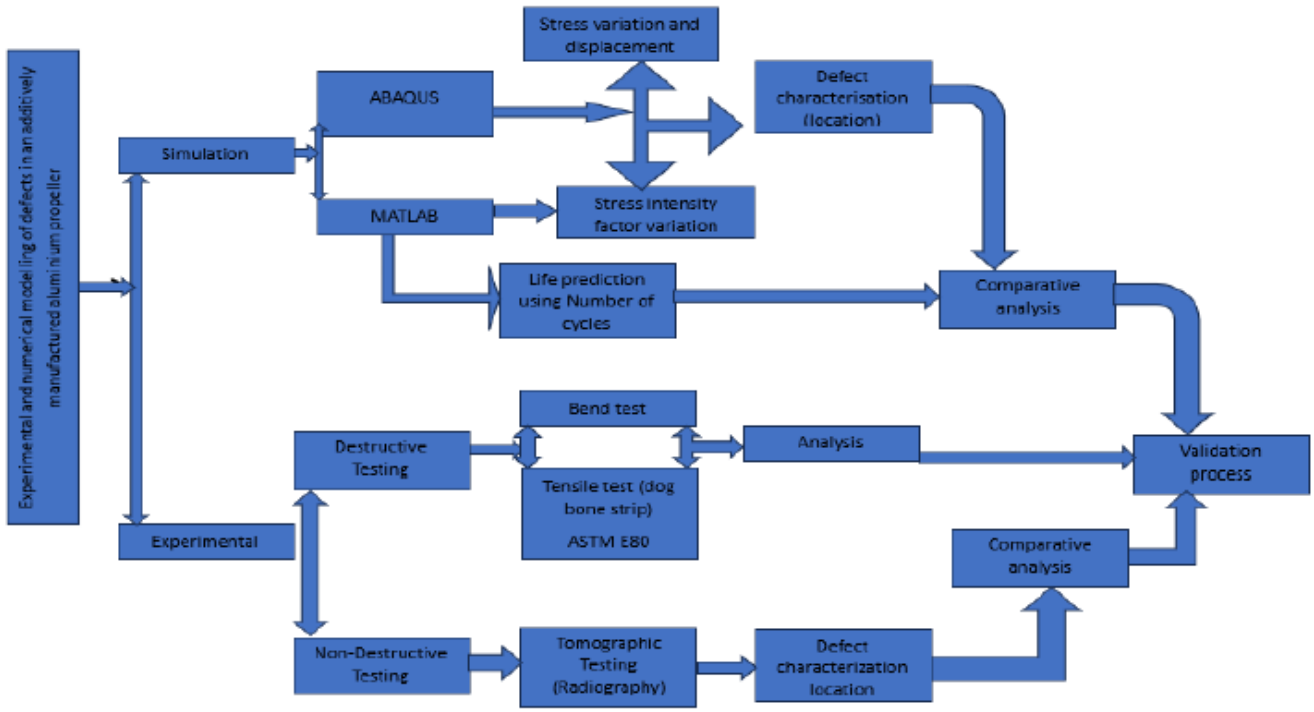

Figure 3.3: Summary of research methodology

3.2 Simulation Methodology/procedure

The components made of aluminium (AlSi10Mg) are perfect for applications which require a mixture of sound thermal and mechanical properties at small weight. The simulation by ABAQUS in this chapter demonstrates the following:

(a) Analysis of stress distribution
(b) Analysis of displacement(deformation)

3.2.1 AM propeller simulation using ABAQUS

Abaqus is one of the software programs which is used in engineering and is based on the finite element method. The Abaqus can solve a wide range of engineering challenges from linear to nonlinear analyses. The below are the stages followed in the simulation.

(a) Importing a Solid works drawing and Meshing

Solid works is the software that drafts engineering designs such as the aluminium propeller and simple to

share designs in 2D or 3D formats to other CAD software. Therefore, in this research the computer aided design (CAD) model for both the defective and non-defective propeller components were created with SolidWorks computer software and were imported into ABAQUS software.

The SOLIDWORKS drawn component was imported to Abaqus and pre-processed finite element modelling later. The file named model-1 was used and the ***part*** module had an option to import the drawing as shown by the black arrow in the figure 3.3 below.

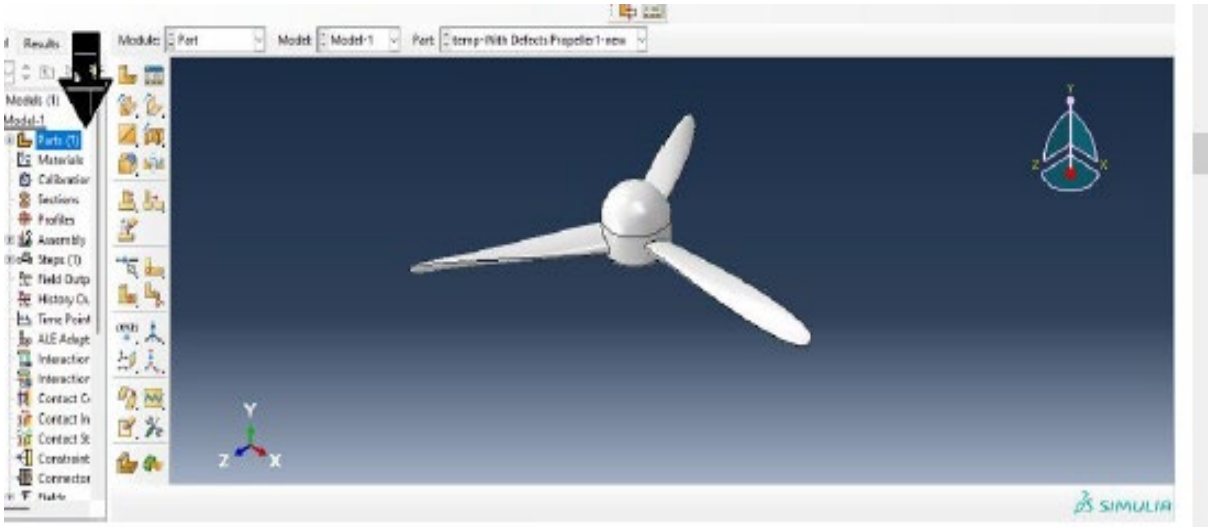

Figure 3.3: Image of an imported propeller.

(b) Material properties Module

The material properties such as density, Young's modulus and Poisson's ratio were assigned and given as 2.67kg/cm3, 68200MPa and 0.33 respectively. The below shows:

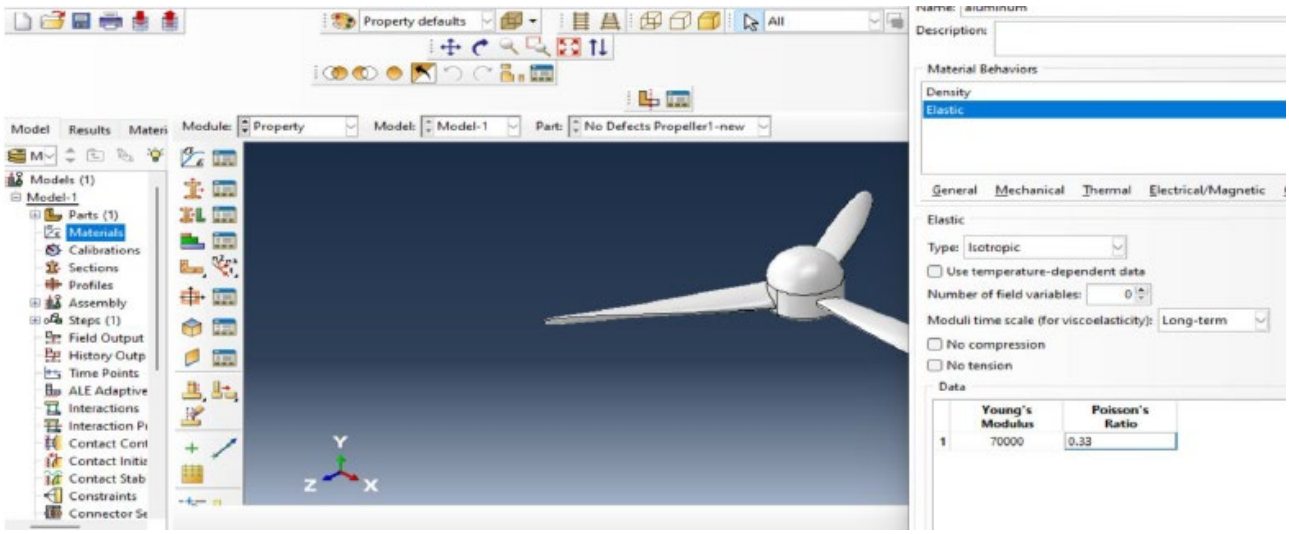

Figure 3.4: *Material module on ABAQUS*

The component was assigned as a homogeneous solid section. The researcher was aware that this model

might not resemble the full characteristics of the AM component however with the availability of modules in ABAQAS software, a solid section was the closest to be assigned. Moreover, the material mechanical properties used resembled those of a fully developed AlSi10Mg AM propeller.

The next step done was on assembly module, followed by the step module where NIgeom was set to **on**, this setting controls the inclusion of the nonlinear effect of large displacement and affects subsequent steps. Once the assembly module was completed, a step module was created with a solid homogeneous section selected.

(c) The loading module

The load module was selected, and the boundary condition named BC-1 was added, a displacement/ rotation was selected for a mechanical category.

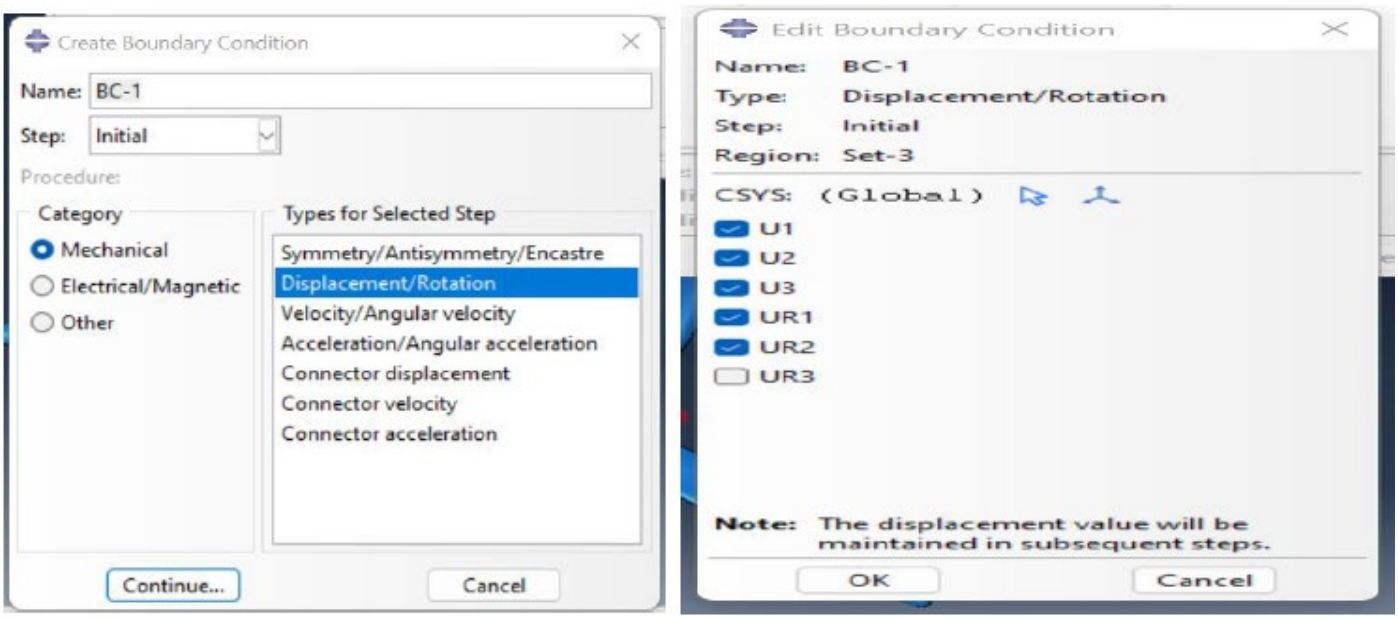

(a) (b)

Figure 3.5: Loading module for boundary condition steps: (a) mechanical category (b) displacement properties

The displacement rotation was selected as shown in figure 3.5 (a) and (b); U1, U2, U3, UR1 and UR2. It should be noted that the most important displacement was U1, U2, U3 though this research included UR1 and UR2, they are suggested not impactful towards the outcome expectation from result. The predefined field was selected to determine the angular velocity of 100 rad/second and the exit point as 0,1,0.

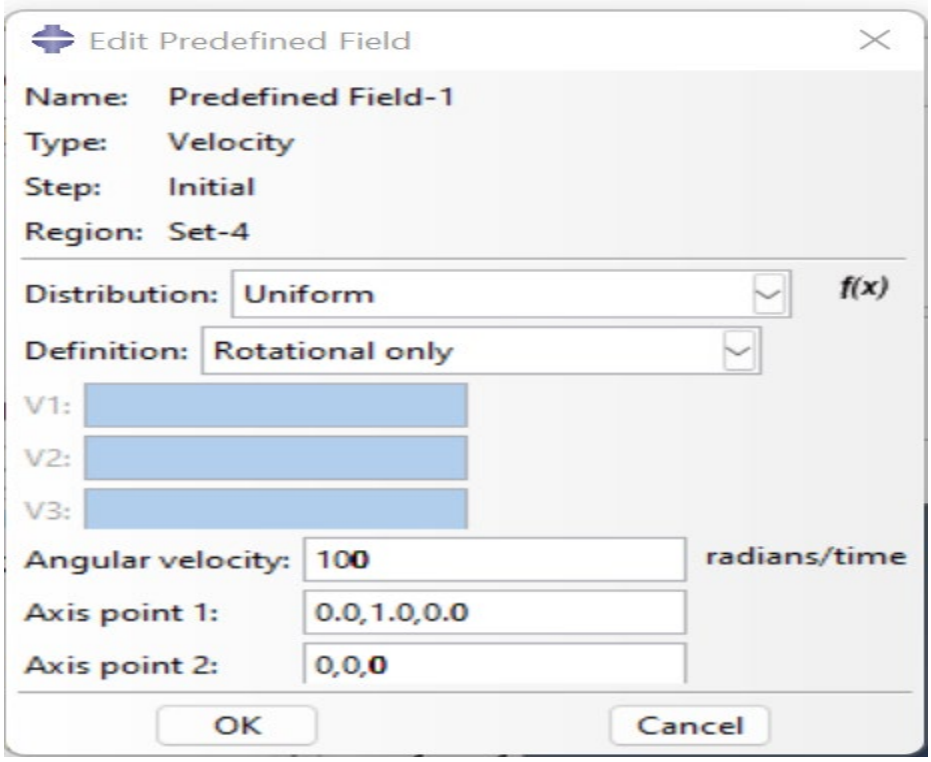

Figure 3.6 ABAQUS predefined field

The axis of rotation was made 750 rad/second. This value was selected as a result of attaining accurate thrust and swirl predictions and would likely result for a high-speed propeller, such as a turboprop engine or experimental aircraft. It can be noted as well that the defects in red colour or irregular boundaries are visible in the homogeneous material structure,

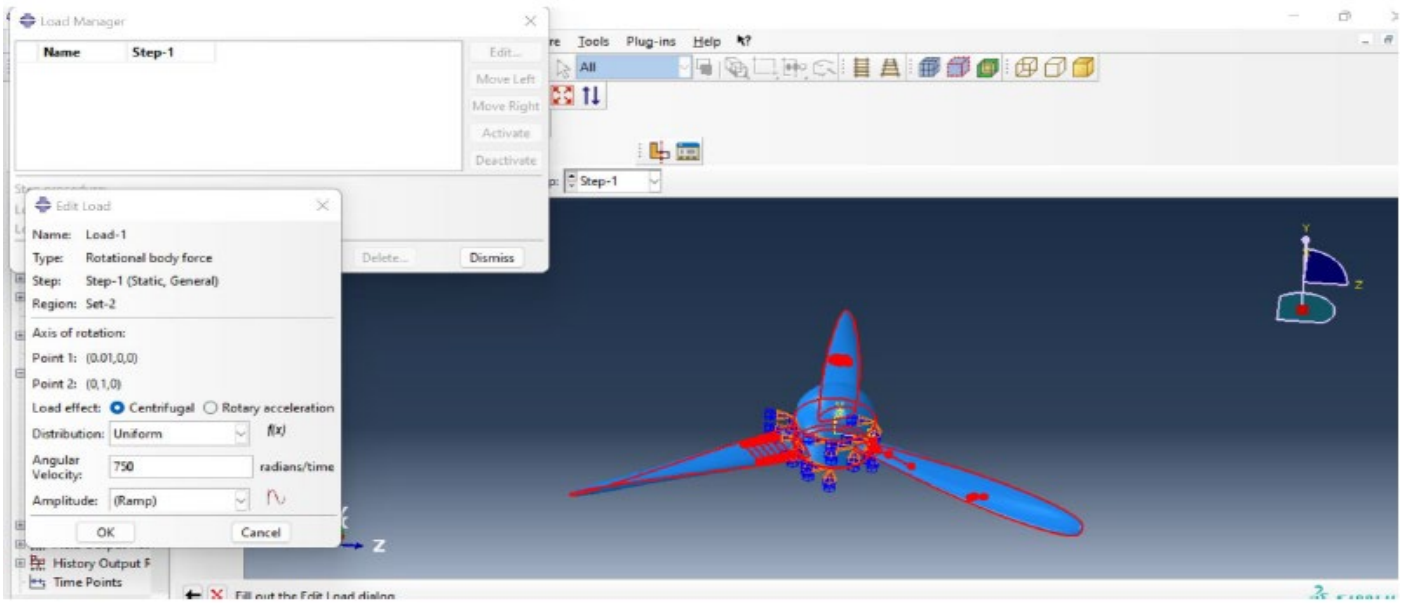

Figure 3.7: The angular frequency, centrifugal force, axis of rotation

(d) The Meshing module

The quadratic hexagonal and quadratic meshing was not supported in this research. A quadratic tetrahedral mesh was the most suitable mesh on this component, and it gave good surface contours. Tetrahedral elements are normally created as equilateral, such as in systems with circular curvature, or they could be constructed as isosceles tetrahedra when a system has asymmetric and could also be totally unstructured and adapted to arbitrary geometries with high accuracy. The resulting meshing was as follows:

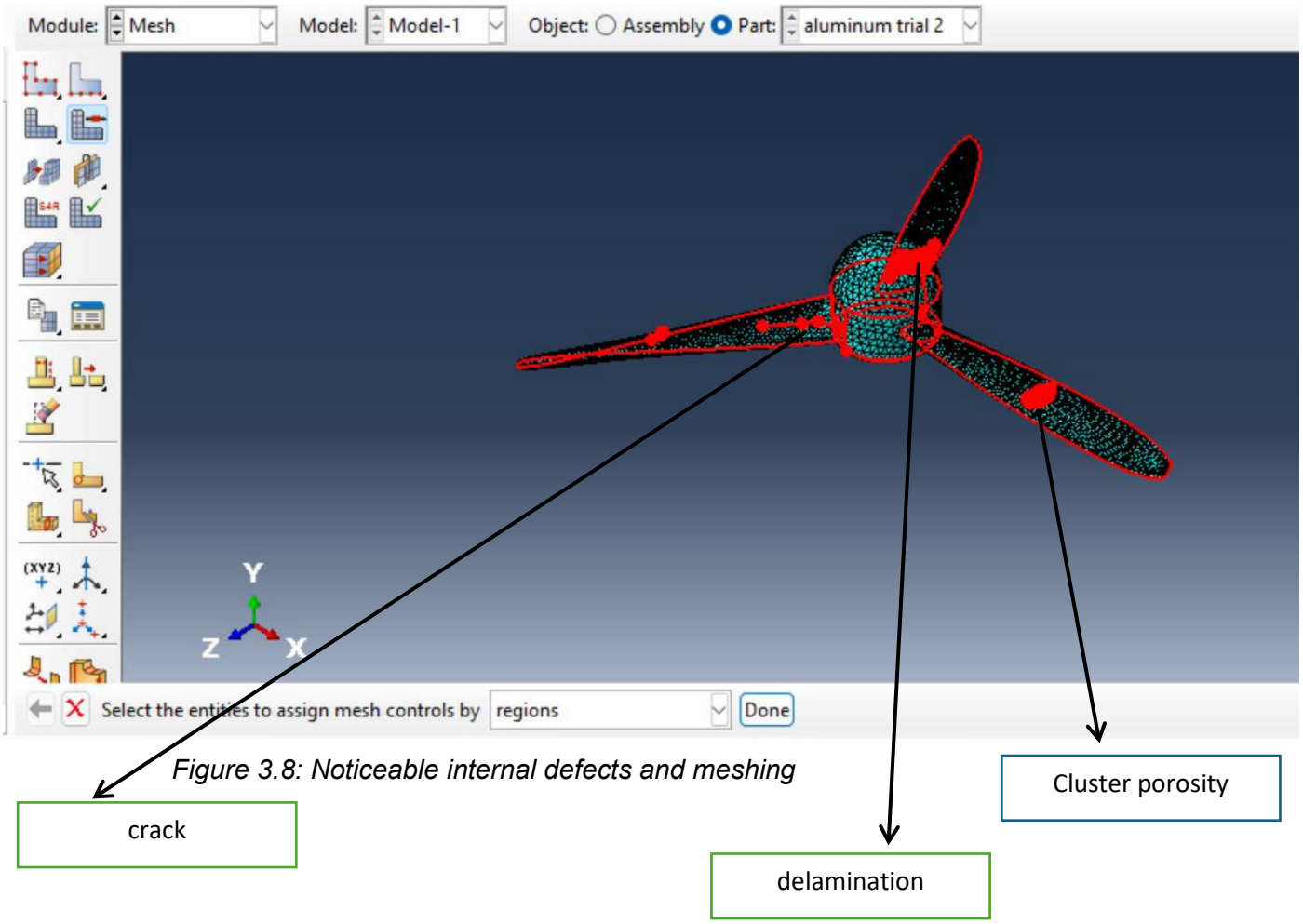

Figure 3.8: Noticeable internal defects and meshing

The entire part (region) was selected for the mesh and remeshing assigning which allows the component to be meshed fully at 4.5.

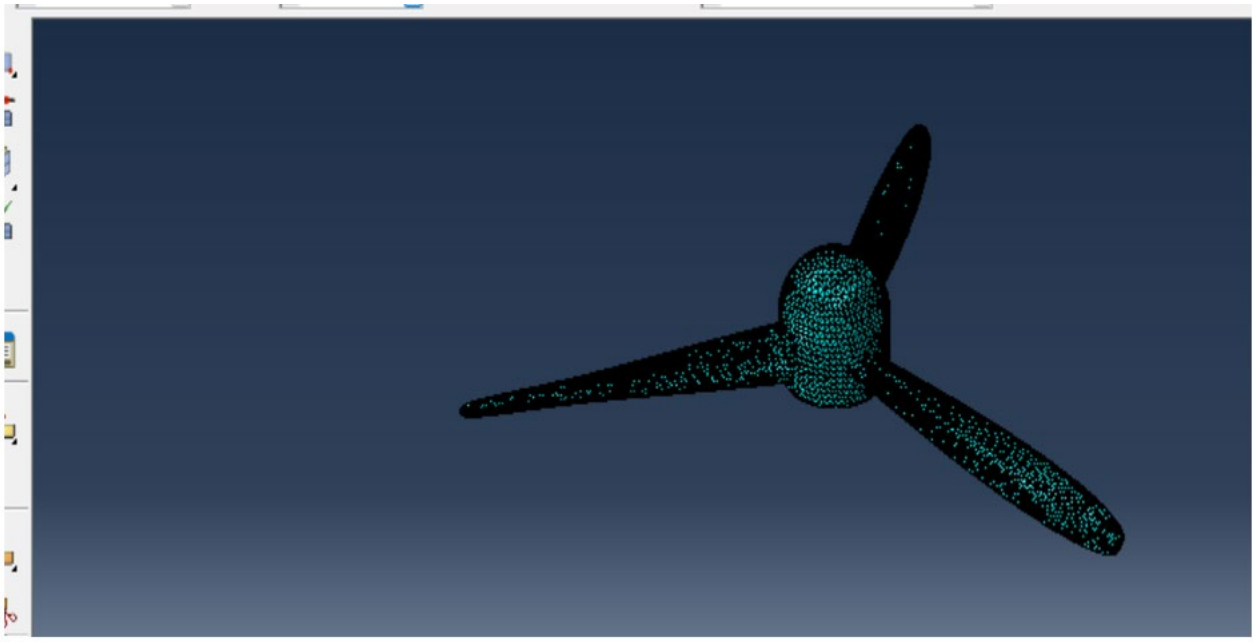

Figure 3.9: Tetrahedral meshing of the propeller blade

The higher-order elements interpolating 10-node tetrahedral elements were used. The system was then run, and the results are shown below.

3.2.2 Results for stress analysis for a defective AM propeller.

The results found on stress were as shown in the images below and twenty-one steps (21) were made and had demonstrated different levels of stresses and deformation. The stress distribution on different (selected) steps is shown below:

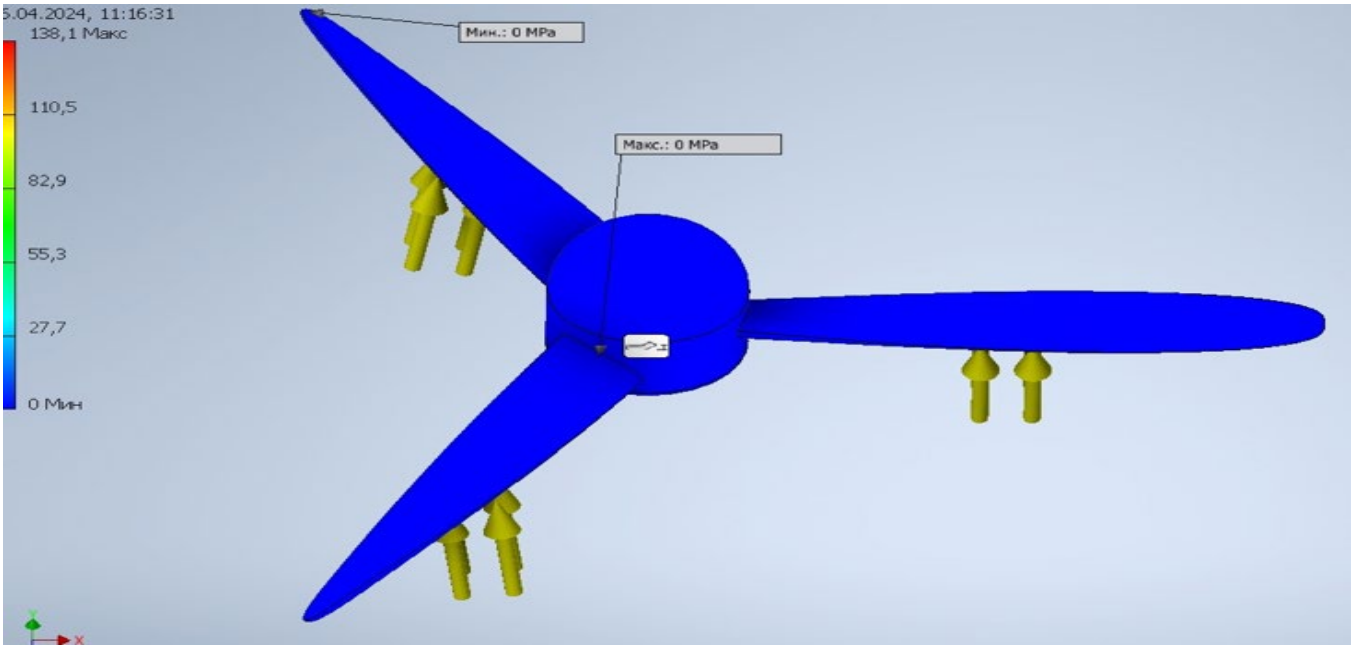

Figure 3.10: Stress distribution on step 1

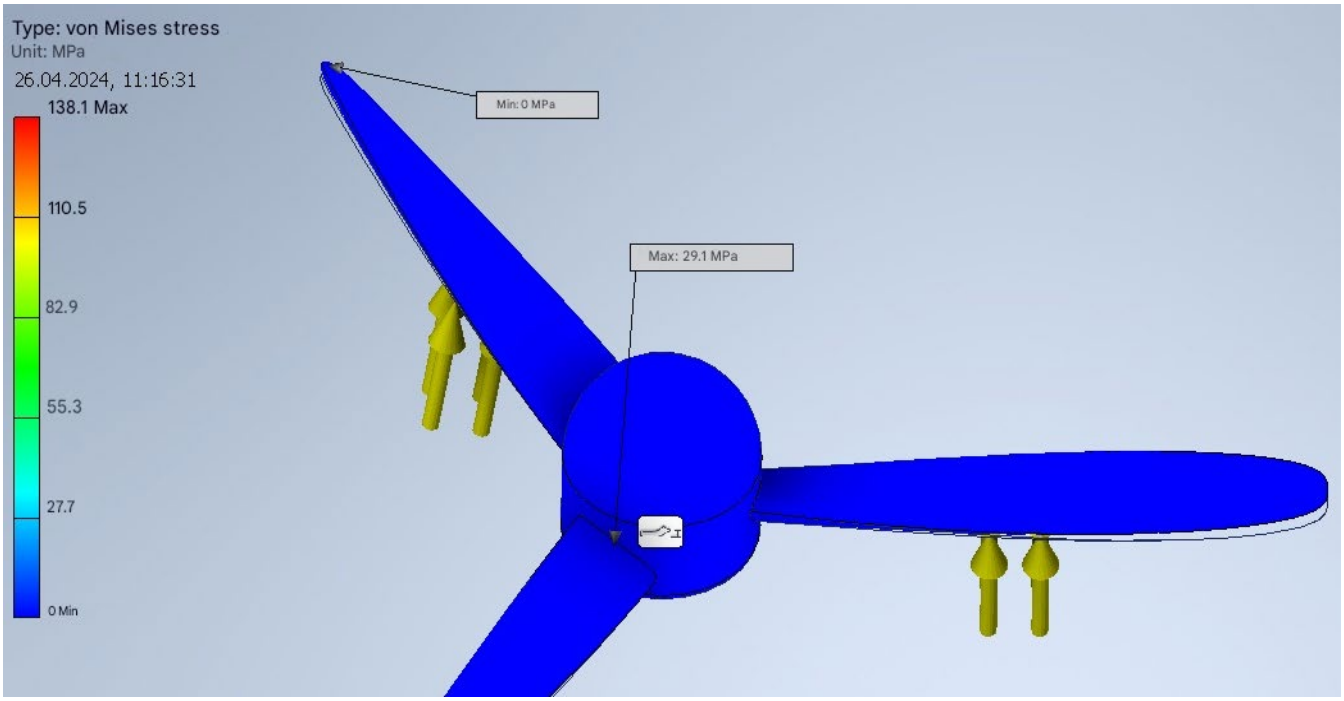

Figure 3.11 Stress distribution on step 5

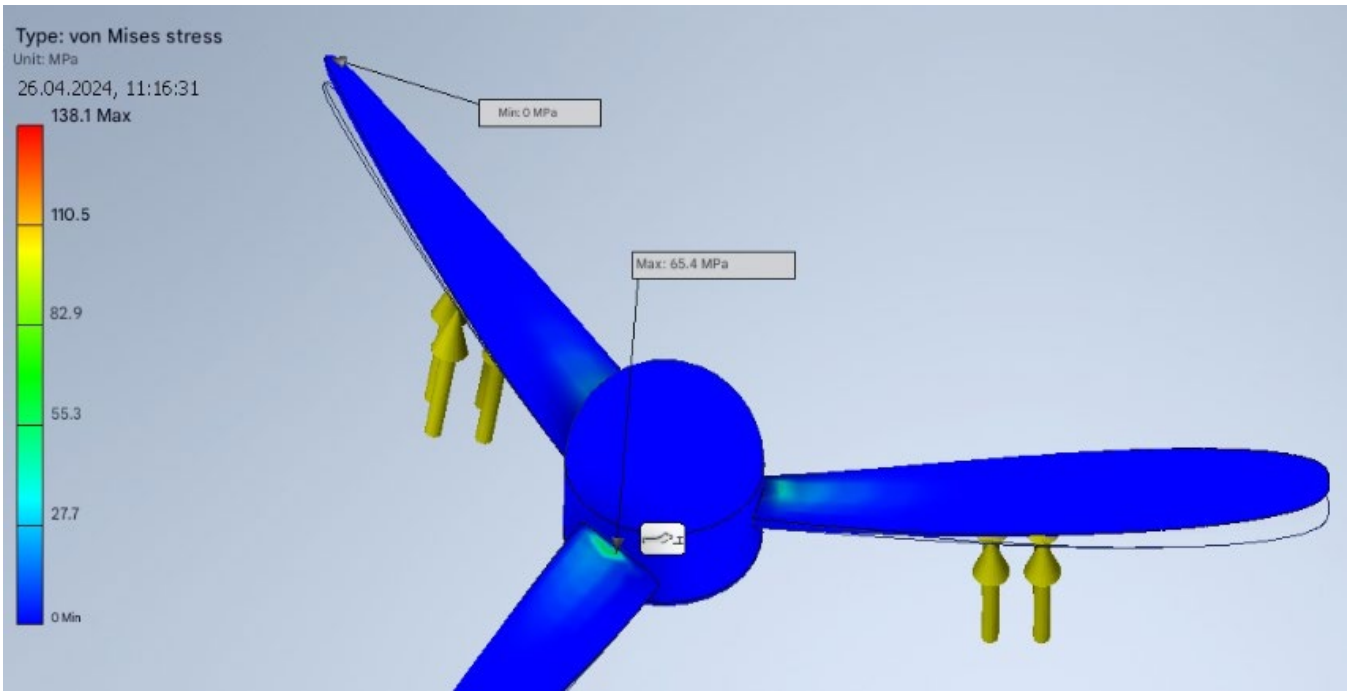

Figure 3.12: Stress distribution on step 10

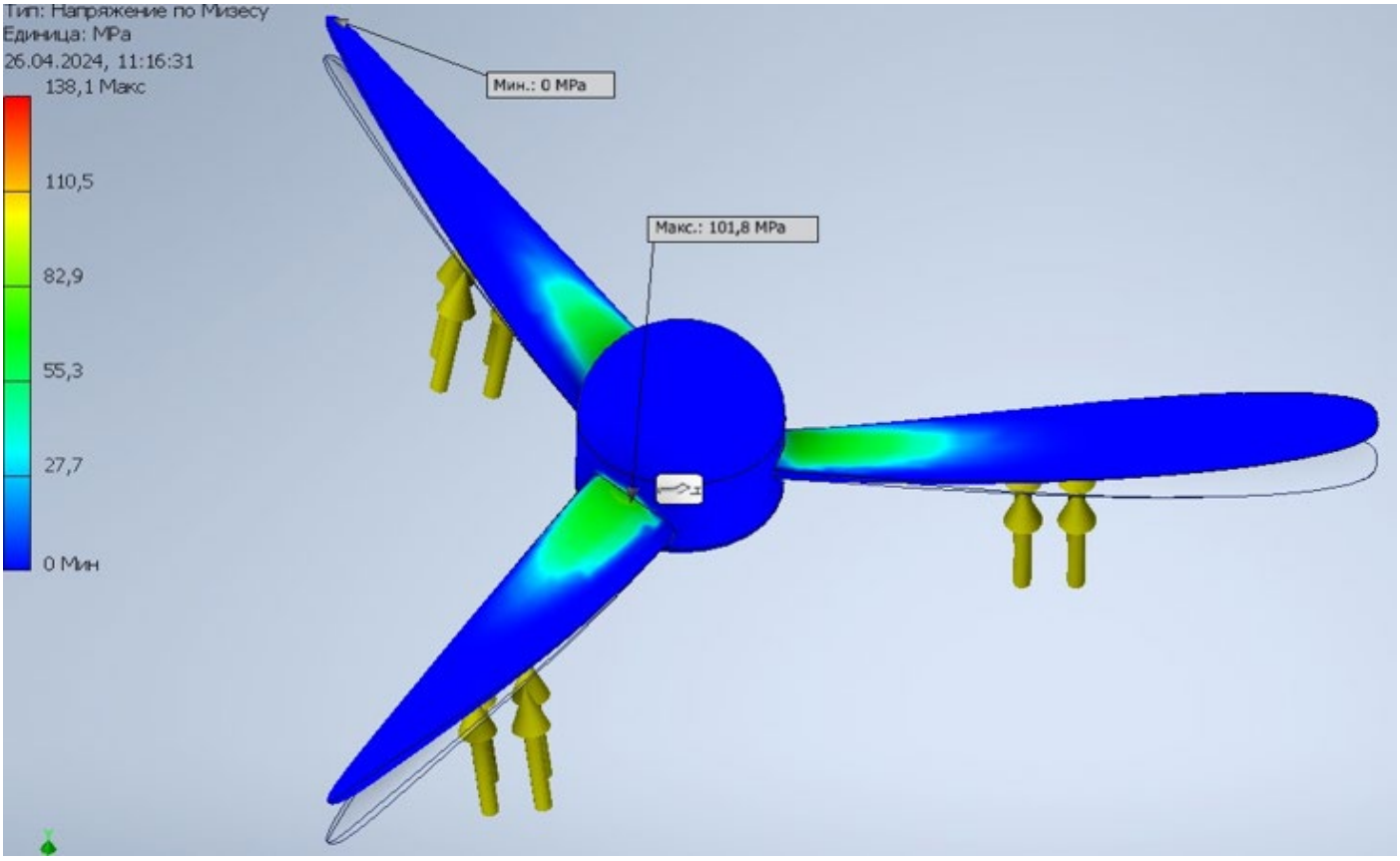

Figure 3.13: *Stress distribution on step 15*

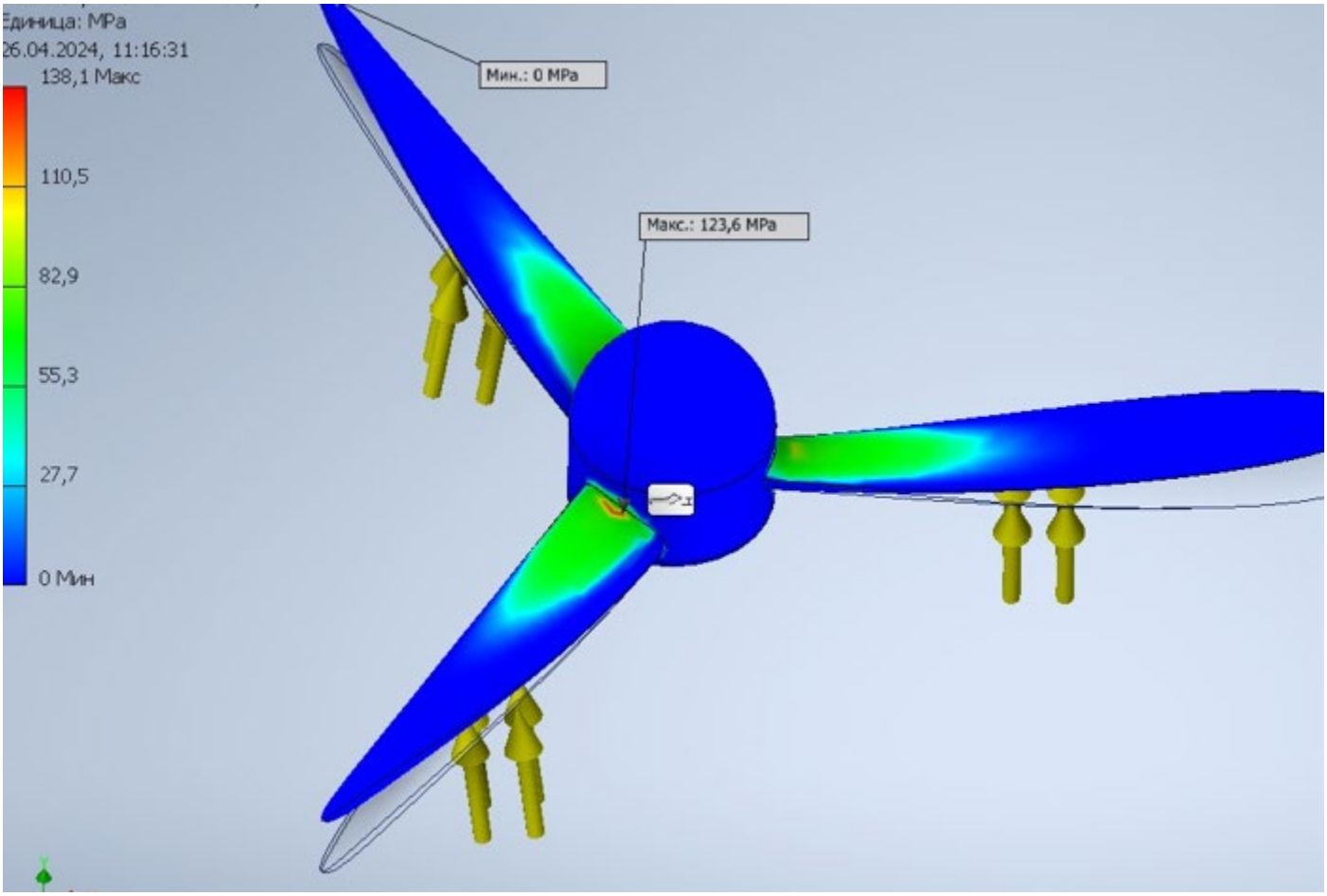

Figure 3.14: Stress distribution on step 18

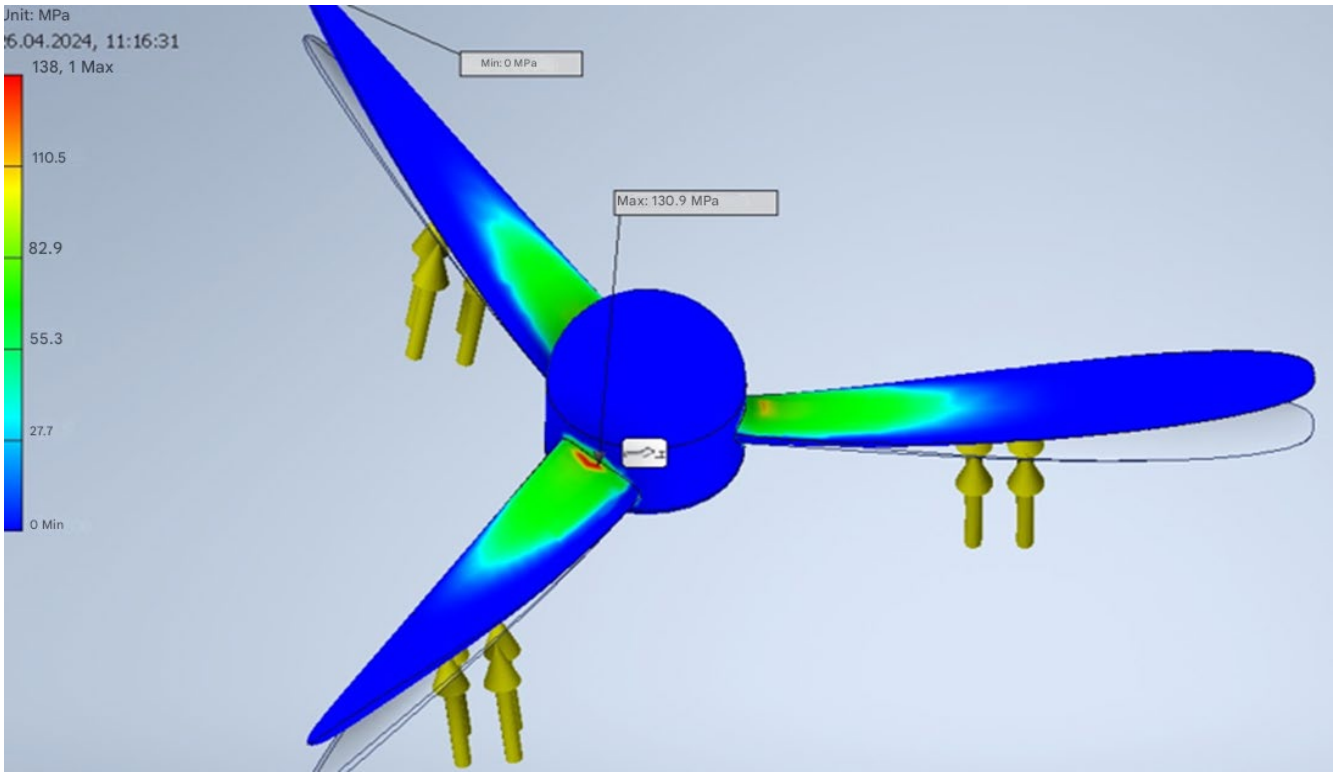

Figure 3.14: Stress distribution on step 19

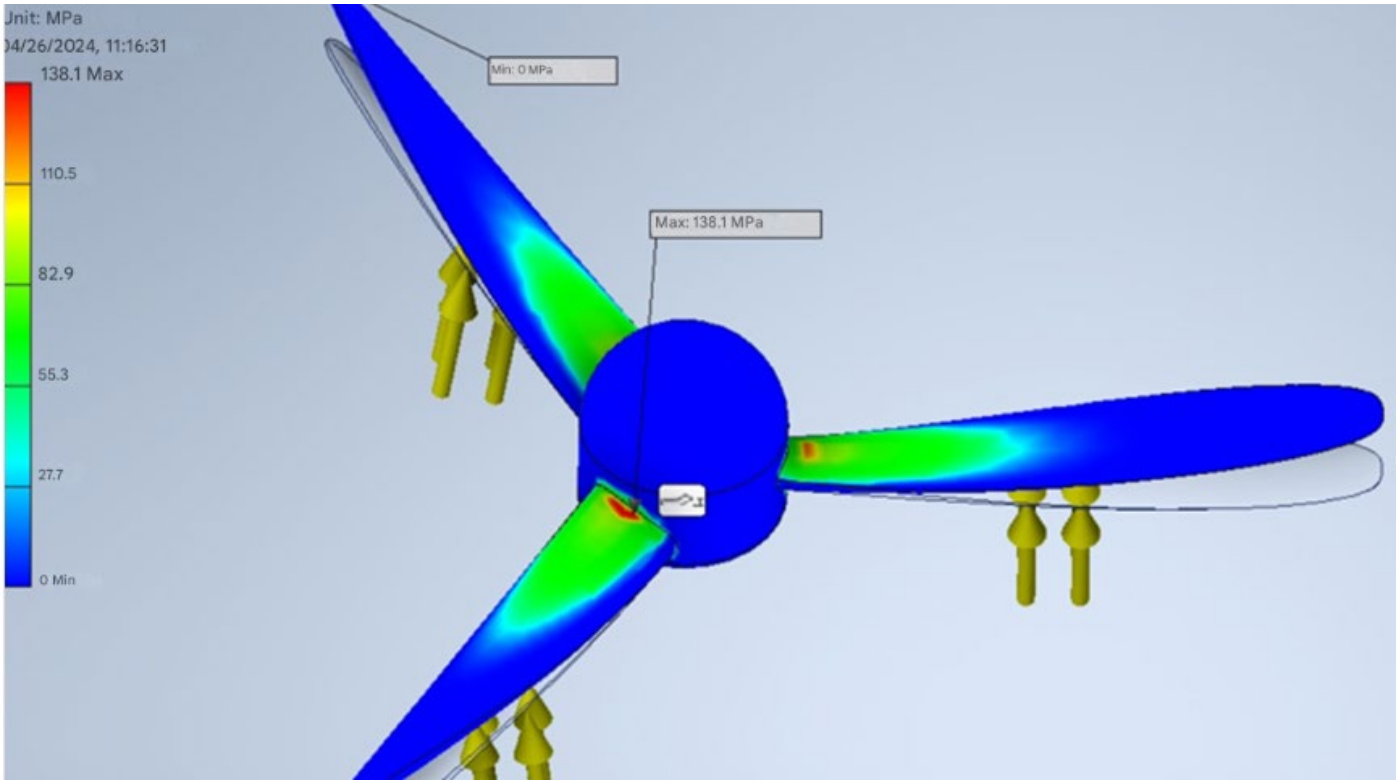

Figure 3.15: Stress distribution on step 20

The stresses acting on the sampled defective blade

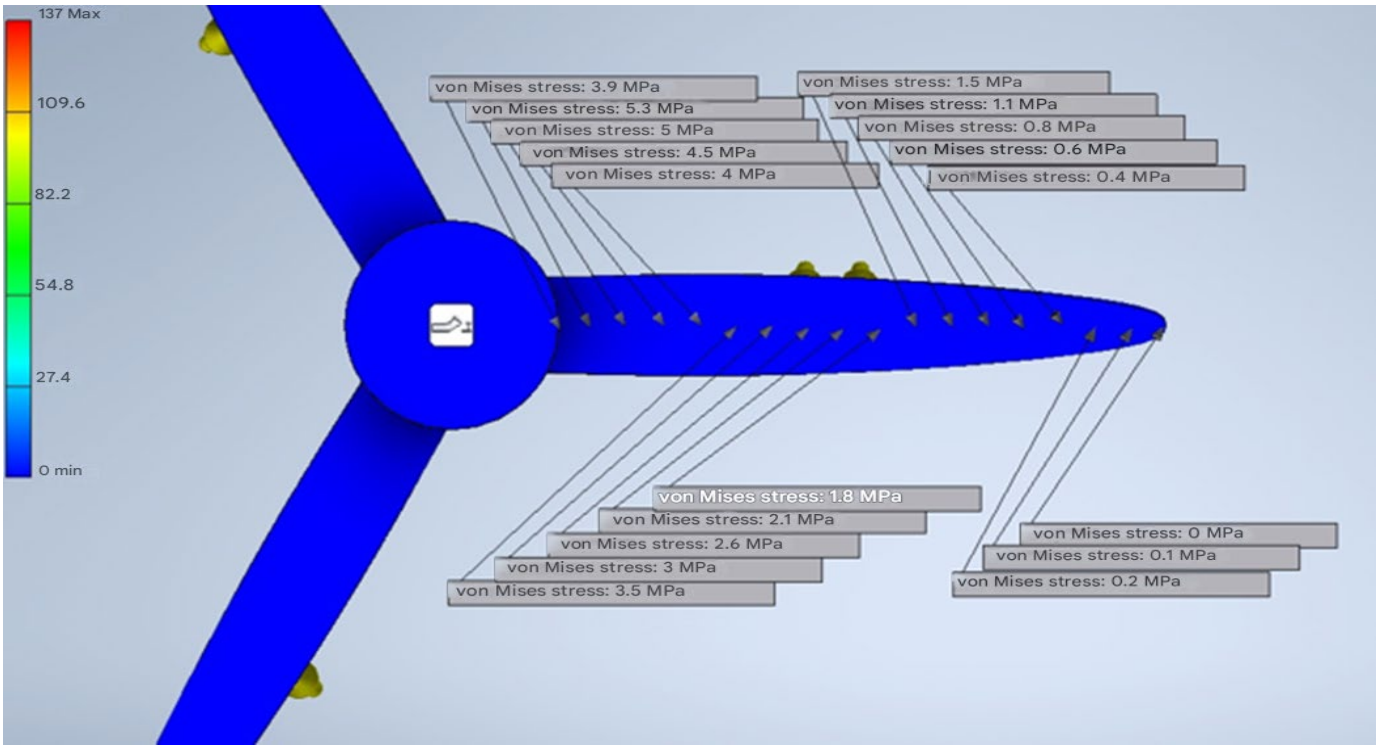

Figure 3.16: Stress distribution on step 2

Graph 3.1: the graphical presentation of stress distribution on the sampled blade

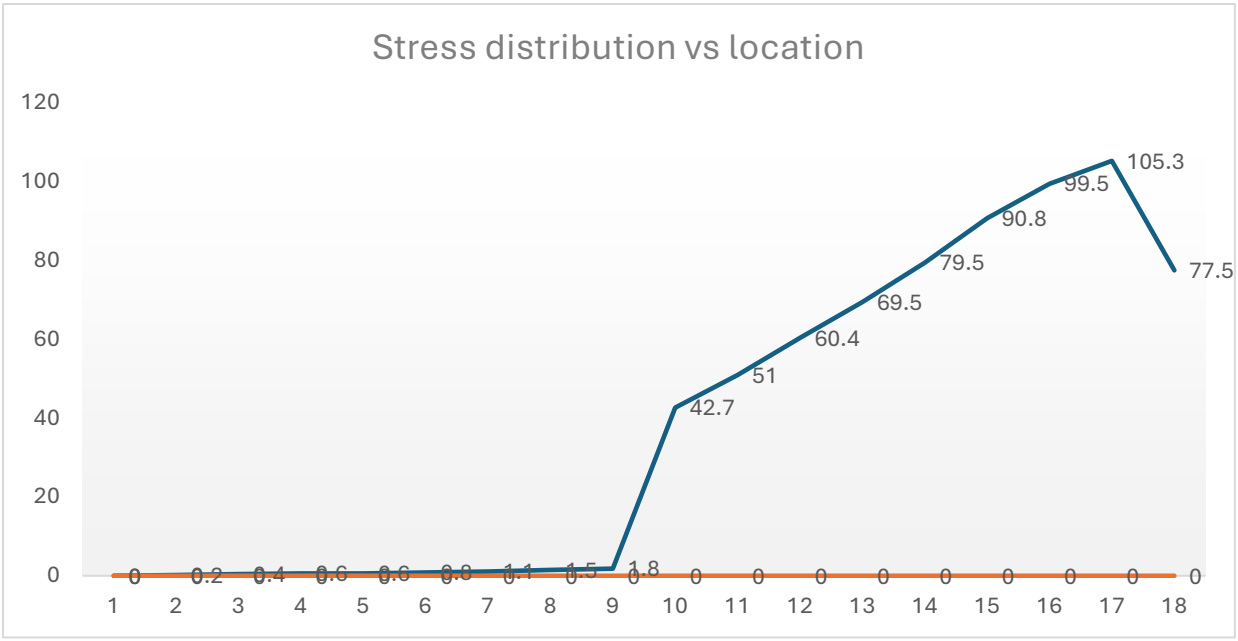

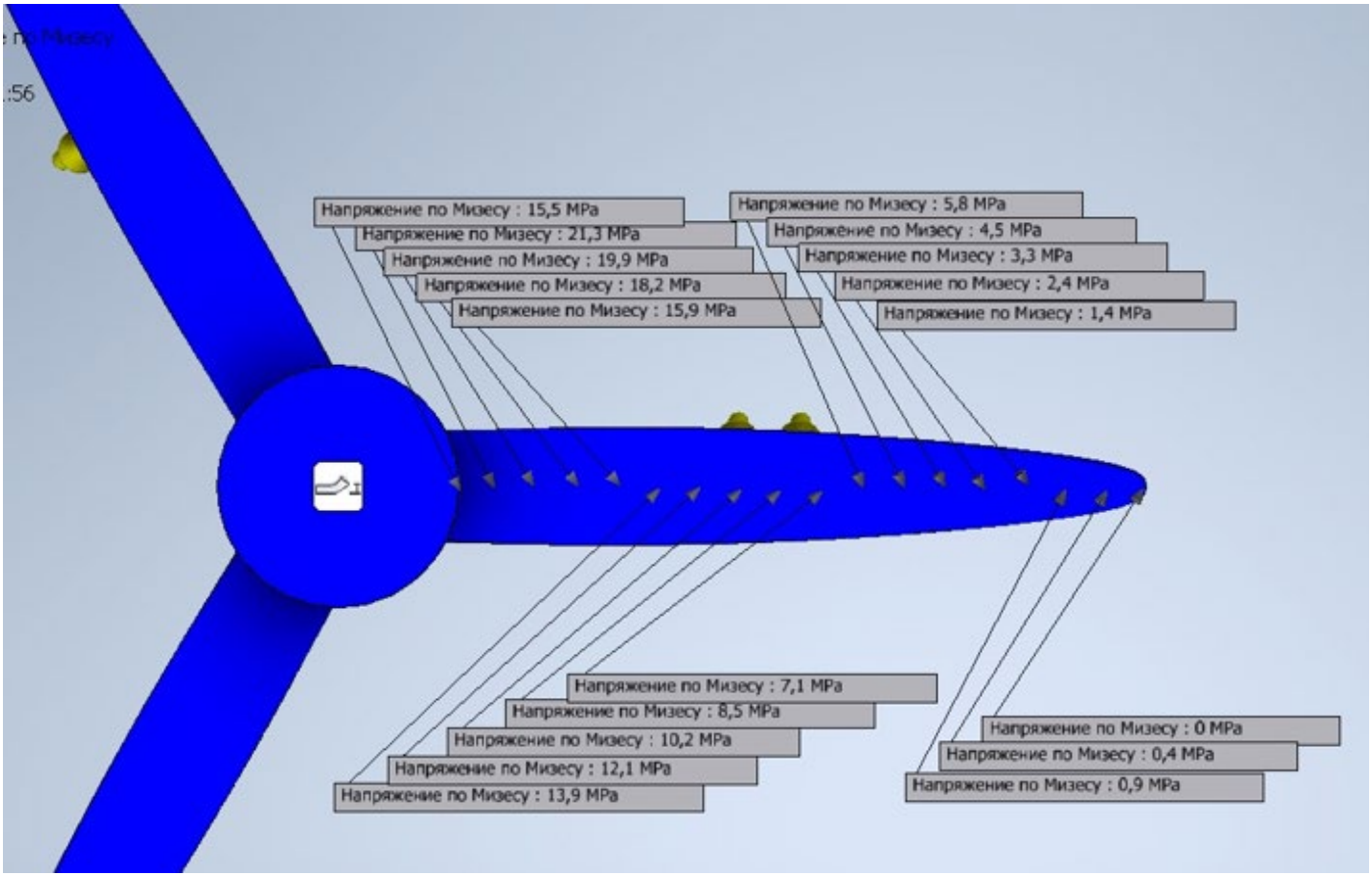

Figure 3.17: Stress distribution on step 5

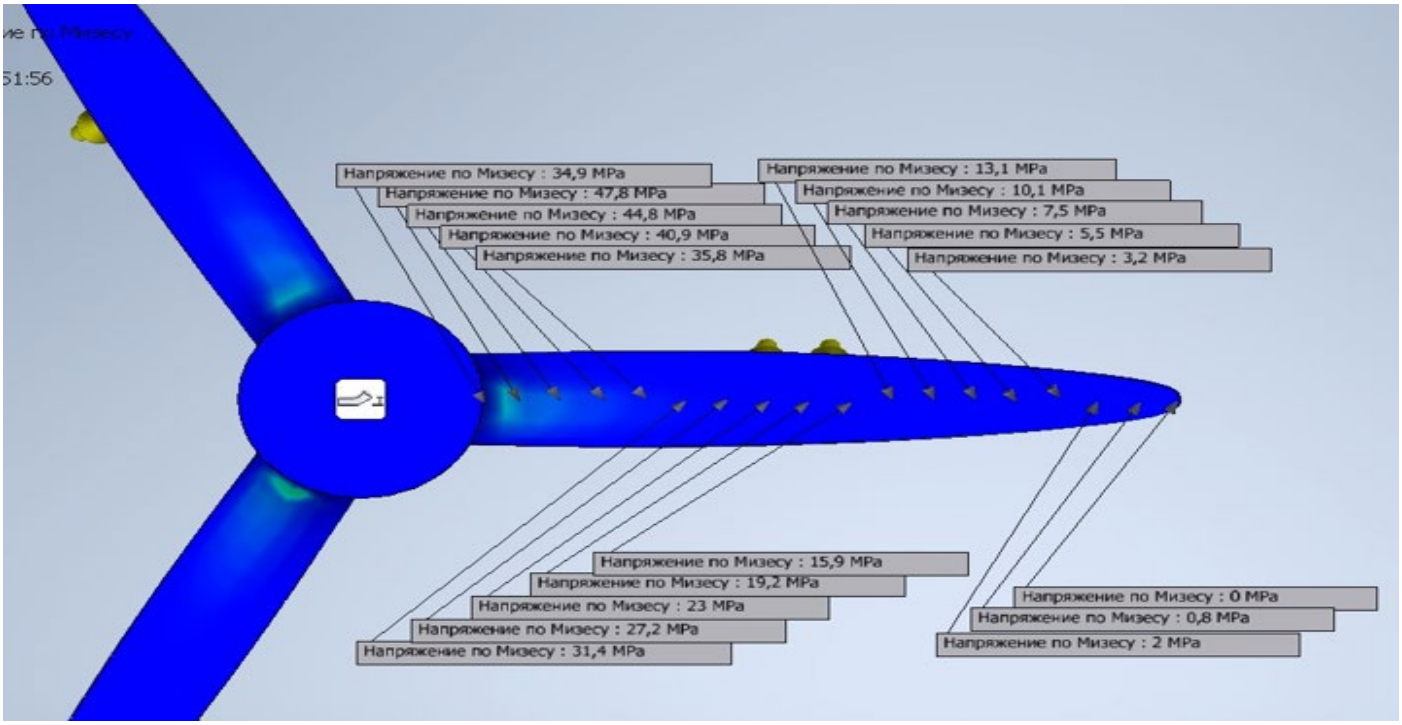

Figure 3.18: Stress distribution on step 10

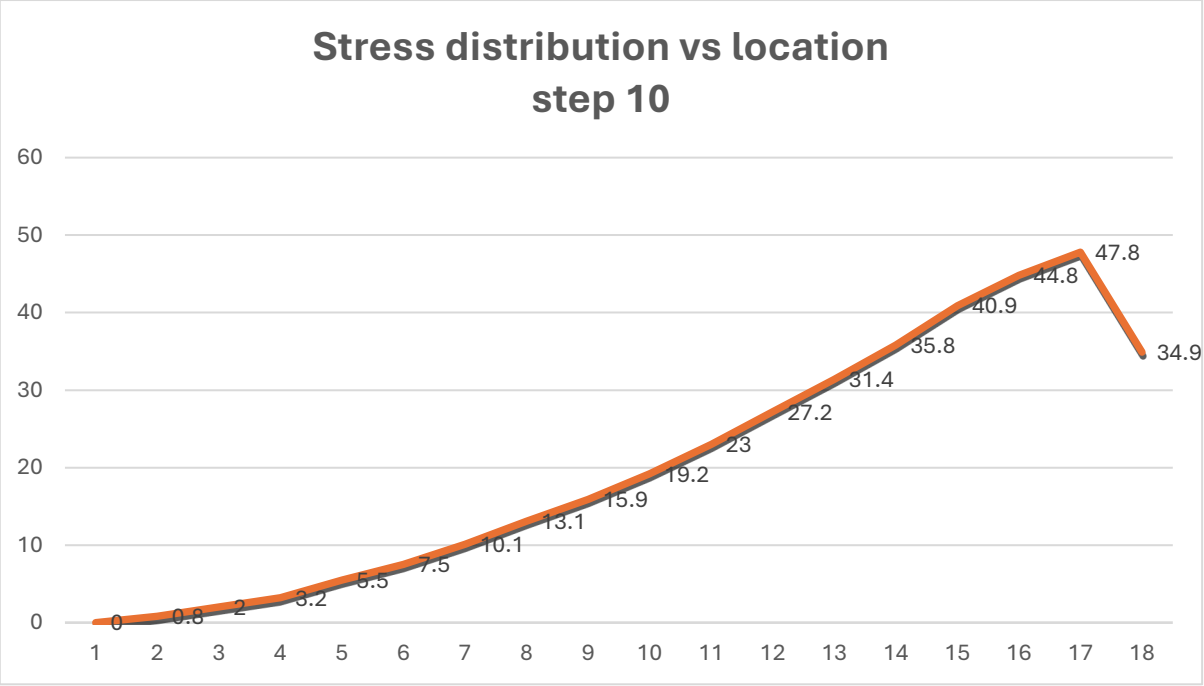

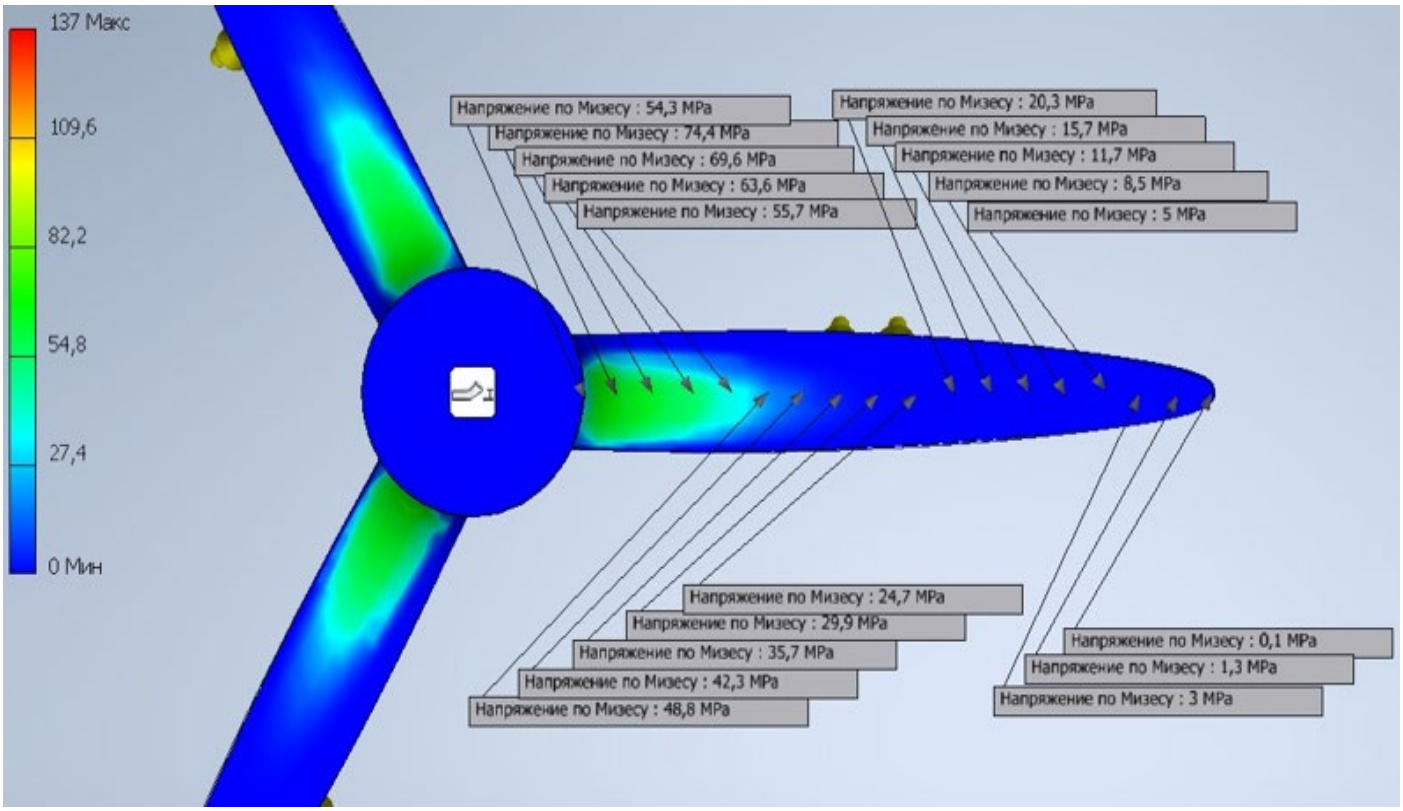

Figure 3.19: Stress distribution on step 15

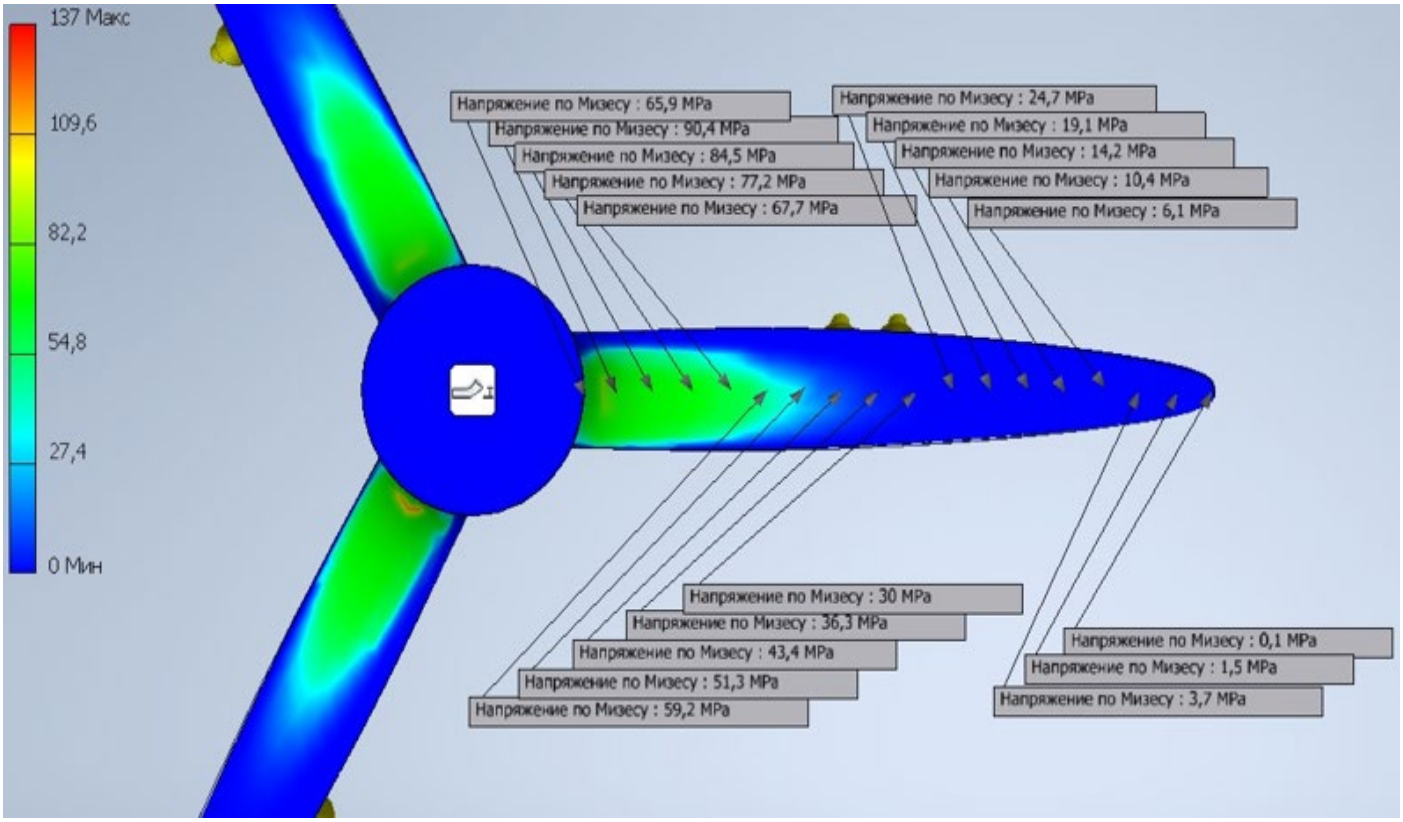

Figure 3.20: Stress distribution on step 18

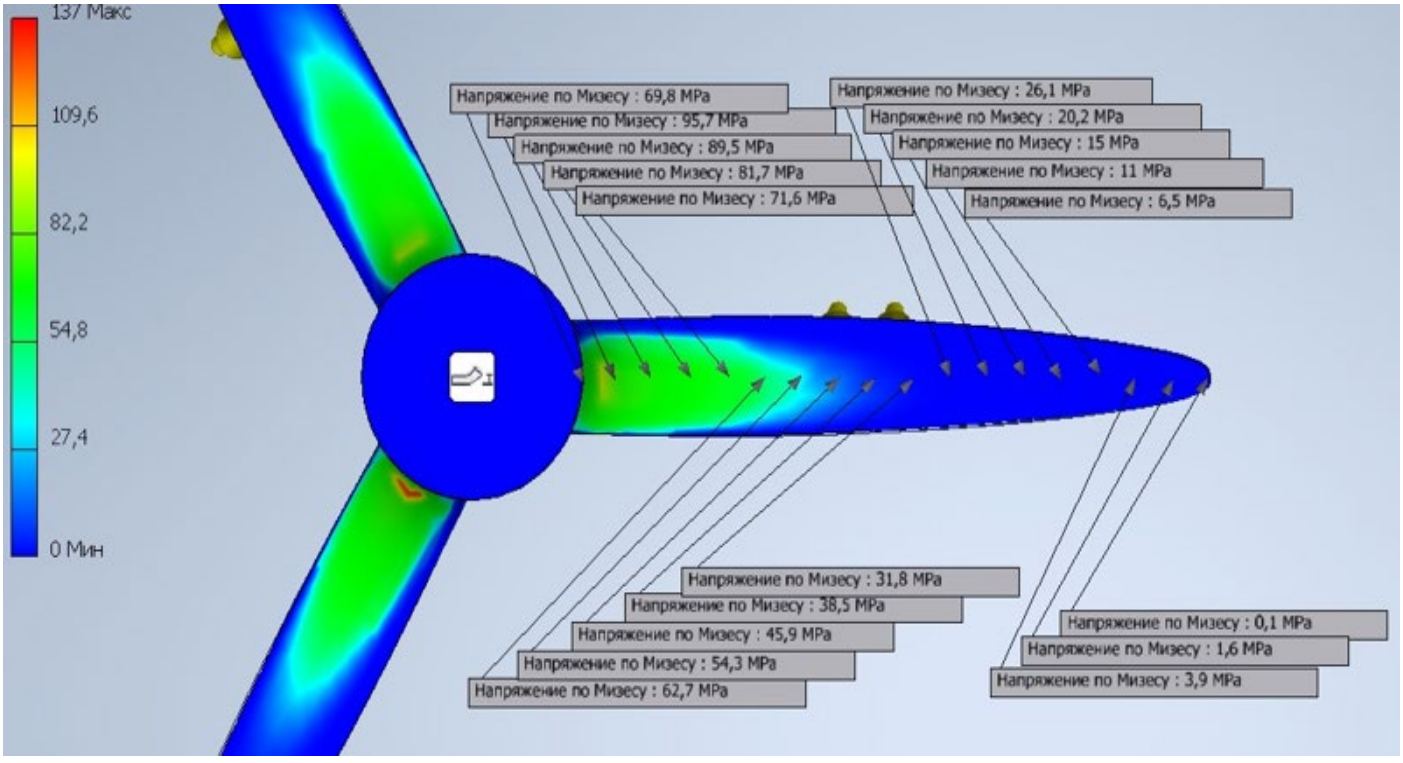

Figure 3.21: Stress distribution on step 19

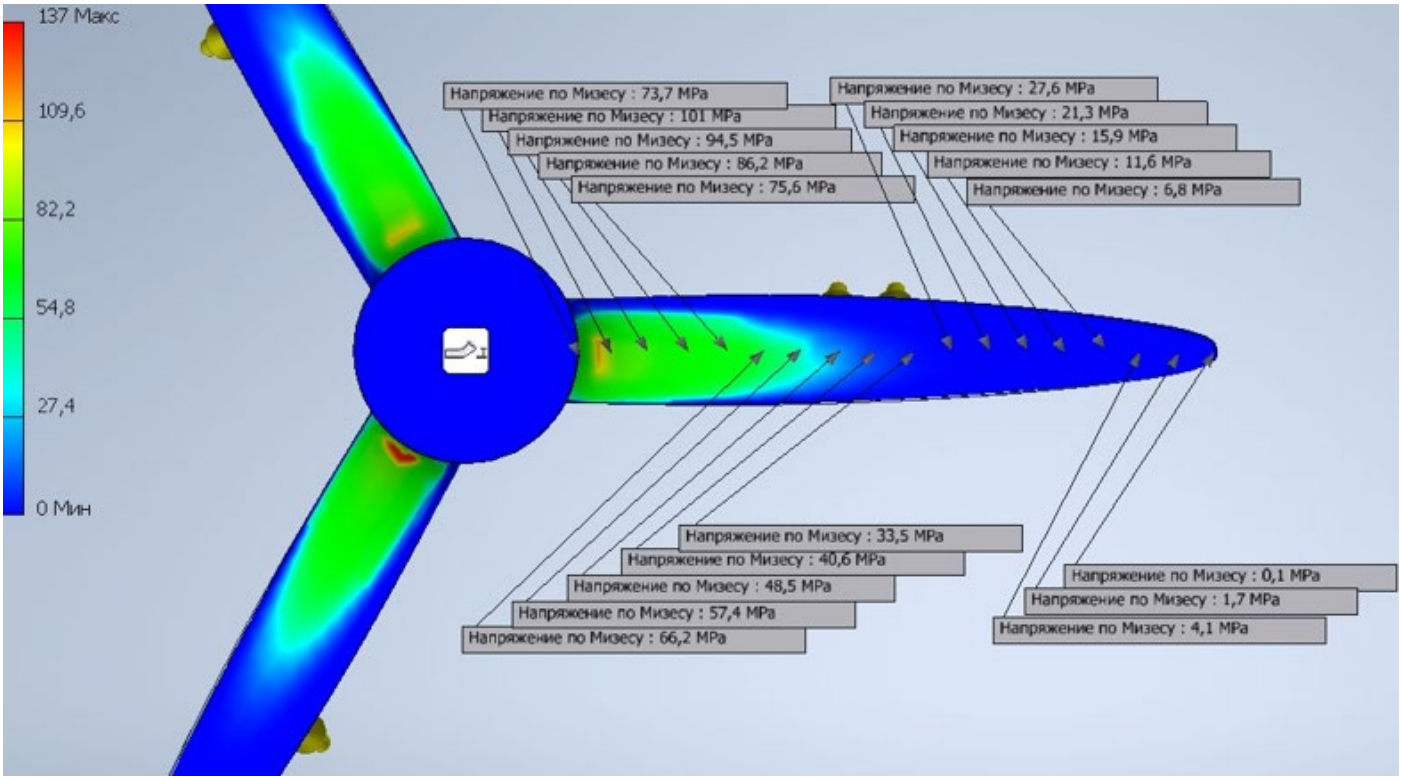

Figure 3.22: Stress distribution on step 21

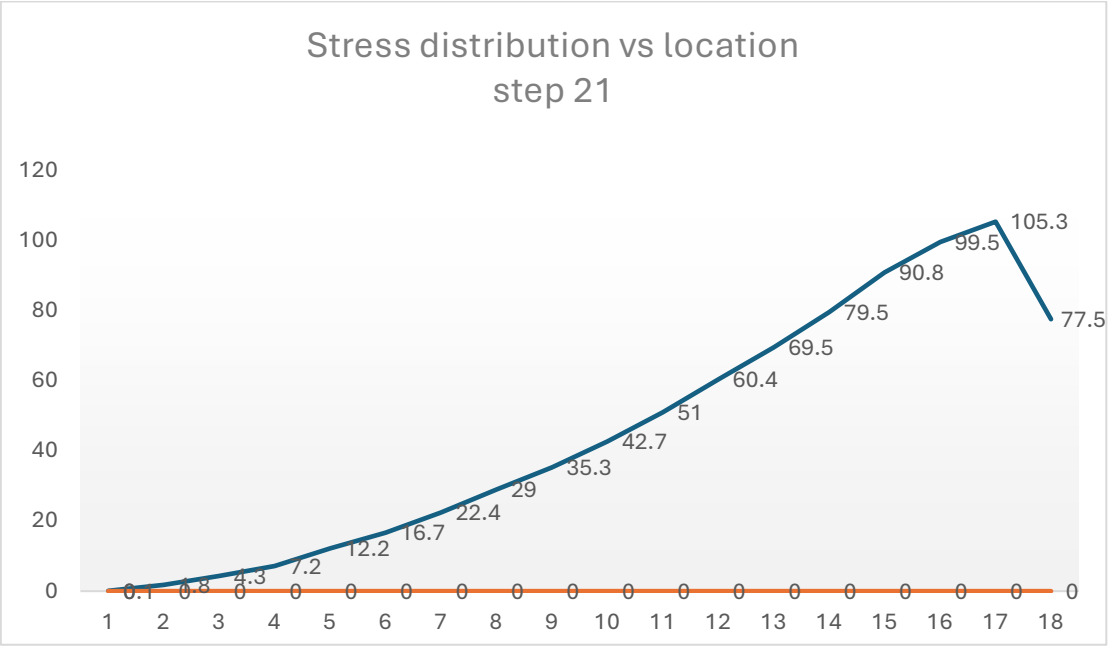

Result of stress intensity factor vs defect length for step 20 based on the stress results found and by applying the Paris Erdogan equation for the defect growth rate in MATLAB the following results were found:

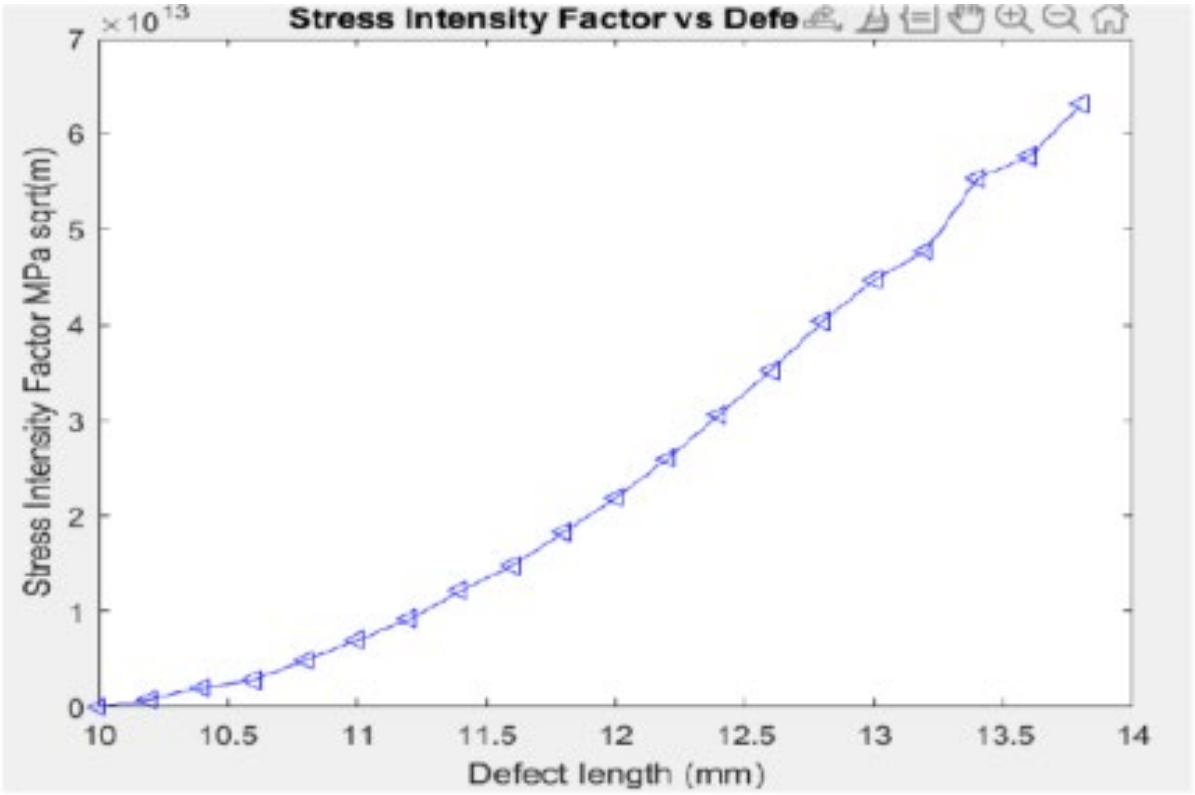

These are the results demonstrated the crack defect behaviour in mode III of fracture.

The results on deformation during rotation per step. A data of 20 steps were made and below is a demonstration of results in different steps.

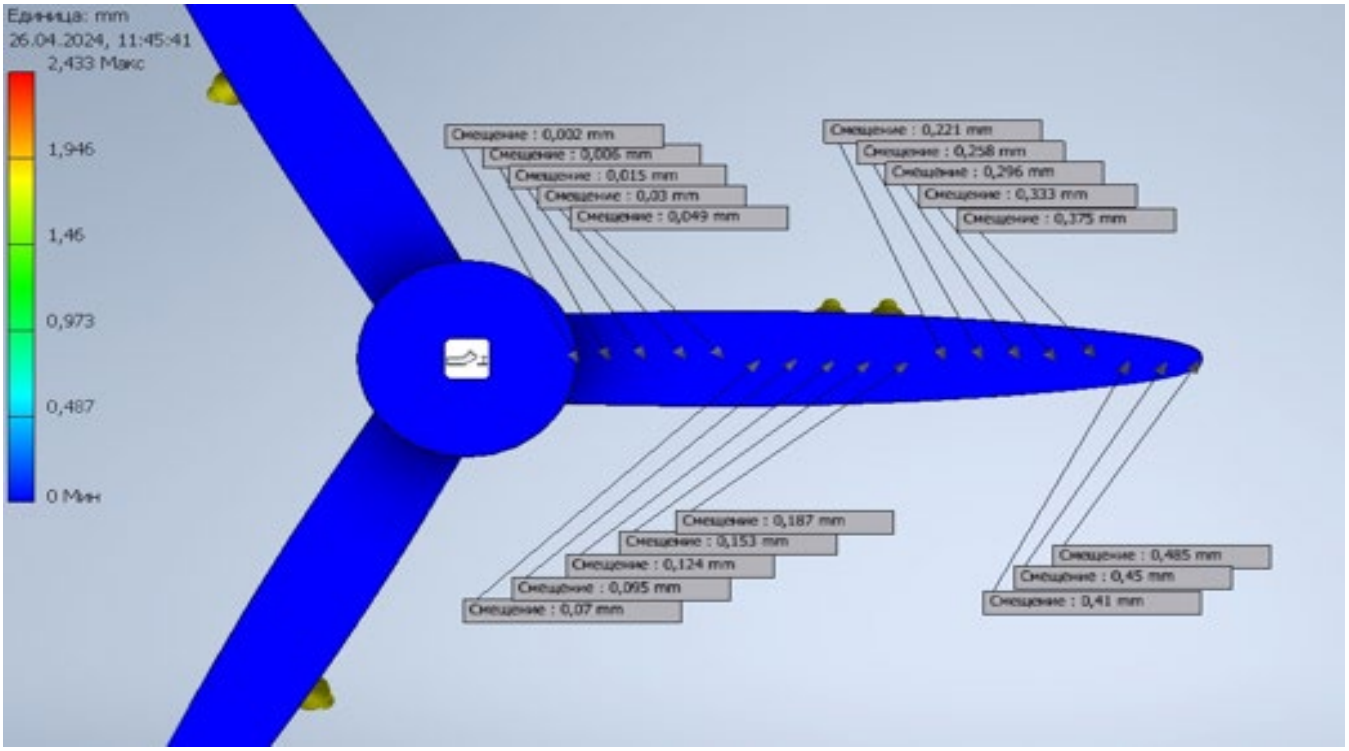

Figure 3.21: Strain distribution on step 5

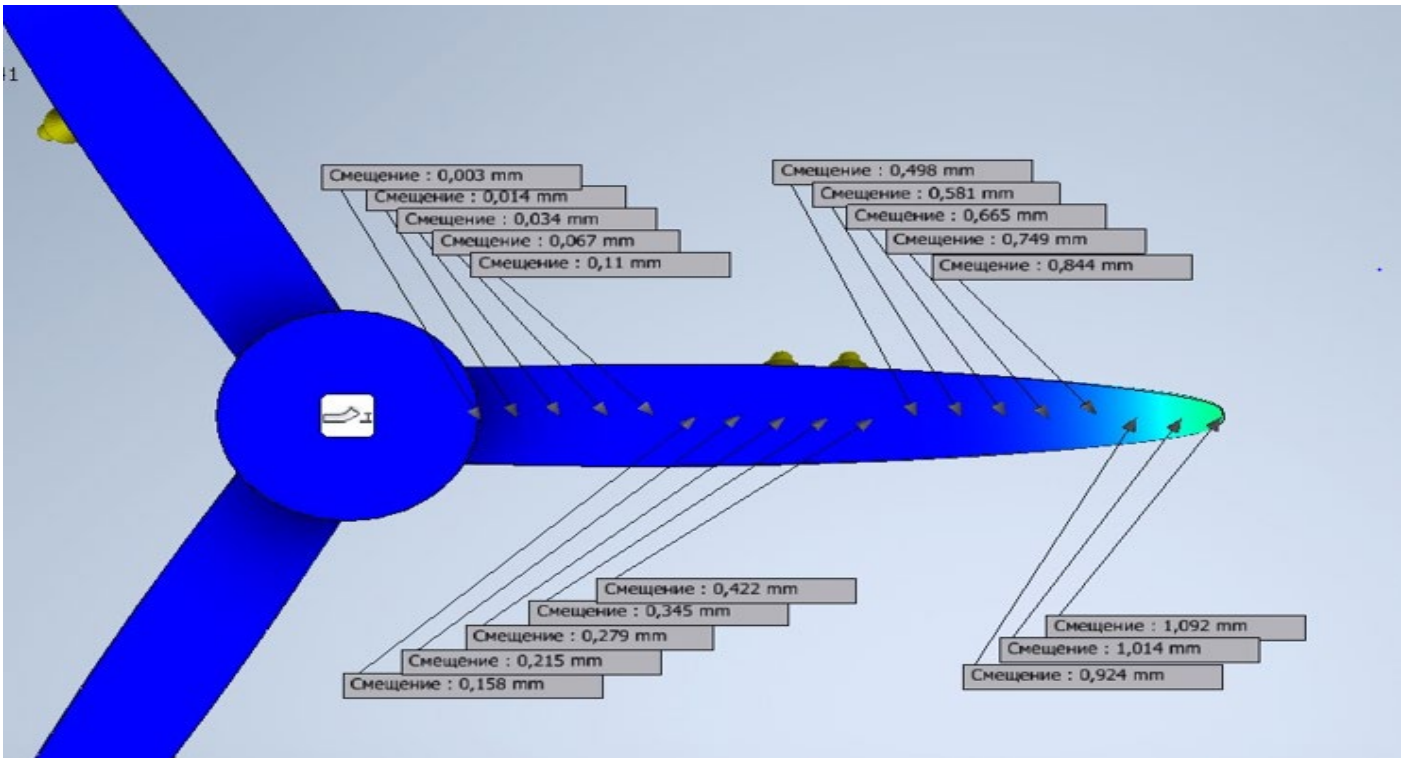

Figure 3.22: Strain distribution on step 10

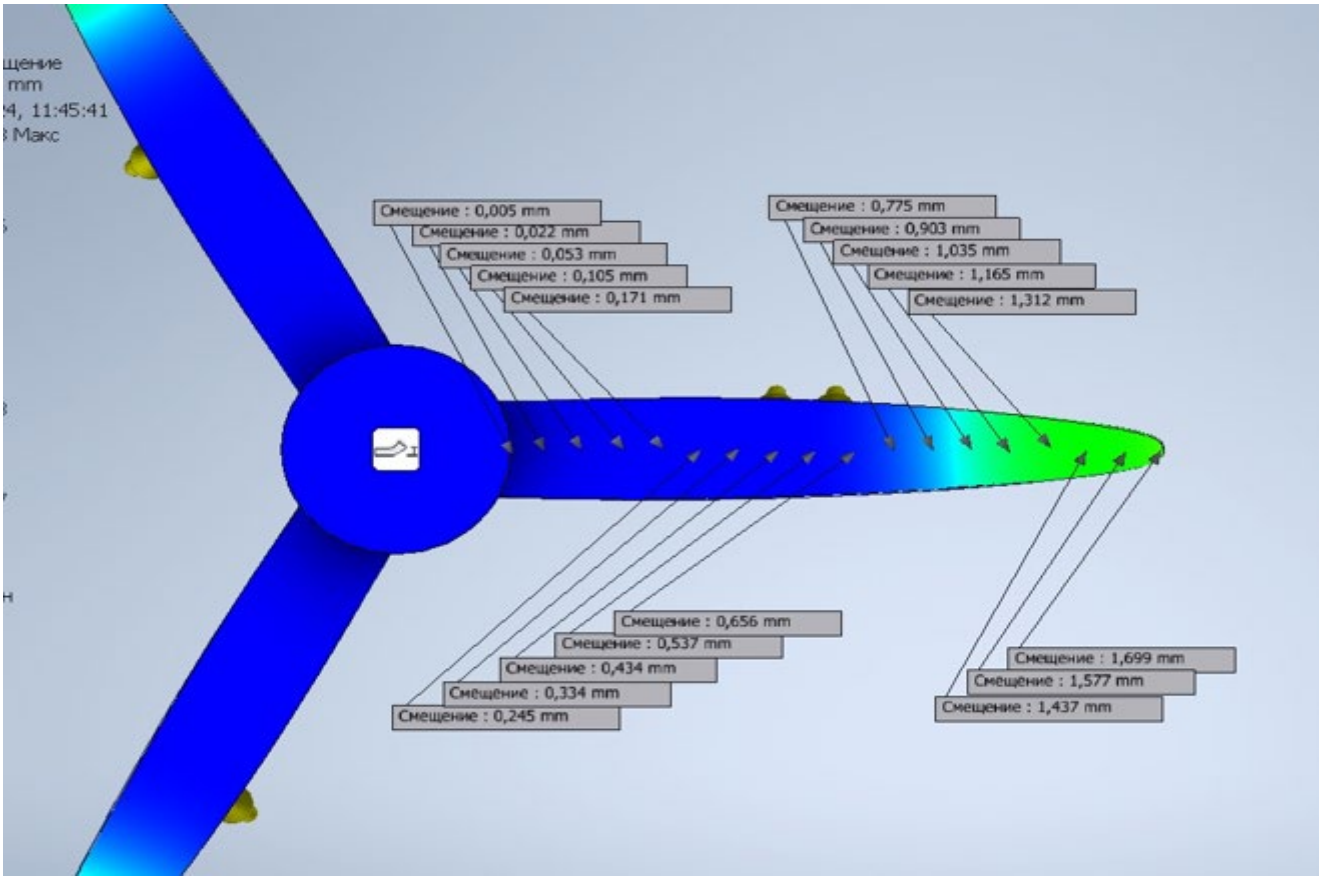

Figure 3.23: Strain distribution on step 15

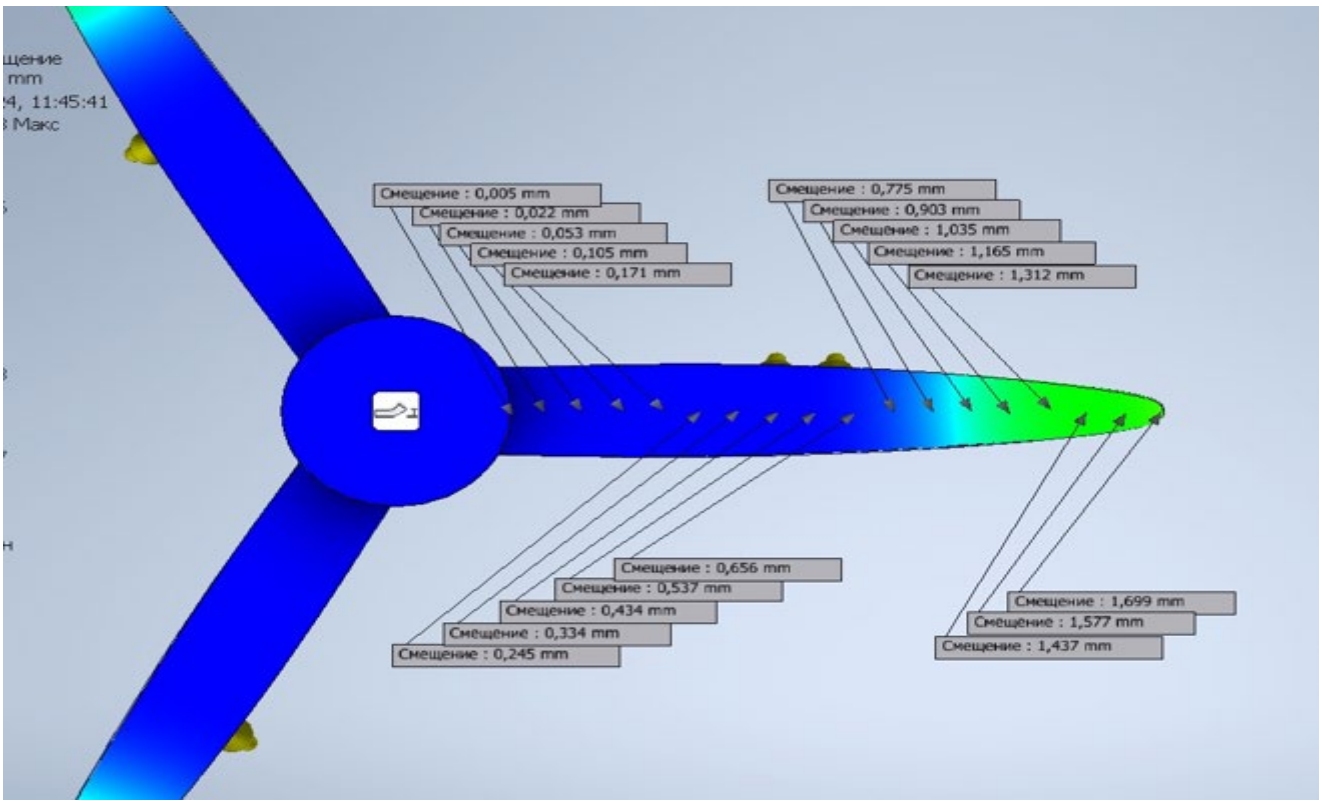

Figure 3.24: Strain distribution on step 18

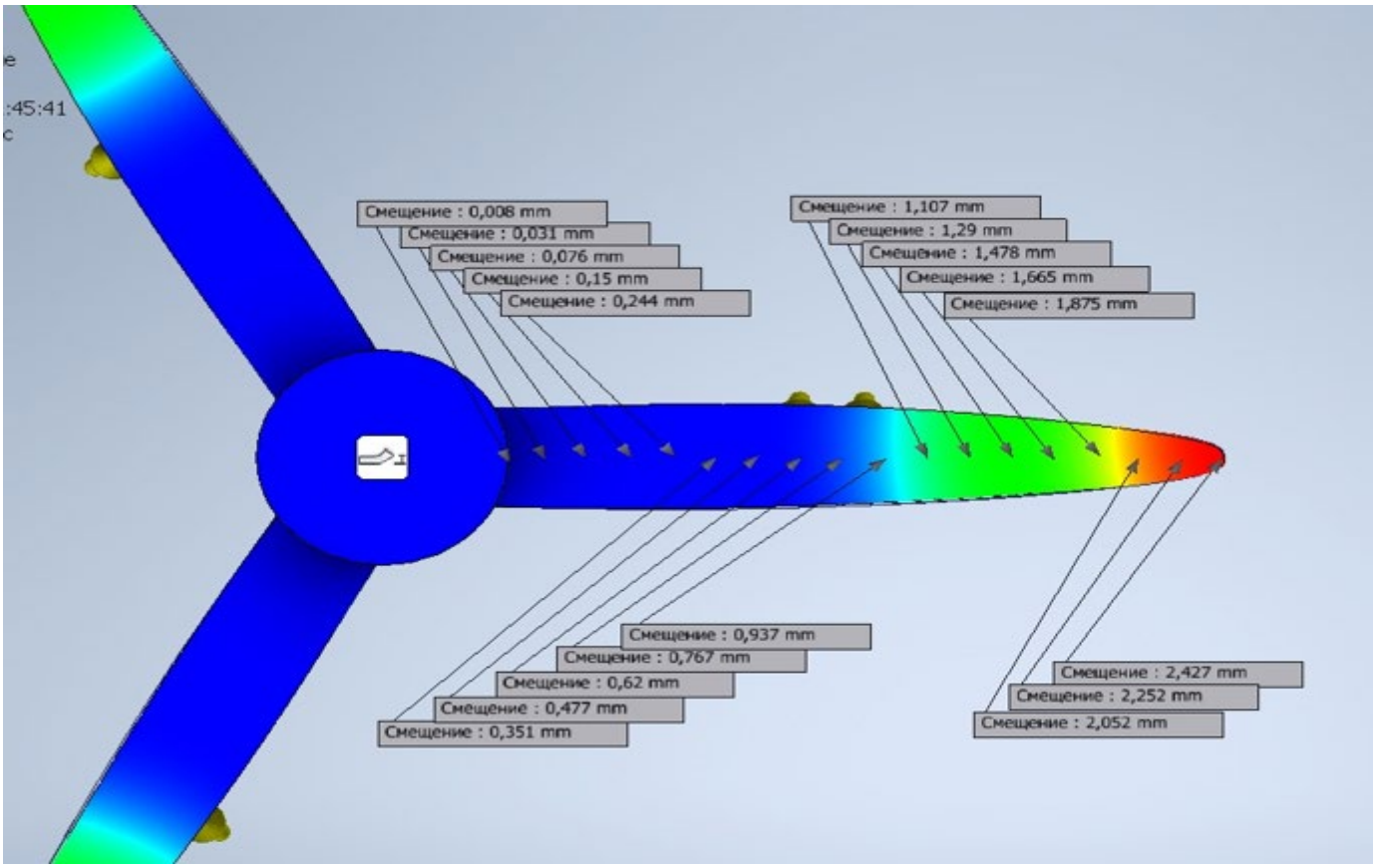

Figure 3.23: Strain distribution on step 20

Chapter 4

Experiments

4.1 Introduction

The Additive manufacturing (AM), by PBF technique has permitted the production of complex aerospace components with reduced material waste and augmented design flexibility. These includes turboprop propeller components which plays a critical role in converting rotational power into thrust in turboprop engines.

The propeller component in this research is manufactured using AlSi10Mg, an aluminium-silicon-magnesium alloy. This propeller material alloy is a known for its excellent strength-to-weight ratio and corrosion resistance amongst others. These properties make it well-suited for aerospace applications, including propeller blades, where performance and reliability are key. The layer-by-layer nature of this AM process presents numerous discontinuities, such as porosity, delamination and cracks. These manufacturing discontinuities create susceptibility of the mechanical properties which affects the integrity and fatigue life of the component. Such defects act as stress concentrators and potentially leading to unplanned cyclic loading failure.

The engineering principles requires amongst others testability and traceability of material including the components which are additively manufactured. Non-Destructive testing in this research specifically Radiographic Testing Computed Tomography was used for validation the defect location, defect geometry and most crucially gaining confidence in defect characterization of additively manufactured components as part of quality assurance. The conformance of Computed tomography was used as a method of inspection to address the second objective mentioned in chapter 1.

This chapter determined the ability X-ray Computed Tomography on finding defects in complex shaped additively manufactured propeller made of AlSi10Mg. These findings were intended to assess the credibility of advanced radiographic testing method in terms of the image resolution (ability of an NT method to determine defects that are close to one another) and the sensitivity (ability of the NDT method to determine the smallest defect). These parameters are the driving force in terms of seeking the appropriate NDT methods.

The experiments in this chapter were also used in determining the possibility of complementation of the results found in chapter 3 and the experiment results. The procedures followed by the researcher were not always standard specific but mainly principle specific and tailored to reproduce a set service conditions (angle

of inspection, radiation penetration power etc.).

The procedure followed had entailed the aim of the experiments; the purpose was outlined; the list of apparatus used, step by step description to every step taken in assessing for integrity of the material and lastly the results in term of digital radiographs were given as evidence.

4.2. Non-Destructive Testing of AM propeller

NDT was applied on the propeller to assess for the presence of defects and localising these defects. This method was used to also validate the results found from the ABAQUS prototype of an AM propeller component and AM tensile samples. The blades were inspected at region of interest (RIO). The ROI was all the blades length as well as where the blade joins the hub.

There were 2 attempts made in this experiment in pursuit of confirming the result outcome.

Aim: The purpose of this experiment was to conduct computed tomography (CT) for validation of defects in an AM propeller Blade 1,2 and 3

Apparatus used.

(a) CT scan machine
(b) AM propeller sample
(c) Computer aided soft were for analysis.
(d) Form for structure support.

Step by step description

- Preheated the X-ray CT machine.

4.1: X-ray CT scan Machine

- Prepared the specimen (propeller) identification by numbering each blade 1,2 and 3 using a masking tape.

Figure 4.2: preparation & identification of propeller blade for CT scans

- Positioned the blade at each time and focused the region of interest (ROI) to the CT scanner into a chamber outfitted with an emitter that emits X-rays from a multitude of different angles. The detector which captures the energy that hits the object as data is mounted opposite the X-ray focal spot. Once X-radiation is attenuated by the complex dimension of the blade wherein will produce computed reconstructed images in three dimensions, meaning that even the defects present will be viewed in three dimensions.

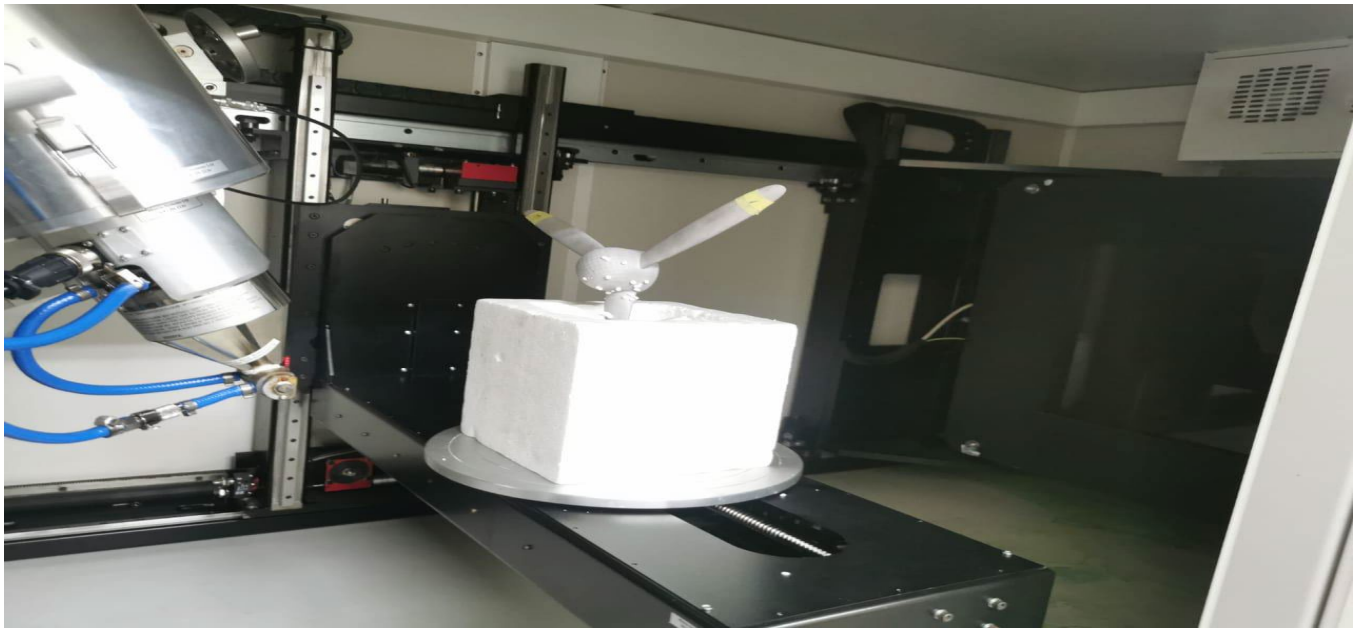

Figure 4.3 CT X-ray focusing cone and positioned propeller

- **3D image results from a CT scan**

(i) Blade 1 CT scan results

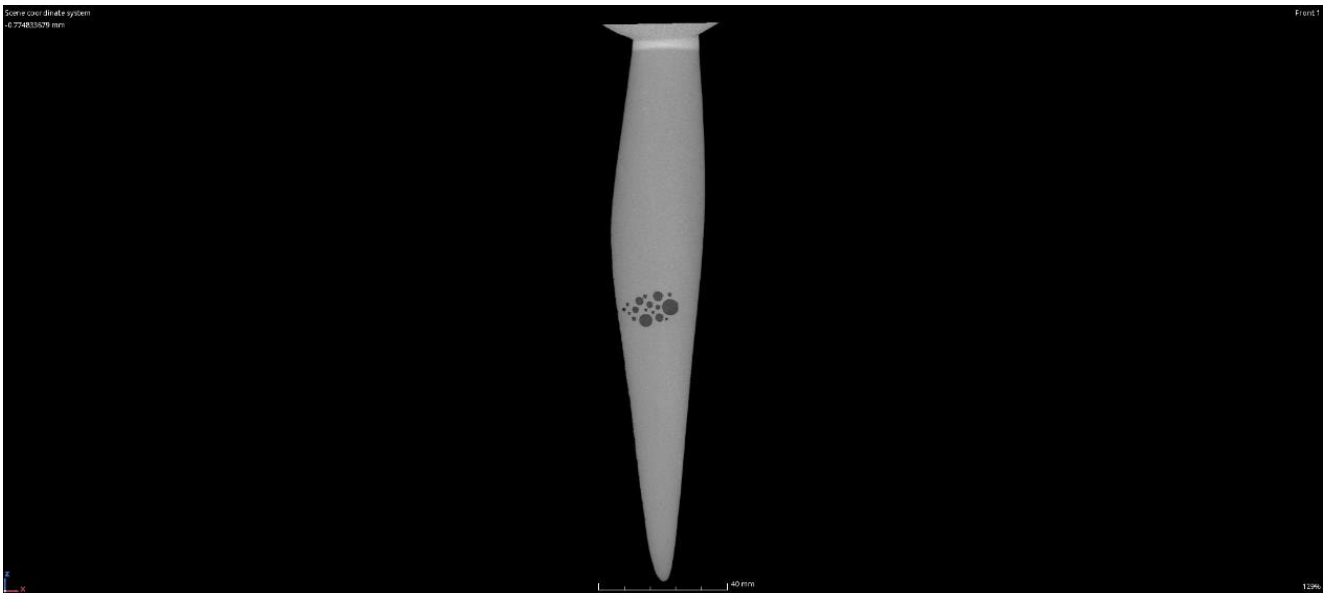

Figure 4.4: View1 image cluster porosity on marked blade 1

Figure 4.5: Projection results on marked blade 1

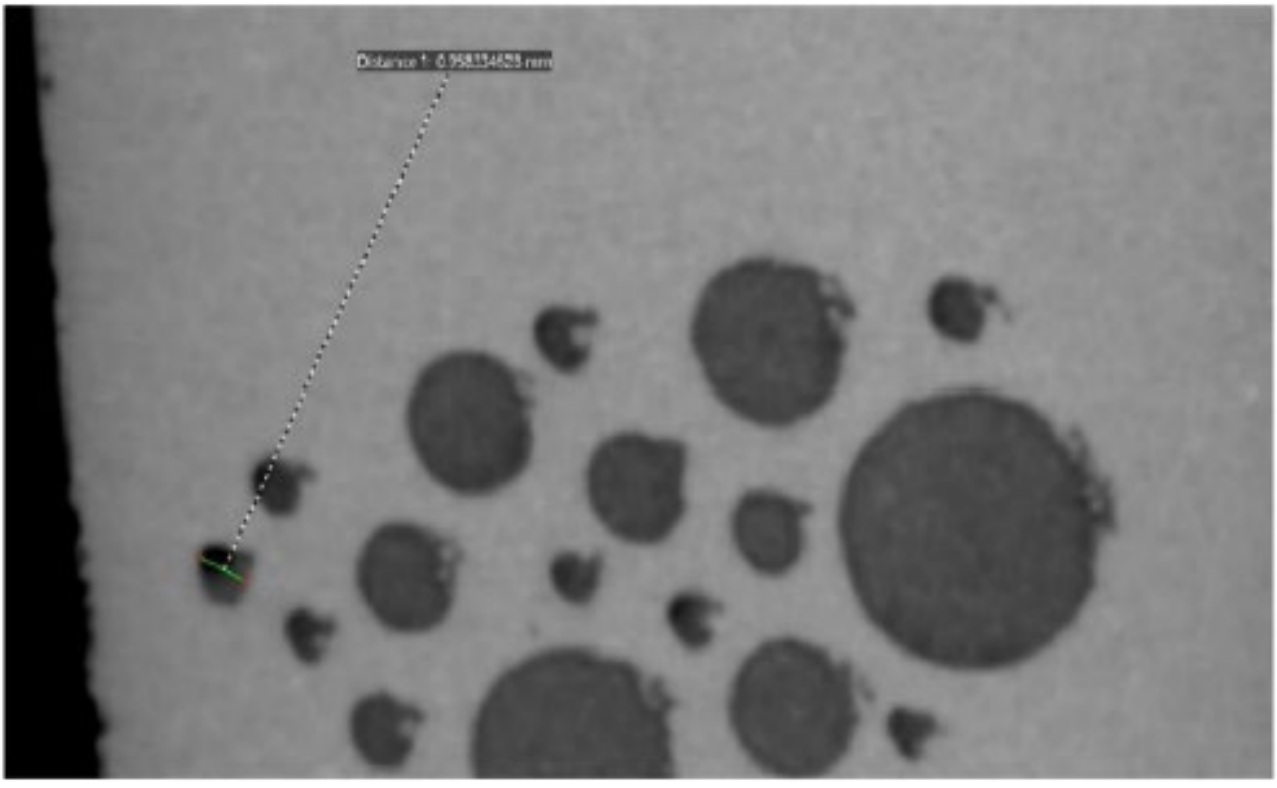

Figure 4.6(a): CT scan projection results of cluttered porosity with diameter of the biggest pore blade 1

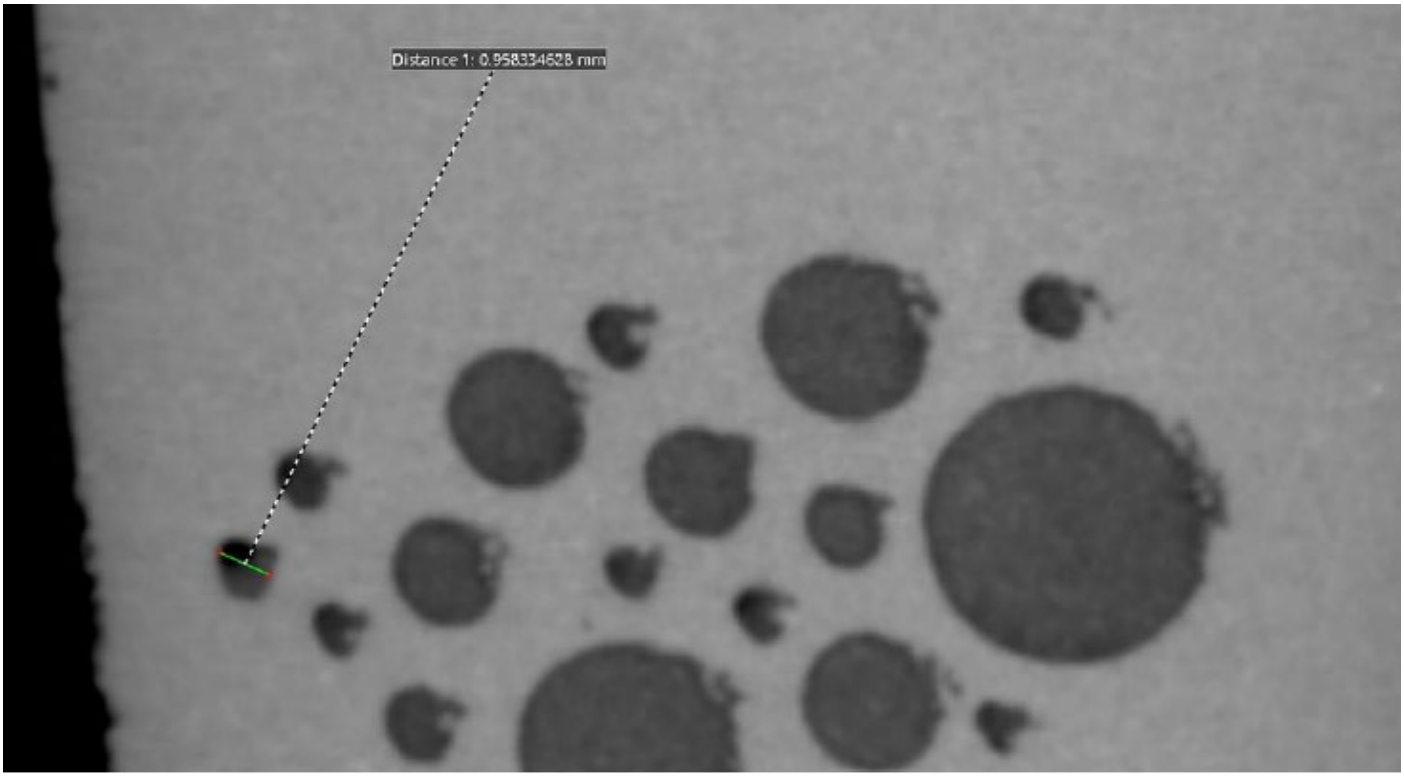

Figure 4.6(b): CT scan projection results of cluttered porosity with diameter of the biggest pore on blade 1

(ii) Blade 2 CT scan results

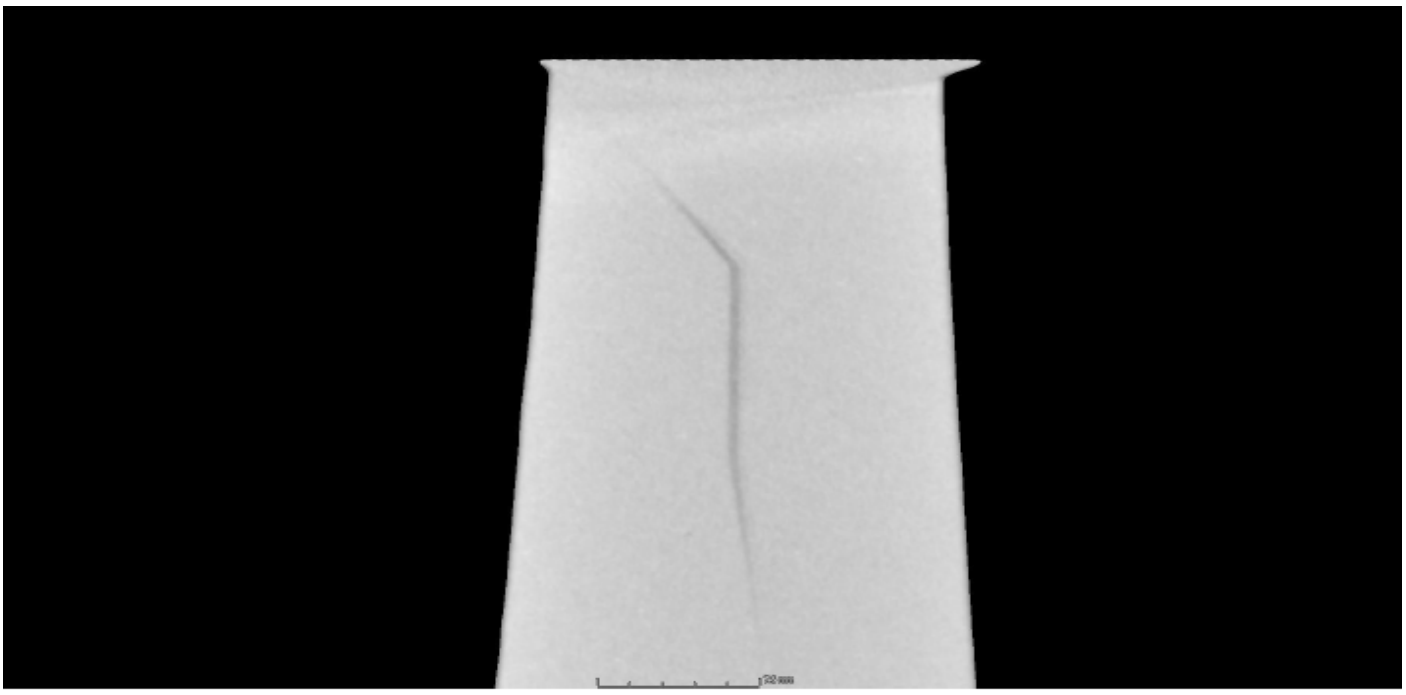

Figure 4.7(a): CT scan projection results of linear indication (crack) on marked blade 2)

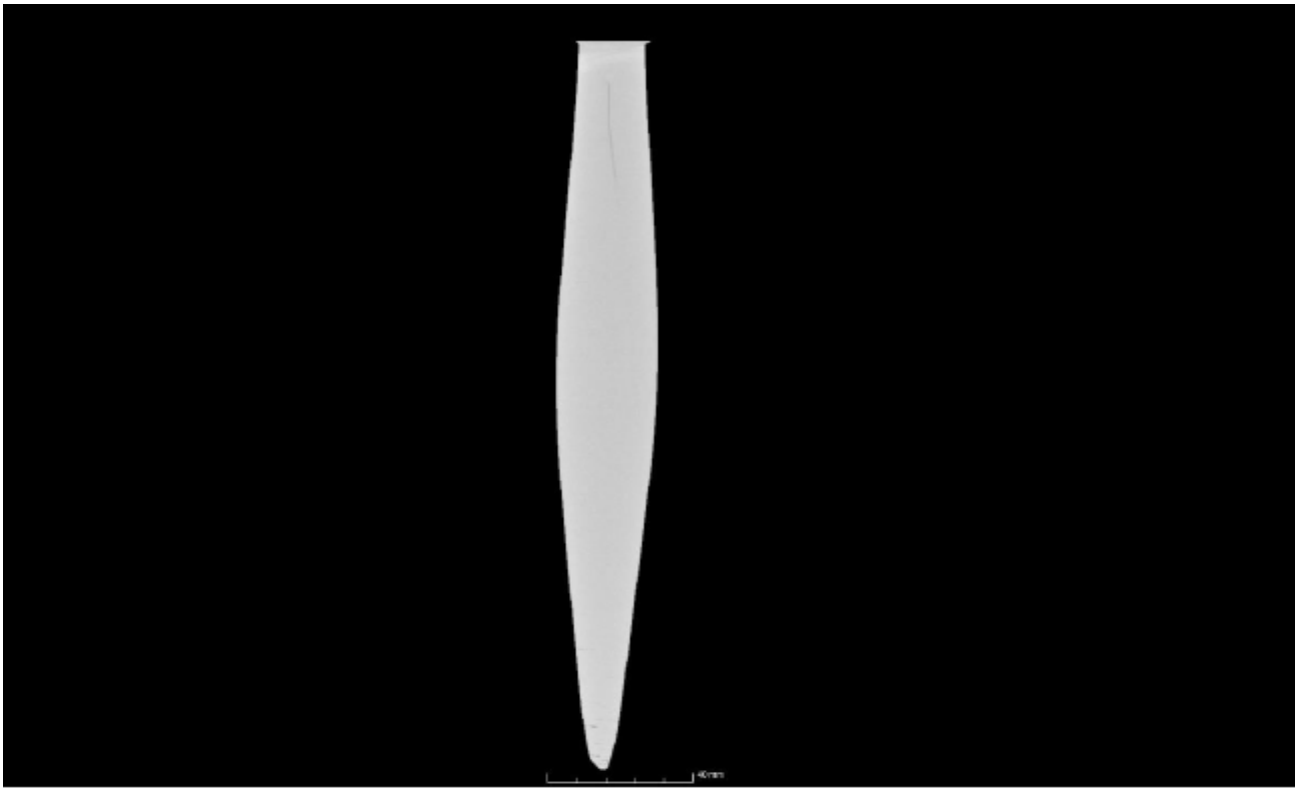

Figure 4.7(b): CT scan projection results of linear indication (crack) on marked blade 2

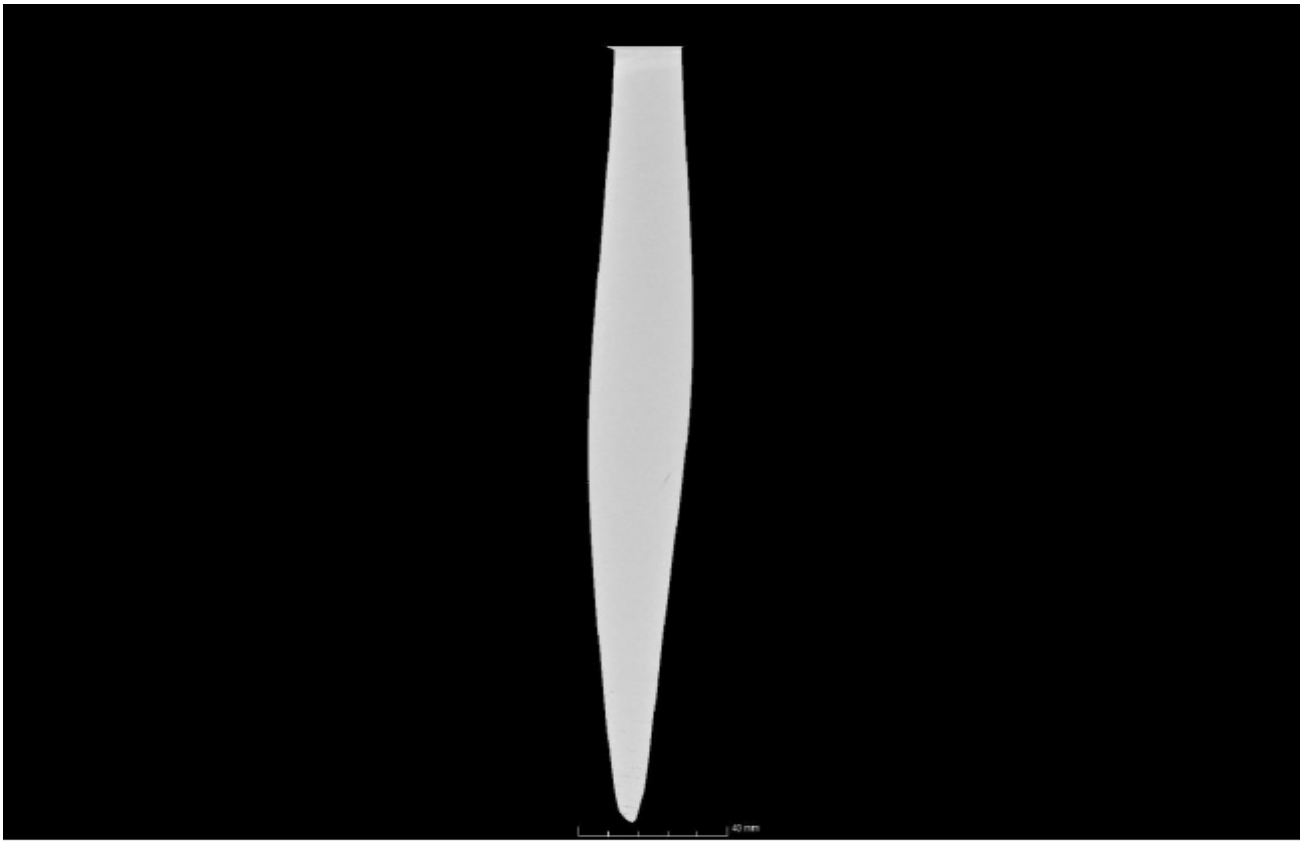

Figure 4.7(c): CT scan projection results of no indication (crack) on marked blade 2 (skewed view)

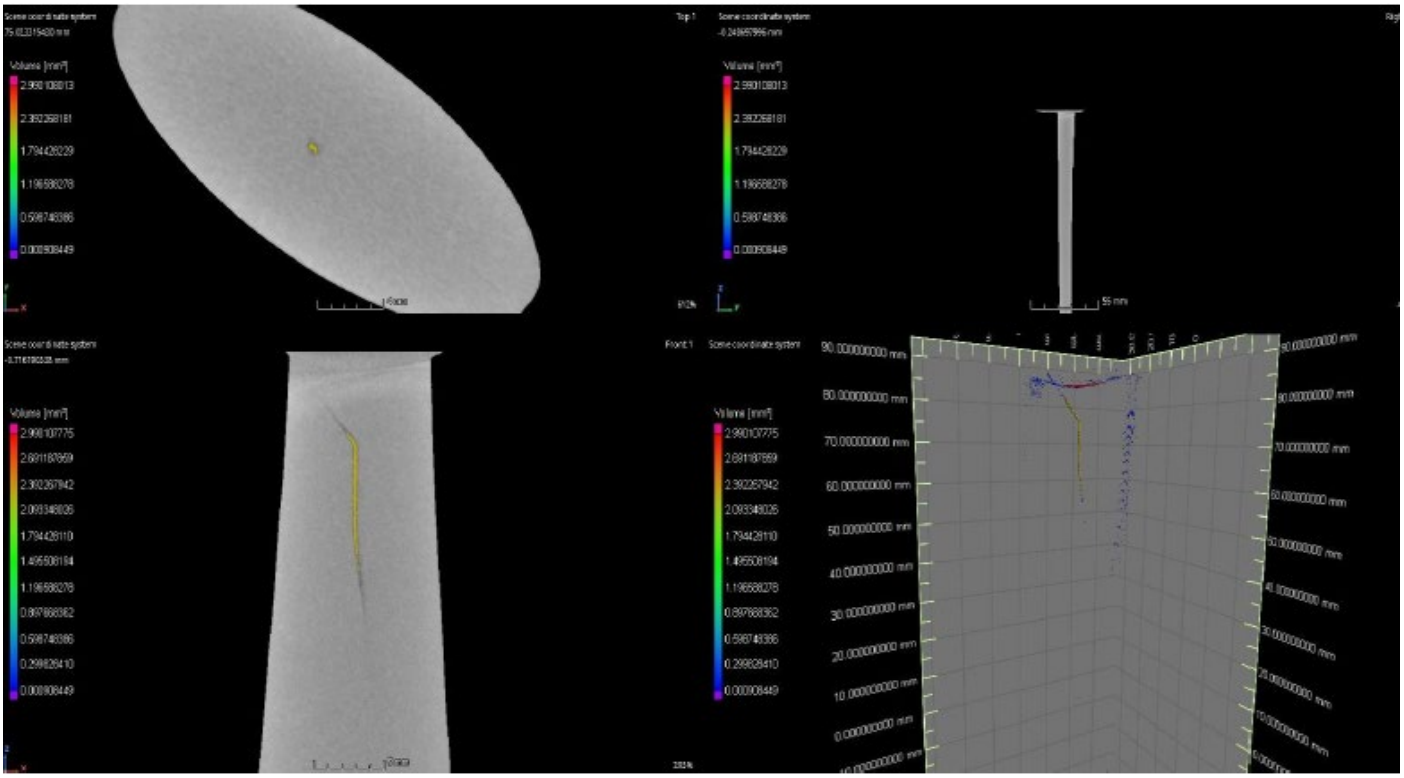

Figure 4.7(d): 3D CT scan projection results of no indication (crack) on marked blade 2

(iii) Blade 3 CT scan results

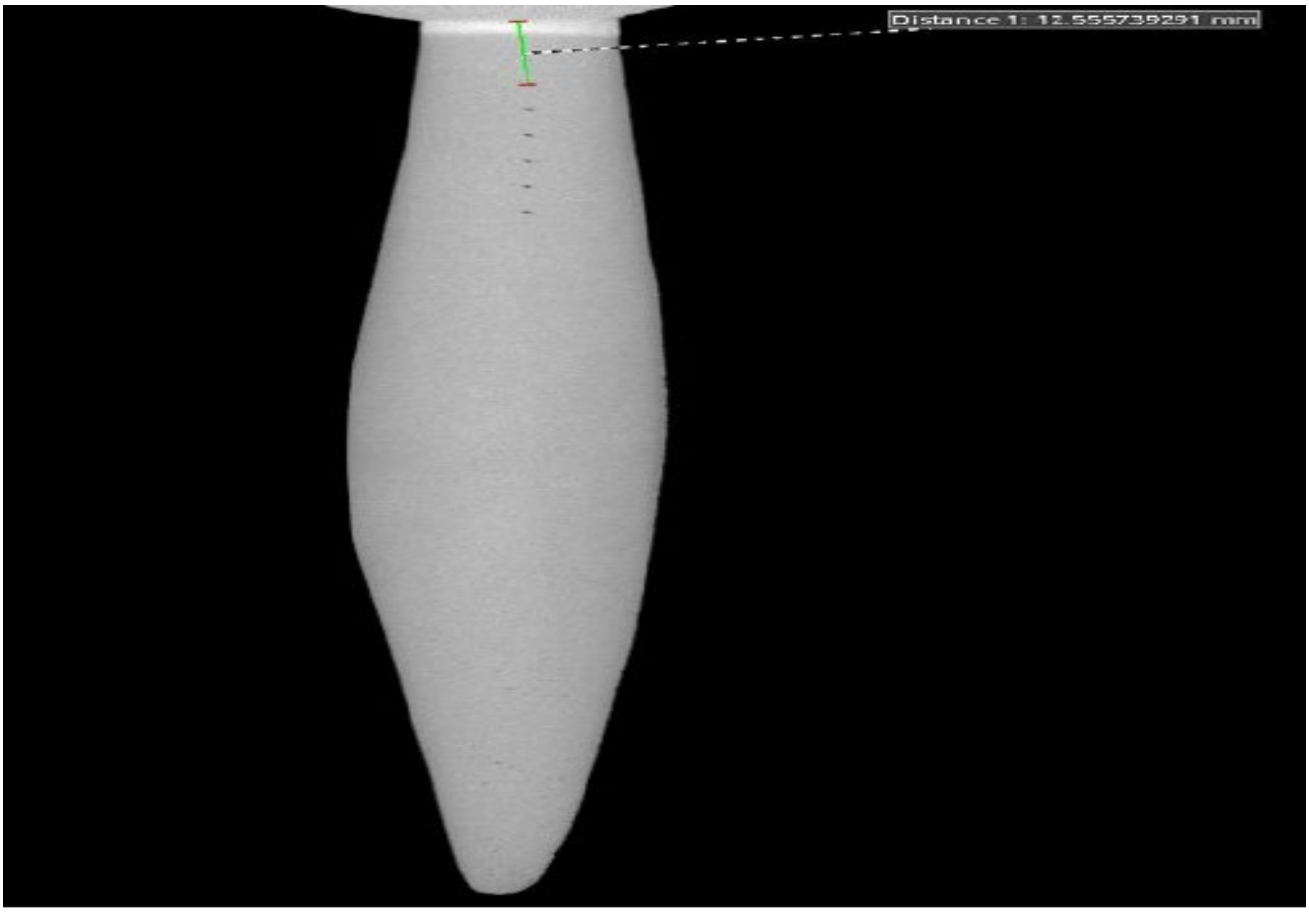

Figure 4.8(a): CT scan projection results of no indication (delamination) on marked blade 3

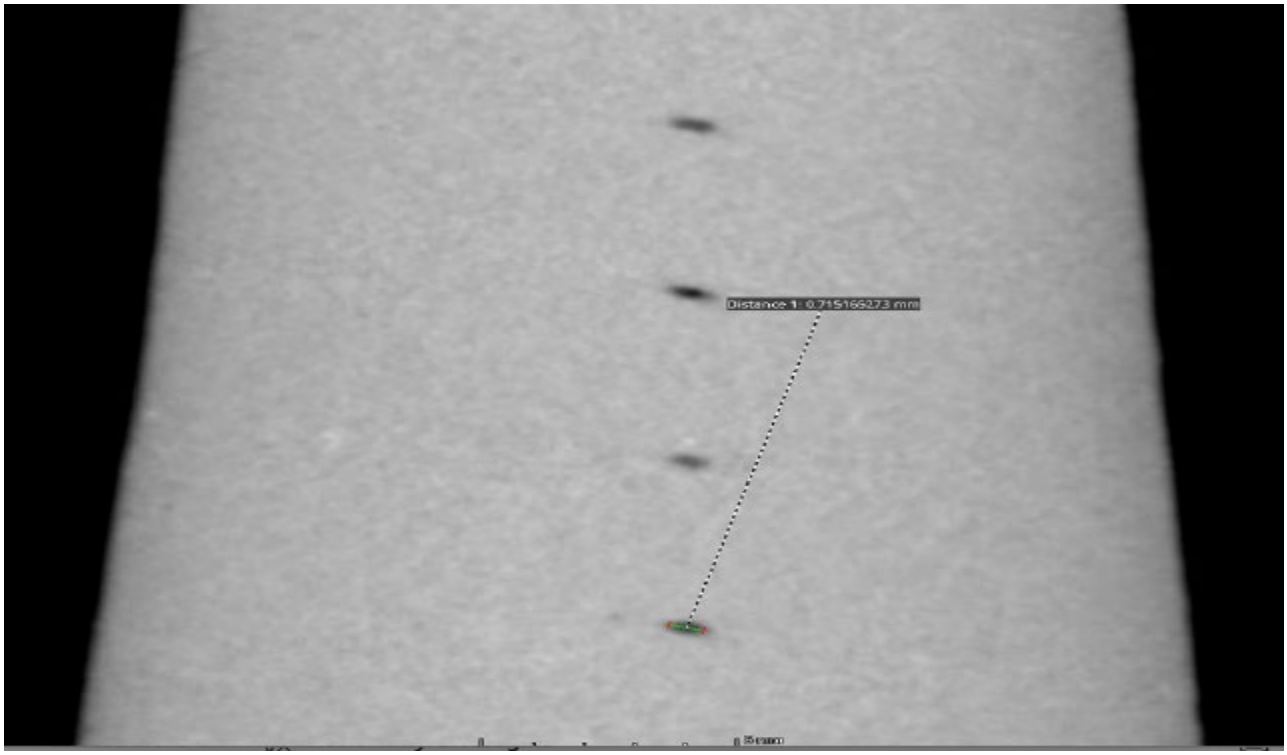

Figure 4.8(b): CT scan projection results of no indication (delamination) on marked blade 3 with sizing

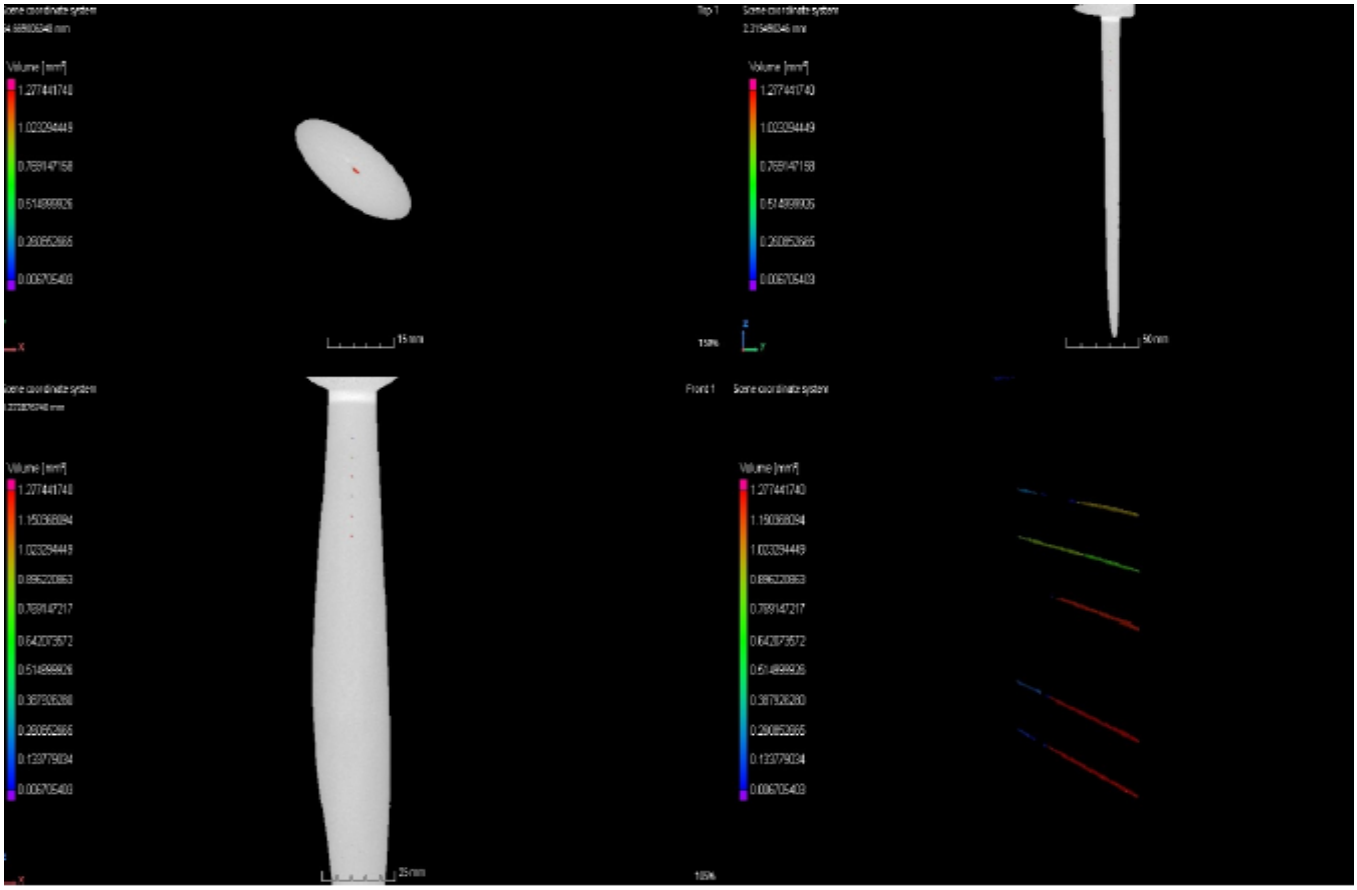

Figure 4.8(c): 3D CT scan projection results of delamination on marked blade

Chapter 5

Results discussion

5.1 Introduction

The production of an additively manufactured aluminium propeller using Powder Bed Fusion (PBF) had suggested to have accurate manufacturing dimensions as drawn by the SolidWorks CAD software for this research. The propeller's material characteristics used in this research for both simulation and production are listed in Table 2.1 in Chapter 2. The defects to be analysed are presented in table 2.2 and assessed in chapter 4 are to be confirmed in this chapter.

This research chapter discusses the outcomes from the data collected through the results of the simulation of an additively manufactured (AM) propeller. The simulation of AM propeller had initially determined the stress distribution around the propeller hub and after had determined the strain distribution. Finite element results to determine the behaviour of stress along the blades of the propeller in relation to defects presence were discussed. The results of the analysis of a randomly sampled blade are discussed here with an intention to understand the effect of the presence of defect when the AM component is under a cyclic loading.

The presentation of Non-Destructive Testing Computed Tomography (NDT-CT) results was discussed to validate the outcomes from the results of finite element analysis. As NDT plays a crucial role in quality control and assurance this chapter saw it fit to also discuss the NDT capabilities on AM complex structures such as AM propeller.

The X-ray Computed Tomography was the used method of inspection for the analysis of internal defects.

5.2 Simulation Results

The finite element method (FEM) was applied in this simulation. It is discussed that the finite element equations in the ABAQUS software were established in Chapter 2 (i.e. eq. 2.10 - 2.21) for the simulation of static analysis. The results for both stress and strain distributions were obtained and observed. It is worth noting that the researcher was mindful of the fact that there were other advanced modelling systems for simulation of additive manufacturing however the parameters used in the ABAQUS software were assumed to demonstrate the mechanical character of an AlSi10Mg AM solid component.

This research distinguished that the hexagonal quadratic meshing was not supported during the simulation when they were selected during the numerical analysis. This occurred due the complexity of the components' geometry on the blades, therefore this research confers that such types of meshes are not precise on finite element analysis of complex structures.

The tetrahedral mesh was the most suitable mesh on this component as shown in Figure 3.9 (tetrahedral meshing of the propeller blade), and it gave results from surface contours because of the complex geometry of the AM propeller. This discussion therefore supports the findings by Mehemert P (2023) who articulated in this research literature that tetragonal meshing is highly considered and recommended in complex-shaped components for FEM analysis. This research conducted 20 tempts of mesh and remeshing of the simulation of the propeller.

The stress around the hub showed to be constant in the y-direction when under rotation. There was a variation of stress distribution during a non-linear static analysis, the component was not rotating, the research simulated the effect of the centrifugal forces caused by the imposed rotational velocity on the three blades when the propeller was under rotation. The centrifugal force, during the rotation of propeller blades had demonstrated to have contributed toward the creation of stresses acting on the propeller blade. The simulation analysis was done to obtain the stress distribution and the corresponding defected area or position. The plane stress distribution was obtained for a static loading of twenty-one (21) steps by satisfying equation 2.13. The simulation of the propeller demonstrated noticeable stresses acting on it. It was equally noticed that no minimum stresses were around the tip of the blade in all twenty-one (21) steps of static loading, this is due centrifugal forces, however there were stresses acting at the joints of hub and blades. It was therefore those variations on blades that address the intent of this research. Chapter 1 mentioned the type of sampling of defects to take place during the analysis. Therefore, a random sampling approach of the blade with defect(s) for analysis was done.

Figure 3.10 (stress distribution on step 1) shows Step 1 at the beginning of the first step of the non-linear analysis there was a 0 MPa of stress distributed around the whole propeller. The progression of steps shown

an increase in stress distributed around the blades closer to the hub as shown in figures 3.11, 3.12,3.13 respectively indicated 29.1MPa, 65.4 MPa and 101.8MPa stresses. These stresses were coded with a colour green, meaning that the stress distribution is still allowable or at the range that is still normal. This result could be the fact that the propeller rotation was slow leading to the propeller to endure 101.8 MPa stress without a cause of susceptibility to failure at step 15. Figure 3.14 show results of Step 18 where a concentrated stress of 123.6MPa was noticed occurring closer to the blade root and consequently in step 21 endured a concentrated stress of 137 MPa (see figure 3.15). The localised stress in colour red were noticed and with this specific blade and more analysis was made.

A random sampling on blade analysis was done with a consideration of a simple one-dimensional (x-direction) analysis. A plotting of eighteen points along the x-axis of the blade were made as shown in figure 3.16 where a variation of stresses distributed started to show in step 2. This was done to assess the stress variations along this blade. The ABAQUS system was ran again to assess the variation of stresses along the blade for the preceding twenty steps.

The stresses started to vary from step 2 showing results of a minimum stress of 0.1 MPa at the tip of blade and maximum of 5.3 MPa near the hub. There was a noticeable sequence that the stress distribution ascends from the tip of the blade to the root at increment of 0,5 MPa however at position 15 to 17 there was a dynamic increase of stresses which is suggested to be an area of a concentrated stress with minimum of 4,5 MPa and maximum of 5.5 MPa. This led to a stress concentration factor of 1.2 and consequently in step 20 the SCF was1.36.

The stress concentration factor (SCF) is a dimensionless factor that quantifies the increase in stress in a material due to the presence of geometric discontinuities such as holes, notches, cracks or changes in cross-section. An SCF of 1.36 means that the maximum stress at the discontinuity is 1.4 times the nominal stress (the average stress calculated without considering the discontinuity). This factor is almost twice the nominal stress.

It was similarly observed that as the steps increase, the stress distribution also increases from the blade root toward the blade tip as shown in Figure 3.20 this could likely be due to the centrifugal force which is the principal acting force during the 750 rad/s rotation speed of the propeller used. The results of stress in Figures 3.17,3.19, 3.20 and 3,21. (*Stress distribution in steps 5,15,18 and 21)* ranged from 0.1 MPa at the tip of the blade to 137 MPa closer to the root (hub). This is due to the propeller being subjected to load leading to the stresses acting on the defective blade varied along the blade's length (from the blade tip to the blade root).

A stress intensity factor (SIF) vs crack length calculation was done by MATLAB and presented graphically. Using equation 2.1 for computing the stress intensity factor *K* for this sampled blade was assessed to obtain result in graph 3.1. The sampled blade had a linear crack of the length 10 mm. The SIF results presented in

suggested that the component with an internal defect which is assumed to be a 10mm linear crack is likely to have a regime 3 fracture or Fracture mode III behaviour, denoting that the was a likelihood of the defect growth rate to be immediately rapid. In the context of Mode III defect propagation, which involves out-of-plane shear (associated with shear loading), the stress intensity factor (SIF) plays a critical role in determining the stability and growth of cracks in materials, including additively manufactured AlSi10Mg components. This mean that the crack growth is not stable or not propagating linearly hence a dynamic growth.

The propagation of a crack in an aluminium blade was seen to likely have several significant impacts, because as the crack propagates, it was likely to compromise the structural integrity of the blade, which could have led to failure during operation. Since the real blade would be exposed micro-impacts through vibrations and unsteady aerodynamic force that will encourage defect growth. Conditions such as thermal vibrations, fatigue loading and environmental pressure will increase the likeliness of compromising the integrity of the blade. This is particularly critical in applications like aerospace, and it is therefore these reasons that such defect should be evaluated and controlled by methods such as NDT.

These stress levels result along the blade, were higher at the area that is assumed to be defective. The defected area demonstrated to have stress values ranging from 105MPa at the defect edges to 137MPa towards the middle of the defect. A Non-Destructive Testing method, Computed Tomography which will be discussed below, validated the presence of defect around this sampled blade. The figures 4.1-4.8 (c), shows the results of an advanced radiographic testing technique using X-rays by which it demonstrated different internal defects in each blade. The defect length was 10mm with an unpredictable growth direction.

These results obtained suggested that the presence of the linear defect affects the deformation at and around the blade tip and the stress to be higher at the defected region. This is argued by the tensile test results as shown in appendix B. these were the result of a sample that was manufactured additively with an interval linear defect. The internal defect (crack) in an AlSi10Mg showed that the stress at maximum load is almost equivalent to a fracture point. These results showed that a sample with defects (linear defects) is likely to endure a higher yielding strength.

Crack is likely to reduce the fatigue life of the material, meaning the blade can fail after fewer cycles of loading and unloading than originally expected. The number of circles to failure are not possible to compute since the defect length is at a critical state meaning it is in a mode III fracture state. The efficiency and performance of the blade may be adversely affected. For example, in an aeroplane blade, a crack could lead to unbalanced forces, causing vibrations and potentially damaging surrounding components. The facts that the original bulk design strengths are not surpassed, and the simplest caution signal of an impending fracture is regularly a crack that direction of propagation is not easily predicted, makes crack damage dangerous (Plessis et al., 2016).

The crack propagation expectation is highly sensitive to stress variations due to load ratio, and thickness, noting that the environmental effects may have influence. This agrees with the findings of Chen et al. (2021) that the presence of the defect affects the mechanical properties of an AM propeller noticeably in this research, the stress, strain, and brittleness. This also supports the article that stated that defect tolerant approaches to component fatigue is to predict consistently on the growth of pre–existing cracks of specified initial size (a_i), shape, location and orientation in a structure subjected to a pre-set cyclic loading (Miloˇ, 2017).

Therefore, providing the defect growth prediction in mode II lead to the suggestion of inspection and service intervals to be established and in this research case the defect size reflect to be on the critical state of mode III which means that the repairs should be immediately or rejected.

This paper also deliberates that monitoring and repairing cracks in AM propellers can increase maintenance costs and downtime, affecting overall operational efficiency as well as the likelihood of altering the local material properties around the crack tip, potentially leading to further degradation or unexpected behaviour under load. This shall significantly cause risks of catastrophic failures.

The interaction between deformation and crack propagation in rotating AM aluminium blades is complex, involving numerous factors that can significantly influence the integrity and lifespan of the component. Monitoring and managing these effects are critical for safe and reliable operation. The presence of a crack demonstrated to have altered the stress distribution in the propeller blade.

This suggests that a crack in an AM aluminium part that has a stress concentration factor of 1.2 should typically lead to rejection. The presence of a stress concentration factor means that stress is amplified in the area around the crack. This increases the likelihood of crack propagation, especially under load (rotation). When the components are under loads, naturally will experience cyclic or high loads, even a small crack can grow over time.

In applications where safety is critical (like aerospace or automotive), any defect that can lead to failure is usually unacceptable. Although there is no definite acceptance standard for AM components, most engineering standards and specifications require components to be free of critical defects.

A crack is typically seen as a major defect and the potential cost of a failure, including injury, loss of life, or damage to other part, far outweighs the cost of rejecting a flawed part. SCF of 1.2 indicates a minor increase in stress, the presence of a crack often raises serious concerns. This paper therefore spots it typically beyond compared to err on the side of caution and consider rejection or further evaluation in this event.

The strain on the other hand is noticed to be the largest at the tip of the blade and gradually decreases toward the root of the blade. The hub had a deformation of 0.006 mm, the centre of the blade had 0.767 mm of

deformation, and the blade tip has 2.427 mm. This shows that due to the thickness variation of the blade, deformation dominates at thinner thickness sections while the stress dominates at the thicker sections. These results are assumed to be a result of centrifugal force that pulls the blade outwards during rotation. Deformation was likely to worsen the stress concentration, potentially leading to crack propagation.

These results also demonstrate that deformation is likely to affect the balance of the propeller. An unbalanced propeller can lead to vibrations, which can further stress the structure and potentially worsen the crack or cause additional failures. Deformation may also lead to changes in the aerodynamic profile of the blades, resulting in decreased efficiency and performance

Additively manufactured aluminium may have slightly different mechanical properties compared to conventionally manufactured materials meaning that the deformation result found in this research simulation were likely led to unexpected behaviour, such as localized yielding or differences in the material's response to stress. This therefore mean that deformation in a cracked rotating AM aluminium propeller poses serious risks and can lead to rapid deterioration of the part, potentially resulting in catastrophic failure. Regular inspection and maintenance are critical to ensure safety and performance. These results on deformation suggest that it may be harder to inspect the crack effectively which could be complicating maintenance and safety assessments of the AM propeller structure.

5.3 Experimental Results

Micro-X-ray Computed Tomography (μX-ray CT) is a non-destructive method, allowing for the evaluation of components without compromising their integrity. This is especially valuable for high-value components where traditional destructive testing methods would be impractical. The experimental results on computed Tomography had demonstrated evidence that the AM component had internal defects at different locations and having different geometries.

The use of a μX-ray CT offered high-resolution imaging and detailed insights into the internal structures of AM aluminium blades, making it an effective tool for defect detection and integrity assessment. The internal defects in this research were suggested to have contributed and influence the stress and deformation distributions in AM component.

A voluntary procedure for NDE μX-ray CT of AM components was developed to provide concise values of kV, amperes, number of slices, extent on examination, source to detector distance etc. The aluminium blade was carefully prepared, positioned and placed in a sample holder within the μX-ray CT system as shown in figure 4.3. The blade was subjected to a series of X-ray beams while rotating around an axis. The X-rays penetrated the material and were absorbed differently depending on the density and any internal structures, such as cracks.

As the X-ray source rotated, 1000 projections for each blade and at high resolution that could detect a defect with a length of 0.2 mm were captured from different angles. This created a comprehensive set of data regarding the internal structure of the blades. The collected projections were processed using algorithms to reconstruct a three-dimensional image of the blade. This 3D model provided a detailed view of the internal features, including any defects such as cracks, porosity or delamination.

The reconstructed image was then analysed to identify and characterize defects. The size, shape, and location of the defects were assessed, allowing for evaluation of their severity and potential impact on the blade's integrity. Advanced software tools provided a quantitative data regarding crack dimensions and other relevant features.

µCT allows for the non-destructive detection of internal defects such as porosity, voids, and inclusions, which are common in AM processes. These defects can significantly impact the mechanical properties and performance of the finished part. The algorithms such as Filter back projections (FBP) and iterative reconstruction (IR) are fundamental to the functioning of µCT in non-destructive testing, enabling detailed internal imaging and analysis of materials.

The microfocus unit with low X-ray penetration energy of 80 kV and a current of 2A was used. The visualization and interpretation were performed through the VG-Studio Max 2.2 software which allowed a 2D and 3D interpretations of defects. The µX-ray CT scan result on blade 1 showed internal cluster porosity of different diameters (see figure 4.4 - 4.6(b)). The smallest diameter found was 0.9mm (see Figure 4.6(b) chapter 4) and the larger diameter was measured to be 5.0mm (see Figure 4.6(a) Chapter 4). CT scan was also able to estimate the depth of the defect from the projection.

Blade 2 had an internal linear indication which could be a crack. The simulation results for the finite element analysis reflect to agree with the results found in the experiments for the Non-Destructive Testing. This defect was difficult to detect at other angles of projections and will reflect the blade to have no defect (see figure 4.7 (c)) at a skewed view. The defect was interpreted to be present at a top view confirmation in figure 4.7(d) top left image projection and bottom left image projection. The length of the defect was measured by the software to be 10 mm. These results agree with the defect design by SolidWorks, therefore demonstrated accuracy in geometric definition.

The defect was located at the root of the hub and the direction of propagation was toward the tip of the blade. These results complement those that are identified in the simulation. This ability of detectability of linear indication by µ X-ray CT demonstrate that NDT is an exceptional tool to be used in investigation of such discontinuities. These results are also supported by Cheng (2021) who is mentioned in the literature that, the crack initiation can be accelerated mainly because the irregular morphology can produce higher stress

concentration. They further noted that the distributions of defect sphericity follow the trend of high localised stress concentration. These trends were like those found by other researchers they had discussed who also mentioned that defect size had an influence on buffer crack nucleation and failure and NDT was the best approach to investigate such defects Cheng (2021).

Blade 3 result demonstrated the presence of delamination which was located 13 mm from the hub.

These results were useful in assisting to assess the influence of presence of defects from the simulation result and the NDT results. a high deformation at the blade tip will promote the defect geometry change, while the high stress at the root will promote defect growth.

The solutions obtained here demonstrate to create a data of effect-of-defect haviour of AM aluminium component that is under load by specifying the values of stress intensity factors of 1.36, maximum stresses of 137MPa. Micro X-ray computed tomography (μCT) is an effective acceptance method for assessing additive manufactured (AM) aluminium components. The mean μX-ray CT can be utilized to measure the geometrical features of complex AM aluminium components with high precision. By comparing the scanned 3D model to the CAD design, manufacturers can ensure that the dimensions meet specified tolerances

In additive manufacturing, layers were built sequentially. μCT demonstrated the ability to assess the integrity of these layers by ensuring proper bonding between them, which is critical for achieving the desired mechanical properties. These capabilities therefore mean the integration of μ X-ray CT into the quality control process will contribute towards manufacturers establishing acceptance criteria for AM aluminium parts. This involve setting limits for defect sizes, porosity levels, and dimensional deviations. The detailed imaging and analysis provided by μCT serves as documentation for compliance with industry standards and regulations. This is particularly important in sectors such as aerospace and medical devices, where safety and reliability are critical.

This research chapter, therefore, supports the idea that regions with higher stress concentrations in a complex additively manufactured structure such as propellers are more prone to defect (crack) initiation and growth, which in turn increases the likelihood of detecting those defects (cracks) through various NDT inspection techniques such as μ X-ray CT. The Chapter therefore had demonstrated that the relationship between stress concentration factors and NDT using micro-CT includes detecting and characterizing defects that influence stress distribution and failure modes in materials. This understanding is crucial for improving the reliability and lifespan of components, particularly those produced through additive manufacturing.

Chapter 6

Conclusion

The research concludes that the lifespan impacting inherent defects for AM AlSi10Mg components contributes toward the compromising the reliability the propeller. This is due to the fact that as the propeller rotates, it experiences significant centrifugal forces. These forces increase the stress on the material, particularly in areas where defects exist. The presence of a defect worsens the effect of these forces, leading to a more rapid increase in localised stress.

This research also found that the type of lifespan impacting inherent defects in AM AlSi10Mg propeller were linear indications such as cracks, lack of fusion; delamination; rounded defects such as voids and porosity; and geometric inaccuracies. This research concludes that such defects were susceptible to result from a poor quality of powder such as powder particle shapes, the presence of satellites, the particle size distribution, oxidation level, humidity, static charge etc.

This research concludes by noting that the finite element method (FEM) was the most suitable method to implement for complex geometry in the determination of stress and deformation distributions. This modelling method used more sophisticated and complex mathematics for its formulation which would have made it difficult to study in manual computations.

The FEM stress distribution on AM blades of a propeller was linear defect was concluded to be exponentially increasing. This was due that fact that the combination of geometric discontinuity, centrifugal forces, fatigue effects, non-uniform material properties, load redistribution, and dynamic loading conditions contributes to an exponential increase in stress distribution in a defective rotating AlSi10Mg propeller. It was noticed by this research and concluded that as defects propagate, there was a load redistribution throughout the AlSi10Mg additively manufactured propeller. This redistribution led to increased stresses in adjacent areas, causing a cascading effect where stress levels grew rapidly in response to the presence of a linear defect. Defects such as porosity due to incomplete fusion of powder particles leading to small voids within the material, cracks due to thermal stresses during the cooling and solidification processes, particularly in area with high geometrical complexity, or irregularities created during the additive manufacturing process were likely to influence stress concentration points. When the propeller rotates, these stress concentrations amplified the local stresses.

This thesis concludes to notice that the deformation along the length of the root is higher at the tip of blade under rotation and lower at and around the hub(root). Therefore, the researcher emphasizes the importance of quality control and defect detection in additive manufacturing processes to ensure component reliability.

This research concludes that crack propagation of inherent defects in additive manufactured (AM) components is significantly influenced by the following:

- Stress Concentration: Linear defects like cracks create localized stress concentrations. When the component is subjected to loading, these areas experience higher stress, which can accelerate crack initiation and growth.
- Under cyclic loading conditions, defective AlSi10Mg AM components, will have a cracks propagating easily along the interfaces, leading to delamination or inter-layer cracking.
- AM processes often introduce residual stresses due to rapid heating and cooling. These residual stresses can drive crack propagation, particularly if they are tensile in nature, creating a favourable environment for crack growth.

Consequently, an inherent linear defects of length 10 mm crack and above is likely to propagate rapidly and uncontrollably on AM blades. The results also conclude that a 10 mm crack defect propagation in such AM components will satisfy mode 3 of defect fracture and noticeably linear discontinuities resulting from the production by PBF in AM components create conditions that can accelerate crack initiation and propagation which compromise the structural integrity and lifespan of the AlSi10Mg propeller components, hence understanding and mitigating these defects is critical for improving the reliability of AM components.

The interaction between deformation and crack propagation in rotating aluminium blades is complex, involving multiple factors that can significantly influence the integrity and lifespan of the component. Monitoring and managing these effects are critical for safe and reliable operation. deformation in a cracked rotating aluminium propeller poses serious risks and can lead to rapid deterioration of the part, potentially resulting in catastrophic failure. Regular inspection and maintenance are critical to ensure safety and performance.

The research had proven the different NDT methods used in industry for inspection such as magnetic particle testing (MPT), liquid penetrant testing (LPT), eddy current array testing (ECAT), computed tomography radiographic testing (R, T), and ultrasonic testing (UT), phased array that maybe employed in AM components however danced improvement was needed. It is concluded that based on the capabilities and limitations of each method, the advanced radiographic testing technique, i.e. computed tomography (CT) was most capable of determining the internal integrity of the complex components that were made by additive manufacturing.

Micro X-Ray CT of 1000 projections for each blade and at high resolution detected various defects internally of the AM propeller blades. The 3D model provided a detailed view of the internal features of defects such

as cracks, porosity or delamination.

This capability showed that µCT offers high-resolution imaging and detailed insights into the internal structures of AM aluminium blades, making it an effective tool for crack detection and assessment. this also show that µCT serves as a comprehensive acceptance method for additive manufactured aluminium by enabling detailed analysis of internal structures, dimensional accuracy, and material quality. Its non-destructive nature and ability to provide quantitative data make it a vital tool in ensuring the reliability and performance of AM components. The research further concludes that adequate defect sizing from the use of VG-Studio Max 2.2 software was possible however requires knowledge of interpretation of radiographs. The CT system uses high-intensity radiation to penetrate through the material thickness and records the thickness variations on a radiation-sensitive plate called a detector. This made it possible for the researcher to assess the component internally and compared the results of the FEA by ABAQUS.

This therefore mean that Non-destructive testing (NDT) methods are essential for uncovering and characterizing lifespan-impacting defects in additive manufactured (AM) components since µ X-ray CT provides detailed 3D images of the internal structure of AM components, allowing for the identification of voids, inclusions, and other internal defects and it has the ability to quantify defect sizes, shapes, and distributions, helping assess their impact on mechanical properties.

Currently, NDT radiography adopts standards based on ASME V article 2 and ISO 17636-2 for the conduct of radiation penetration into material and also use ISO 5817 levels as acceptance criteria. This research however concludes to note that there is no regulated standard that focuses on the acceptance criteria of discontinuities. This research also validates that NDT is a useful tool that contributes to fracture mechanics and the determination of the initial defect size so that other computations such as stress intensity factor, and when the reasonable number of cycles expected for the component to fail. Advanced NDT computed radiography can be perceived as a reliable tool for assessing internal integrity of complex shaped AM components.

This research therefore contributes to the knowledge hub a view that Simulation of Additive manufacturing components during design process gives guidance to understand the additive material behaviour under cyclic loads which leads to the corresponded of utilising NDT methods. µ X-ray CT is essential for uncovering and characterizing lifespan-impacting defects in additive manufactured (AM) components and also that fact that the linear defect such as a crack of 10mm has a dynamic defect growth in rotating AM propellers that are made of AlSi10Mg. Such defects reflect a mode III fracture meaning that they poses a critical stress intensity factor which lead to conclude that such defects are rejectable. The mechanical properties such as stress and strain, were observed in this research, and it is seen that from the presence of linear defects may cause a brittle fracture of a AlSi10Mg material in Additive Manufacturing (see Appendix B). This mean that the desired manufacturing process related properties in the final product should be included in the product specifications

in the design phase so that they are considered in the pre-production phase during the process engineering.

Future study

This research has identified gaps in studies on the effect of defects on the heat-treated AM aluminium materials, this will contribute to assessing the mechanical properties, electrical properties, and thermal properties of AM aluminium. This research may further suggest corrective measures to address inherent defects such as cracks. Another gap that this research has identified is the crack growth rate of ductile materials that are manufactured additively in comparison with other manufacturing processes of similar materials. There is a lack of acceptance standards for additive manufacturing defect hence a development of such standards shall contribute to satisfying the engineering principles and quality.

References

Grasso, M. *et al.* (2018) 'ScienceDirect ScienceDirect CIRP CAT Conference , process May 2018 , monitoring Nantes , France and quality Data fusion methods for statistical characterization in metal additive manufacturing A new methodology to analyze the functional and physical architecture of existing products for an assembly oriented product family identification', *Procedia CIRP*, 75, pp. 103–107. doi: 10.1016/j.procir.2018.04.045.

Chua, Z. Y., Ahn, I. H. and Moon, S. K. (2017) 'Process Monitoring and Inspection Systems in Metal Additive Manufacturing: Status and Applications', 4(2), pp. 235–245. doi: 10.1007/s40684-017-0029-7.

Klahn, C., Leutenecker, B. and Meboldt, M. (2014) 'Design for Additive Manufacturing – Supporting the Substitution of Components in Series Products', *Procedia CIRP*, 21, pp. 138–143. doi: 10.1016/j.procir.2014.03.145.

Cherfaoui, M. (2012) 'Innovative techniques in non-destructive testing and industrial applications on pressure equipment', *Procedia Engineering*, 46(0), pp. 266–278. doi: 10.1016/j.proeng.2012.09.472.

Krishnamoorthy, K. (2009) 'Quality Assurance in NDT Abstract: The Role of the NDT Operator in Quality Assurance', *Atomic Energy of Canada Limited*, pp. 1–15. Available at: https://www.ndt.net/article/ndt-canada2009/papers/21.pdf.

Lopez, A. B. *et al.* (2019) 'Phased Array Ultrasonic Inspection of Metal Additive Manufacturing Parts', *Journal of Non-destructive Evaluation*, 38(3), pp. 1–11. doi: 10.1007/s10921-019-0600-y.

Charalampous, P., Kostavelis, I. and Tzovaras, D. (2020) 'Non-destructive quality control methods in additive manufacturing: *a survey'*, 4(December 2019), pp. 777–790. doi: 10.1108/RPJ-08-2019-0224.

Chen, Y. *et al.* (2021) 'Defect inspection technologies for additive manufacturing'.

Singh, R. et al. (2020) 'Powder bed fusion process in additive manufacturing : An overview Materials Today : Proceedings Powder bed fusion process in additive manufacturing : An overview', Materials Today: Proceedings, (March). doi: 10.1016/j.matpr.2020.02.635.

Rao, R., Mohan, S. and Kumar, G. (2016) 'Determination of Fatigue Life of Surface Propeller by Using Finite Element Analysis', *International Journal of Engineering Science*, 2492(8), pp. 2492–2503. doi: 10.13140/RG.2.2.22463.43688.

Sharma, A. and Sinha, A. K. (2018) 'Ultrasonic testing for mechanical engineering domain: present and future perspective', International Journal of Research in Industrial Engineering, 7(2), pp. 243–253. doi: 10.22105/riej.2018.100730.1018.

Vo, T. H. et al. (2018) 'ScienceDirect ScienceDirect 15th CIRP Conference on Computer Aided Tolerancing – CIRP CAT 2018 France Melting Typology geometrical defects A new methodology to analyze the and physical of assembly oriented product family identification'. doi: 10.1016/j.procir.2018.04.033.

Kharfi, F. (2019) 'Mathematics and Physics of Computed Tomography (CT): Demonstrations and Practical Examples', (September). doi: 10.5772/52351.

Du Plessis, A. *et al.* (2018) 'X-Ray Microcomputed Tomography in Additive Manufacturing: *A Review of the Current Technology and Applications*', 5(3), pp. 227–247. doi: 10.1089/3dp.2018.0060.

Rohib, R. and Irawan, A. (2018) 'Additive manufacturing for steels: *a review'*. doi: 10.1088/1757-899X/285/1/012028.

Senck, S. *et al.* (2020) 'Additive manufacturing and non-destructive testing of topology-optimised aluminium components', *Nondestructive Testing and Evaluation*, 35(3), pp. 315–327. doi: 10.1080/10589759.2020.1774582.

Villarraga, H. *et al.* (2015) 'Assessing Additive Manufacturing Processes with X-ray CT Metrology assessing additive manufacturing processes with x-ray ct metrology', (May).

Chen, Y. *et al.* (2021) 'Defect inspection technologies for additive manufacturing'.
Diego, S. (2016) 'NDT for Additive Manufactured (AM) / 3D-Printed Parts Introduction to AM AM Approach for Service'.

Muhsen, A. A. (2022) 'Non-Destructive Testing Methods and their Application in Technology Non-Destructive Testing Methods and their Application in Technology', (November 2021). doi: 10.6084/m9.figshare.16926127.

Siddique, A. et al. (2021) 'Mode I fracture toughness of fiber-reinforced polymer composites: A review', Journal of Industrial Textiles, 50(8), pp. 1165–1192. doi: 10.1177/1528083719858767.
Kharfi, F. (2019) 'Mathematics and Physics of Computed Tomography (CT): Demonstrations and Practical Examples', (September). doi: 10.5772/52351.

Khorshidi, A., Khosrowpour, B. and Hosseini, S. H. (2020) 'Determination of defect depth in industrial

radiography imaging using MCNP code and SuperMC software', *Nuclear Engineering and Technology*, 52(7), pp. 1597–1601. doi: 10.1016/j.net.2019.12.010.

Obaton, A. (2020) 'Efficient volumetric non-destructive testing methods for additively manufactured parts', pp. 1417–1425.

Rohib, R. and Irawan, A. (2018) 'Additive manufacturing for steels: a review'. doi: 10.1088/1757-899X/285/1/012028.

Bajaj, P. *et al.* (2020) 'Materials Science & Engineering A Steels in additive manufacturing : A review of their microstructure and properties', 772(October 2019). doi: 10.1016/j.msea.2019.138633.

Charalampous, P., Kostavelis, I. and Tzovaras, D. (2020) 'Non-destructive quality control methods in additive manufacturing : a survey', 4(December 2019), pp. 777–790. doi: 10.1108/RPJ-08-2019-0224.

Haghdadi, N. *et al.* (2021) 'Additive manufacturing of steels : a review of achievements and challenges', *Journal of Materials Science*, 56(1), pp. 64–107. doi: 10.1007/s10853-020-05109-0.

Hilgendorff, P. *et al.* (2016) 'ScienceDirect Modeling and simulation of temperature-dependent cyclic plastic deformation of austenitic stainless steels at the VHCF limit deformation of austenitic stainless steels at the VHCF limit Thermo-mechanical modeling of a high pressure turbine blade of an gas', *Procedia Structural Integrity*, 2, pp. 1156–1163. doi: 10.1016/j.prostr.2016.06.148.

Hosseini, Z. S. *et al.* (2018) 'On the theoretical modeling of fatigue crack growth', *Journal of the Mechanics and Physics of Solids*, 121(June 2019), pp. 341–362. doi: 10.1016/j.jmps.2018.07.026.

Kharfi, F. (2019) 'Mathematics and Physics of Computed Tomography (CT): Demonstrations and Practical Examples', (September). doi: 10.5772/52351.

Khorshidi, A., Khosrowpour, B. and Hosseini, S. H. (2020) 'Determination of defect depth in industrial radiography imaging using MCNP code and SuperMC software', *Nuclear Engineering and Technology*, 52(7), pp. 1597–1601. doi: 10.1016/j.net.2019.12.010.

Kristensen, P. K., Niordson, C. F. and Martínez-pa, E. (2020) 'Applications of phase field fracture in modelling hydrogen assisted failures', 110(November).

Miloˇ, I. (2017) 'ScienceDirect E ff ects of Inclusions on the Very High Cycle Fatigue Properties of a ff ects of Inclusions on the Very High Cycle Fatigue a High Strength Martensitic Steel within the Transition Area High

Strength Martensitic Steel within the Transition Area of a high turbine blade of an a pressure airplane gas turbine engine'. doi: 10.1016/j.prostr.2017.11.096.

Muñiz-Calvente, M. and Fernández-Canteli, A. (2020) 'Special issue: Probabilistic mechanical fatigue and fracture of materials', *Materials*, 13(21), pp. 1–5. doi: 10.3390/ma13214901.

Plessis, A. *et al.* (2016) 'Directionality of Cavities and Porosity Formation in Powder-Bed Laser Additive Manufacturing of Metal Components Investigated Using X-Ray Tomography', 3(1), pp. 48–55. doi: 10.1089/3dp.2015.0034.

Price, C. T. and Muszynski, M. J. (2014) 'Motorboat Propeller Injuries: Report of Thirteen Cases with Review of Mechanism of Injury and Bacterial Considerations', *Journal of Trauma & Treatment*, 04(03). doi: 10.4172/2167-1222.1000267.

Teng, W. S. *et al.* (2021) 'A past, present, and prospective review on microwave non-destructive evaluation of composite coatings', *Coatings*, 11(8), pp. 1–25. doi: 10.3390/coatings11080913.

Gbenga, E. E. (2016) 'Using Non-Destructive Testing for the Manufacturing of Composites for Effective Cost Saving: A Case Study of a Commercial Prepreg CFC', *International Journal of Materials Engineering*, 6(2), pp. 28–38. doi: 10.5923/j.ijme.20160602.02.

Chandra, P. and Bhagi, R. (2014) 'Basics Eddy Current Testing : Basics', (March 2011).
Klahn, C., Leutenecker, B. and Meboldt, M. (2014) 'Design for Additive Manufacturing – Supporting the Substitution of Components in Series Products', *Procedia CIRP*, 21, pp. 138–143. doi: 10.1016/j.procir.2014.03.145.

Bhagi, Purna Chandra. (2011). Eddy Current Testing: *Basics. Journal of Non-Destructive Testing & Evaluation*. 10. 7-16.

Sacarea, A. I., Oancea, G. and Parv, L. (2021) 'Magnetic particle inspection optimization solution within the frame of ndt 4.0', Processes, 9(6). doi: 10.3390/pr9061067.
Kamar V. et al. (2020) 'Performance Characteristics of Weld Defect Inspection by Magnetic Particle Testing', *International Journal of Innovative Technology and Exploring Engineering*, 9(3), pp. 2270–2276. doi: 10.35940/ijitee.c8856.019320.
Ma, Z., Liu, W., Li, S., Lu, X., Bessling, B., Guo, X., & Yang, Q. (2022). A local to global (L2G) finite element method for efficient and robust analysis of arbitrary cracking in 2D solids. Computer Methods in Applied Mechanics and Engineering, 398, 115205. https://doi.org/10.1016/j.cma.2022.115205

Foudil, K. et al. (2013) ‘Modeling of Fatigue Crack Propagation in Aluminum Alloys Using an Energy Based Approach’, (August). doi: 10.48084/eta
Zenzinger, G. et al. (2014) ‘Process Monitoring of Additive Manufacturing by Using Optical Tomography Process Monitoring of Additive Manufacturing by Using Optical Tomography’, (July). doi: 10.1063/1.4914606.

Montanari, R. *et al.* (2023) ‘Additive Manufacturing of Aluminum Alloys for Aeronautic Applications: Advantages and Problems’, *Metals*, 13(4). doi: 10.3390/met13040716.

Obaton, A. (2020) ‘Efficient volumetric non-destructive testing methods for additively manufactured parts’, pp. 1417–1425.

Amin S (2024) et al.’ Exploring the stress concentration factor in additively manufactured materials: A machine learning perspective on surface notches and subsurface defects’ pp. Volume 130, April 2024, 104298

APPENDIX A

Mode I

```
close all;
clc;
clear all;
% the stress intensity factor computation for AM propeller%
a=[10:0.2:13.8];%mm%
s=[0,2,5,7,12,17,22,29,35,43,51,60,70,80,91,100,106,122,126,137];
Y=70.*10^9;%Pa%
K=Y.*s.*(sqrt(pi.*a));
plot(a,K,'b<-');
title ('Stress Intensity Factor vs Defect length')
x-label ('Defect length (mm)');
y-label ('Stress Intensity Factor MPa sqrt(m)')
```

Mode III

```
close all;
clc;
clear all;
% the stress intensity factor computation for AM propeller%
a=[10:0.2:13.8];%mm%
F=[0,2,5,7,12,17,22,29,35,43,51,60,70,80,91,100,106,122,126,137];
A=[400:0.1:403] %mm^2%
Z=1;%geometrical correction factor%
K=Z.(F/A).*s.*(sqrt(pi.*a));
plot(a,K,'b<-');
title ('Stress Intensity Factor vs Defect length')
x-label ('Defect length (mm)');
y-label ('Stress Intensity Factor MPa sqrt(m)')
```

APPENDIX B

Results of a tensile test of a defective component

Aim: To conduct a tensile stress analysis of an AM Aluminium strip sample that is prepared in accordance with ASTM E88 dimension specification to understand its tensile strength, yield strength, and fracture.

Apparatus used.

a three samples with same defects, which are.

b tensile machine.

c calibrated ruler for measuring dimensions.

d Stationery for recoding

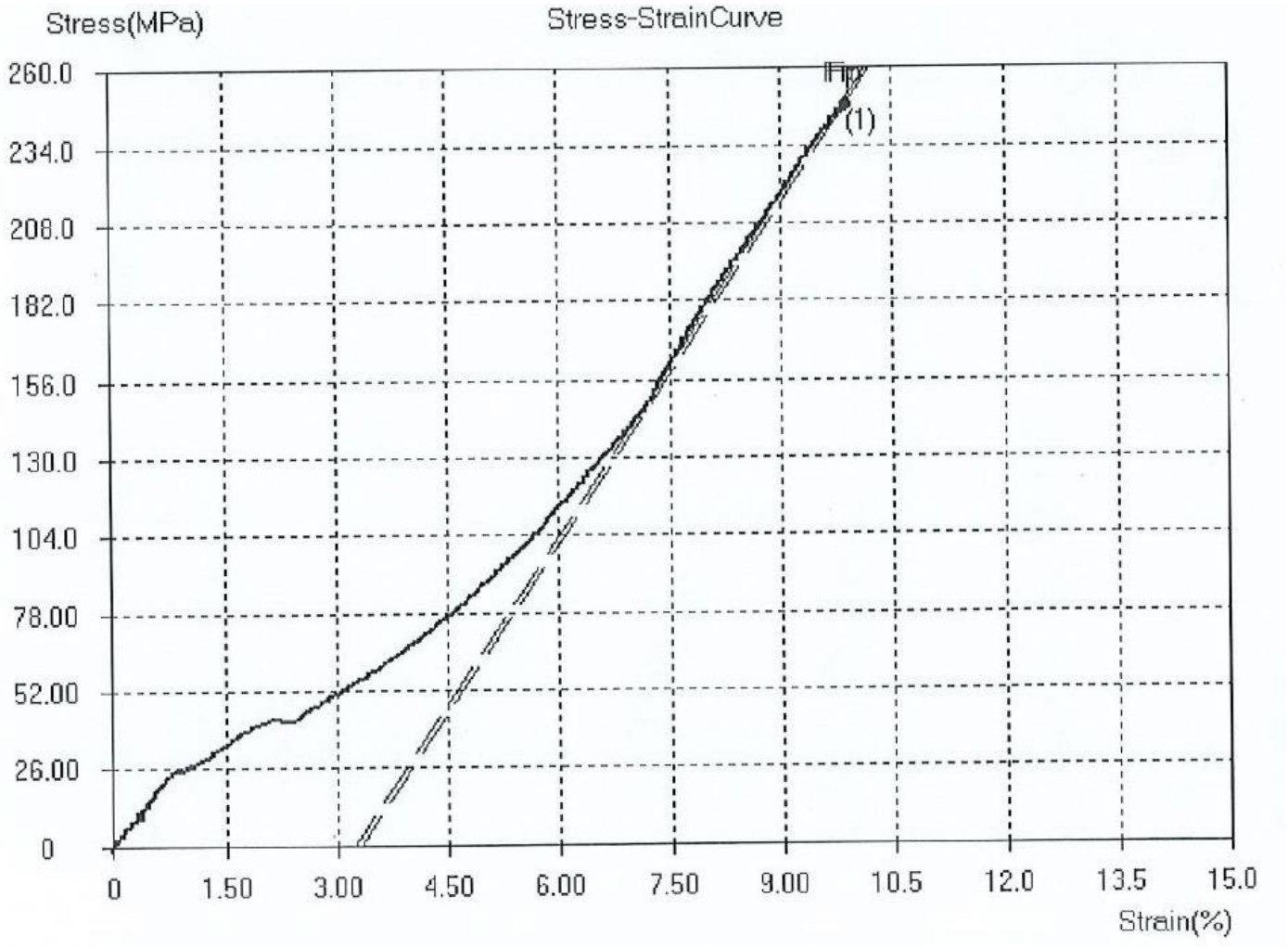
Stress(MPa)
Stress-StrainCurve
260.0
234.0
208.0
182.0
156.0
130.0
104.0
78.00
52.00
26.00
0
(1)
0
1.50
3.00
4.50
6.00
7.50
9.00
10.5
12.0
13.5
15.0
Strain(%)